Fakultät für Medizin der Technischen Universität München

Avidity dependent evolution of the T cell receptor repertoire during chronic viral infection

Florian Maximilian Voit

Vollständiger Abdruck der von der Fakultät für Medizin der Technischen Universität München zur Erlangung des akademischen Grades eines

Doktors der Medizinischen Wissenschaft

genehmigten Dissertation.

Vorsitz:	apl. Prof. Dr. Klaus-Peter Janssen
Prüfer*innen der Dissertation:	1. Prof. Dr. Dirk Busch
	2. Priv. Doz. Dr. Caspar Ohnmacht
	3. Prof. Dr. Angela Krackhardt

Die Dissertation wurde am 02.03.2021 bei der Technischen Universität München eingereicht und durch die Fakultät für Medizin am 13.10.2021 angenommen.

Parts of this thesis have already been published:

Schober, K., Voit, F., Grassmann, S. *et al.* Reverse TCR repertoire evolution toward dominant low-affinity clones during chronic CMV infection. *Nat Immunol* **21,** 434–441 (2020). https://doi.org/10.1038/s41590-020-0628-2

These authors contributed equally: Kilian Schober, Florian Voit.

Content

List of Figures

Abbreviations

ACT *ammonium chloride Tris*
AIDS *acquired immune deficiency syndrome*
ANOVA *analysis of variance*
APC allophycocyanin
APL *altered peptide ligand*
BSA *bovine serum albumin*
CAR *chimeric antigen receptor*
CD *cluster of differentiation*
CFM *complete freezing medium*
CMV *cytomegalovirus*
DMSO *dimethyl sulfoxide*
DNA *deoxyribonucleic acid*
EBV *Epstein–Barr virus*
EC50 *half maximal effective concentration*
EDTA *ethylenediaminetetraacetic acid*
EMA *ethidium monazide bromide*
Fab *antigen-binding fragment*
FACS *fluorescence-activated cell sorting*
Fc *fragment crystallizable*
FCS *fetal calf serum*
FITC *fluorescein isothiocyanate*
Gy *gray*
hCMV *human cytomegalovirus*
HLA *human leukocyte antigen*
i.p. *intra-peritoneal*
IE *immediate early*
IFNγ *interferon gamma*
IL *interleukin*
IONO *ionomycin*
IRP *immune risk phenotype*
k_{bleach} *bleaching rate*
K_d *dissociation constant*
k_{off} *off-rate*
k_{on} *on-rate*
LCMV *Lymphocytic choriomeningitis virus*
LN *lymph node*
mCMV *murine cytomegalovirus*
MHC *Major histocompatibility complex*
NGS *next generation sequencing*
NSCLC *non-small-cell lung carcinoma*
p.i. *post infectionem*
PB *pacific blue*, *peripheral blood*
PBMC *peripheral blood mononuclear cells*
PBS *phosphate buffered saline*
PCR *polymerase chain reaction*
PE *phycoerythrin*
PerCP *peridinin-chlorophyll-protein complex*
PFU *plaque-forming unit*
PI *Propidium iodide*
PMA *phorbol 12-myristate 13-acetate*
pMHC *peptide major histocompatibility complex*
Rag *recombination activating gene*
RNA *ribonucleic acid*
rpm *revolutions per minute*

SC$^+$ *Supplement complete*
SD *standard deviation*
SEM *standard error of mean*
SP *spleen*
SPF *specific pathogen free*
SPR *surface plasmon resonance*
$t_{1/2}$ *half-life time*
Tcm *central memory T cell*
TCR T cell receptor
tg *transgenic*
wt *wild type*

1 Introduction

1.1 T cell repertoire and precursor frequency

Cluster of differentiation 8 positive ($CD8^+$) T cells play a key part in killing virally infected or cancerous cells. Immunotherapeutic approaches targeting $CD8^+$ T cells like immune checkpoint inhibitors or adoptive T cell therapy have already shown great clinical success (Li et al., 2019). As part of the adaptive immune system, T cells are not a homogeneous cell population, but all bear a unique T cell receptor (TCR). A better understanding of how T cell fate is regulated by the TCR will be of great importance for improving clinical application.

The main cellular components of the adaptive immune system are T cells and B cells. T cells confer only cell-mediated immunity, whereas B cells are also involved in the humoral immune response (Kenneth Murphy, 2016). One of the hallmarks of the adaptive immune system is its antigen specificity. An antigen-specific response is rendered possible by a highly diverse repertoire of receptors that provides robust recognition of a plethora of potential pathogens. This huge spectrum of antigen specificities is created by the processes of genetic recombination (VDJ rearrangement) and random insertion or deletion of nucleotides within the genes that encode the antigen receptors (Kenneth, 2013). For T cells, combinatorial and junctional diversity during TCR gene rearrangement would theoretically allow for assembly of up to 10^{20} unique TCR (Laydon, Bangham, & Asquith, 2015; Zarnitsyna, Evavold, Schoettle, Blattman, & Antia, 2013). Since the processes governing somatic recombination are not entirely random and T cells have to undergo thymic positive and negative selection, the actual number of unique TCRs present in a human individual is dramatically lower, approximately in the range of 10^8 (Miles, Douek, & Price, 2011; Ouyang et al., 2003; Qi et al., 2014; Quigley et al., 2010; Venturi et al., 2006). The total naïve (that is, antigen-unexperienced) T cell repertoire in the mouse is estimated to contain about 2×10^6 separate clones of ten cells each (Casrouge et al., 2000).

The frequency of naïve T cells specific for one epitope is the so-called precursor frequency. By adoptive transfer of titrated amounts of TCR-transgenic cells Rafi Ahmed's

group estimated the precursor frequency for one lymphocytic choriomeningitis virus (LCMV) epitope to be one in 2×10^5, which would translate to 100–200 epitope-specific cells in an uninfected mouse (Blattman et al., 2002). Using major histocompatibility complex (MHC) multimer and magnetic-bead technology the total number of precursor cells for different epitopes was shown to be in the range of 80 to 1200 cells per mouse (Obar, Khanna, & Lefrançois, 2008). Precursor frequencies for different epitopes vary in size substantially. This was partly explained by the fact that the amino acid sequence of some peptides is more suited to interact with TCRs than others (Chu, Moon, Kruse, Pepper, & Jenkins, 2010; Jenkins, Chu, McLachlan, & Moon, 2010; Turner et al., 2005). Despite the fact that random processes are involved in the generation of the TCR repertoire, the precursor frequency for a defined epitope is remarkably conserved between different individuals (Alanio, Lemaitre, Law, Hasan, & Albert, 2010).

The naïve T cell precursor pool for a given epitope is not a homogeneous entity but consists of T cells that have different TCRs. These differences in the amino acid sequence of the TCR translate to differences in the strength of interaction between the TCR and its peptide major histocompatibility complex (pMHC). The strength of interaction has a major impact on the outcome of a T cell response and next, different methods of measuring it are presented.

1.2 T cell avidity

T cell avidity (functional or structural) and T cell affinity are terms used inconsistently and oftentimes interchangeable in the literature. For the understanding of this project the terminological differences are crucial and will be elaborated below (see also Figure 1).

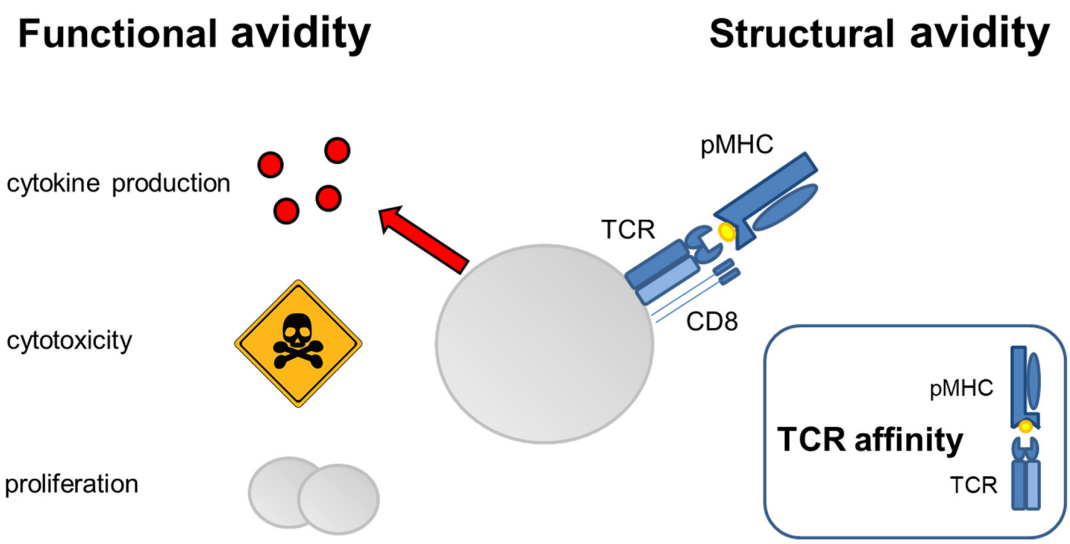

Figure 1. T cell avidity: Differences between functional avidity, structural avidity and TCR affinity. Schematic illustration of the key elements of functional avidity, structural avidity and TCR affinity. Functional avidity describes the sensitivity of a T cell to antigen. Readouts include proliferation capacity, cytotoxic activity and cytokine production upon stimulation with titrated amounts of antigen. T cell affinity is defined as the biophysical strength of interaction between one pMHC molecule and one TCR. T cell structural avidity describes the biophysical strength of interaction between the TCR to pMHC together with co-receptor binding via CD8 or CD4 (Viganò et al., 2012).

1.2.1 T cell affinity

T cell affinity describes a monomeric binding event. It is defined as the biophysical strength of interaction between one pMHC molecule and one TCR (Stone, Chervin, & Kranz, 2009; Viganò et al., 2012) (see Figure 1). The gold standard for determining T cell affinity is surface plasmon resonance (SPR) (Alam et al., 1996). SPR makes use of the optical phenomenon of total internal reflection of light at a metal film-liquid. Both components of the interaction, the TCR and the pMHC, are purified. One is immobilized on a bio-specific interface, while the other is flowed over it in solution (Fägerstam, Frostell-Karlsson, Karlsson, Persson, & Rönnberg, 1992). By this method, the dissociation constant (k_d) can be derived from the on-rate (k_{on}) and off-rate (k_{off}) of the receptor–ligand equilibrium ($k_d = \frac{k_{off}}{k_{on}}$) (Merwe & Davis, 2003).

SPR measurements are performed in three dimensions and investigate protein interactions in their simplest form with no influence from other forces. However, physiologically the interaction between the TCR and the pMHC takes place on two opposing cell membranes. In this cellular context additional factors become relevant that are not

accounted for by SPR (Martinez & Evavold, 2015). Also, since SPR uses purified ligands, it requires recombinant expression of both TCR and pMHC, making the analysis time consuming and not suitable for fast and high-throughput *ex vivo* analysis.

1.2.2 T cell structural avidity and the TCR-ligand k_{off}-rate assay

The term avidity in general relates to the strength of multimeric interactions. T cell structural avidity more specifically describes the biophysical strength of interaction between the TCR to pMHC together with co-receptor binding via CD8 or CD4 (see Figure 1; Nauerth et al., 2013). First assays determining T cell structural avidity in the most rudimental form became possible with the availability of recombinant pMHC multimers (Altman et al., 1996). Since the strength of interaction between the TCR and a pMHC is weak, only the multimerization of the pMHCs via a backbone allowed stable labelling of epitope-specific T cells. The fluorescence intensity of cell surface bound, fluorochrome labelled pMHC multimers was taken as measure for structural avidity, sometimes in combination with a titration of the pMHC multimer reagent (Crawford, Kozono, White, Marrack, & Kappler, 1998; Slifka & Whitton, 2001). Other groups, however, have found only weak correlation between pMHC multimer staining intensity and functional avidity, making sole staining intensity a questionable readout (Echchakir et al., 2002; Lawson et al., 2001; Palermo et al., 2001). A great progress in readouts for structural avidity was the development of dissociation experiments using pMHC multimers (D H Busch & Pamer, 1999; Holmberg, Mariathasan, Ohteki, Ohashi, & Gascoigne, 2003; Savage, Boniface, & Davis, 1999; Wang & Altman, 2003). Here, high temperature or blocking agents (e.g. anti-MHC antibodies, unlabeled MHC multimers or antigen-binding fragment (Fab) fragments) were used to facilitate the dissociation of pMHC multimers. The dissociation rates or half-life times ($t_{1/2}$) were taken as estimators for structural avidity. However, the dissociation of one pMHC multimer requires the disruption of multiple TCR-pMHC interactions. Rebinding events have to be considered and are hard to predict, and therefore higher order dissociation kinetics can occur. Also, dissociation kinetics can be influenced by the concentration of blocking agents or the degree

of multimerization (Wang & Altman, 2003). The great advantage of pMHC multimer dissociation experiments in comparison to SPR is that they can be performed directly *ex vivo*. Nonetheless they are susceptible to some degree of variability due to the multimeric nature of the dissociation and the use of blocking reagents.

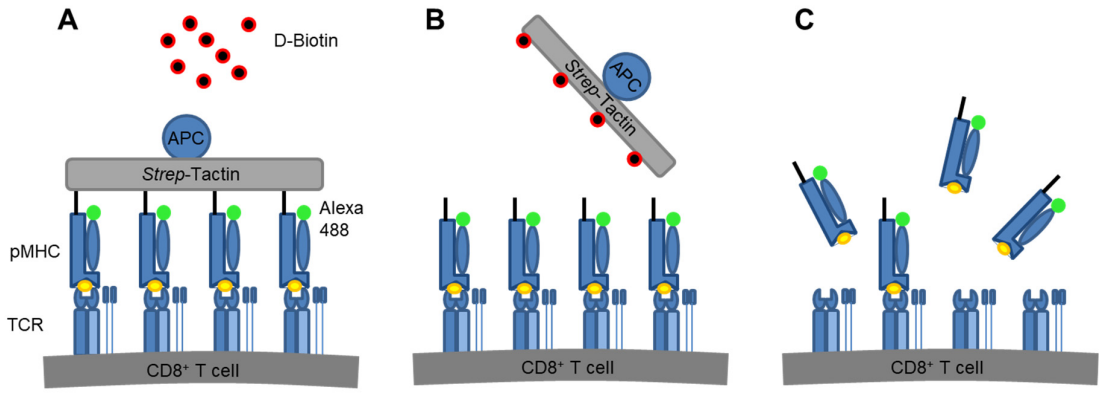

Figure 2. Principle of the TCR-ligand k_{off}-rate assay. (A) A CD8⁺ T cell is stably labelled with a *Strep*tamer consisting of pMHCs multimerized by a *Strep*-Tactin backbone. Both the pMHC and the *Strep*-Tactin are conjugated with a fluorochrome (Alexa Fluor 488 and allophycocyanin (APC) respectively). **(B)** Upon addition of D-biotin the *Strep*tamer complex gets disrupted leaving monomeric pMHCs bound on the TCRs. **(C)** Dissociation of pMHC: Dissociation rate k_{off} is depended on T cell avidity; Adapted from (Nauerth et al., 2013).

In contrast, the TCR-ligand k_{off}-rate assay assesses structural avidity by the dissociation of truly monomeric pMHCs (Knall, 2007; Nauerth, 2012; Nauerth et al., 2013; Weißbrich, 2015). Its key element is a reversible pMHC multimer staining, a so called *Strep*tamer staining (Knabel et al., 2002, Figure 2). The *Strep*tamer consists of two parts: recombinant MHC I molecules loaded with the specific peptide of interest and a *Strep*-Tactin backbone which multimerizes the pMHC molecules via binding to their *Strep*-tag III region. Both the pMHC molecules and the *Strep*-Tactin backbone are conjugated with a fluorochrome allowing stable labelling of living epitope-specific T cells. The *Strep*tamer complex can be disrupted in a controlled manner by the addition of D-biotin, which has a higher affinity to the *Strep*-tag binding sites on *Strep*-Tactin. Consequently, monomeric pMHC are left bound to the TCRs expressed on the T cell surface. Since pMHC monomers do not stably bind to the TCR, their dissociation can be monitored as a gradual decrease in fluorescence intensity. By plotting the fluorescence intensity values over time, the dissociation rate (k_{off}-rate) and $t_{1/2}$ of the dissociation can be calculated. Due to the dissociation's monomeric nature and

the expendability of blocking reagents, TCR-ligand k_{off}-rate measurements are highly reproducible compared to conventional pMHC multimer dissociations. First studies indicated a good correlation between the measured dissociation rate, functional avidity and *in vivo* protectivity (Nauerth et al., 2013), which demonstrated the predictive power of the assay for *in vivo* outcomes. How robustly these parameters indeed correlate, will need to be addressed in large-scale and systematic future studies. Overall, however, the TCR-ligand k_{off}-rate represents the assay that most efficiently combines high-throughput assessment of structural avidity and reliability.

Two versions of the TCR-ligand k_{off}-rate assay have been established so far: the microscopic k_{off}-rate assay and the flow cytometry-based k_{off}-rate assay (Nauerth et al., 2016, 2013). The k_{off}-rate of individual T cells can be measured by the microscopic k_{off}-rate assay (see Figure 3). This single-cell resolution is of particular interest for analyzing polyclonal T cell population by revealing the repertoire composition and heterogeneity of the population in terms of structural avidity. Indeed it could be shown for human cytomegalovirus (hCMV) positive blood donors, that the spectrum of structural avidities of epitope-specific T cell populations can be remarkable broad for one individual, while being narrow for another (Nauerth et al., 2013). Modifications of the assay rendered it applicable for flow cytometry (see Figure 4). Here, the assay measures the average k_{off}-rate of an epitope-specific T cell population, which for monoclonal populations should in theory coincide with the k_{off}-rate obtained for individual cells by the microscopic assay. By using a second non-reversible multimer staining specific for the same epitope the assay can also be performed in the presence of non-specific T cells without the need for prior epitope-specific cell sorting. By this sort-free approach, fast and high-throughput structural avidity measurements became feasible which renders potential clinical applications within reach.

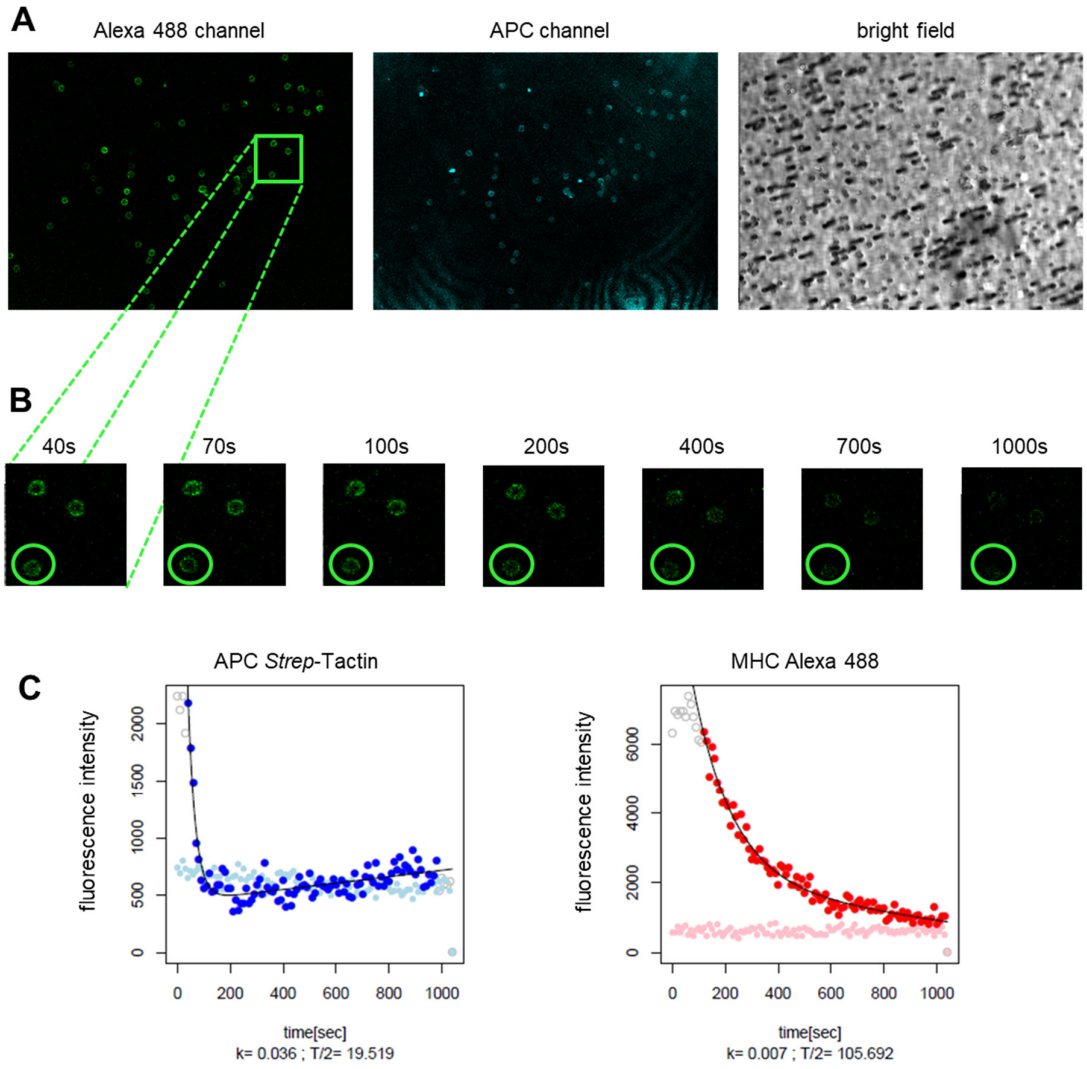

Figure 3. The microscopic TRC-ligand k_{off}-rate assay. (A) Sorted *Strep*tamer+ cells are placed onto a confocal laser scanning microscope. Field of view (different channels) show cells before addition of D-biotin. **(B)** Section of the Alexa Fluor 488 channel in (A) shows three cells at different time points after addition of D-biotin. **(C)** Fluorescence intensity values of the cell marked with a green circle in (B) are plotted over time. Light blue and light red dots depict background fluorescence intensity of the respective channel. Grey dots depict fluorescence intensity before addition of D-biotin.

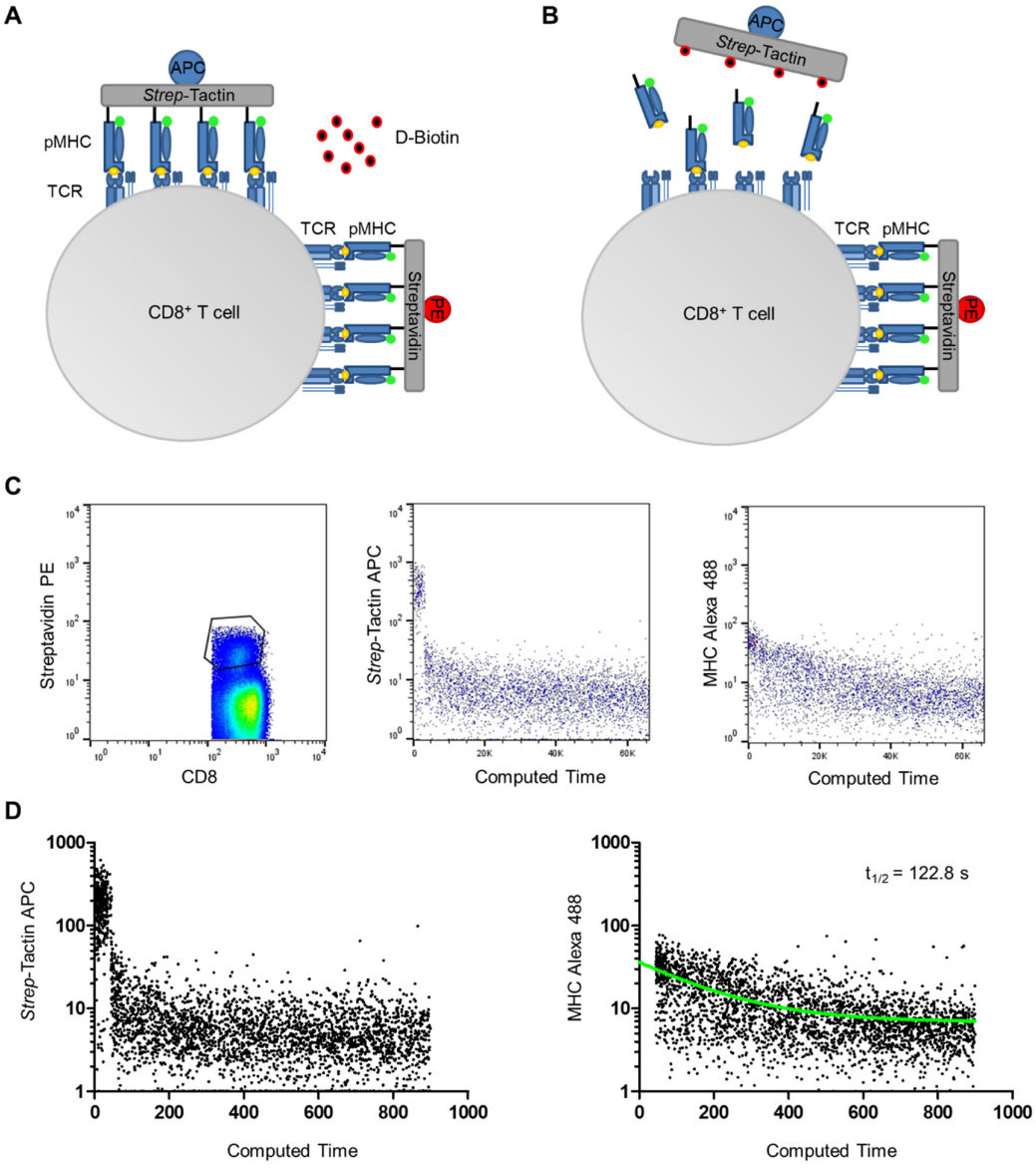

Figure 4. Flow cytometry-based TCR ligand k_{off}-rate assay: a sort-free approach using double multimer staining. (A) Schematic illustration of a T cell stained with a double multimer staining, consisting of a reversible *Strep*tamer staining and a non-reversible multimer staining. **(B)** Upon addition of D-biotin the *Strep*tamer complex is disrupted allowing the observation of the dissociation of monomeric pMHCs. The non-reversible multimer stays stably attached to the T cell. **(C)** Pseudocolor plot of flow cytometry-based k_{off}-rate dissociation; left graph pre-gated on lymphocytes, singlets, living $CD19^-$ and $CD8^+$. Middle and right graph further gated on the gate in left graph **(D)** Dot plot of flow cytometry-based k_{off}-rate dissociation. A one-phase exponential decay curve (green line) is fitted. Note that fitting is started after complete *Strep*-Tactin APC dissociation.

1.2.3 Functional avidity

Functional avidity describes the sensitivity of a T cell to antigen, meaning the ability to exert effector functions in response to limited amounts of antigen. Read-outs of functional avidity include proliferation capacity, cytotoxic activity and cytokine production upon stimulation

with titrated amounts of antigen (see Figure 1). The peptide concentration that elicits half-maximum effector-functions (EC50) is determined. High functional avidity corresponds to a low EC_{50}. Structural avidity (see 1.2.2) has a major impact on functional avidity indicated by a strong correlation of both parameters (Yee, Savage, Lee, Davis, & Greenberg, 1999). This is highlighted by the observation that T cells maintained their functional avidity even after transgenic expression (Johnson et al., 2006). But the interaction between the TCR and the pMHC is not the only factor influencing a functional outcome: other factors are co-receptors and co-stimulatory/co-inhibitory molecules, the phenotype of the cell, the efficacy of intracellular signaling or the level of TCR expression (Scherer, Noest, & de Boer, 2004). For example, a T cell with a high structural avidity could still show a weak response to antigen stimulation due to the expression of inhibitory receptors. As functional avidity shows the functional outcome of stimulation, it is no surprise that it also correlates well with *in vivo* functionality (Zeh, Perry-Lalley, Dudley, Rosenberg, & Yang, 1999).

1.3 T cell activation

T cell activation needs to be tightly regulated to allow an efficient and targeted response against pathogens on the one hand and avoid autoimmunity or allergy on the other hand. The strength of interaction between the TCR and a pMHC is the main determinant of T cell activation and different models have been proposed to explain the exact relationship (Lever, Maini, van der Merwe, & Dushek, 2014). Currently, the kinetic proofreading with limited signaling model is best supported by experimental data. The kinetic proofreading model implies that the dissociation time of the TCR-pMHC interaction must be long enough for the TCR to achieve a signaling-competent state, in other words that there is a threshold for structural avidity to allow T cell activation. A modification of the model with limited signaling includes serial triggering. It proposes that the rate of forming signaling-competent TCRs is proportional to T cell activation. This means there is an optimum for the dissociation time and that very high structural avidities corresponding to dissociation times beyond that optimum will lead to impaired activation (Irving et al., 2012).

1.4 T cell immune response against non-persistent pathogens

During an infection with a non-persistent pathogen naïve epitope-specific $CD8^+$ T cells are activated and undergo a characteristic kinetic sequence of rapid expansion, subsequent contraction and formation of memory cells (Buchholz et al., 2013; Williams & Bevan, 2007). All T cells originating from one naïve precursor T cell bear the same TCR and form a so-called T cell clone (clonal selection theory: Burnet, 1959). The naïve TCR repertoire for a given epitope contains a wide spectrum of different structural avidities and for stochastic reasons the majority of TCRs is believed to be of low structural avidity (Arstila et al., 1999; Hombrink et al., 2013). Using OT-I T cells and SIINFEKL altered peptide ligand (APL) expressing Listeria monocytogenes, Dietmar Zehn and Michael Bevan could show that above a certain structural avidity threshold even very low structural avidity T cells get activated and recruited into an acute T cell response (Zehn, Lee, & Bevan, 2009). Unlike B cells, T cells cannot undergo avidity maturation through somatic hypermutation. Instead, it has been shown that secondary/recall responses against non-persistent pathogens or after immunization consist of T cells with higher structural avidity than the primary response due to selective expansion of high avidity T cells (D H Busch & Pamer, 1999; Savage et al., 1999; Figure 5). As an additional adaption mechanism, individual T cells can increase their functional avidity during the primary response, a process called functional avidity maturation (Slifka & Whitton, 2001; Zehn et al., 2009).

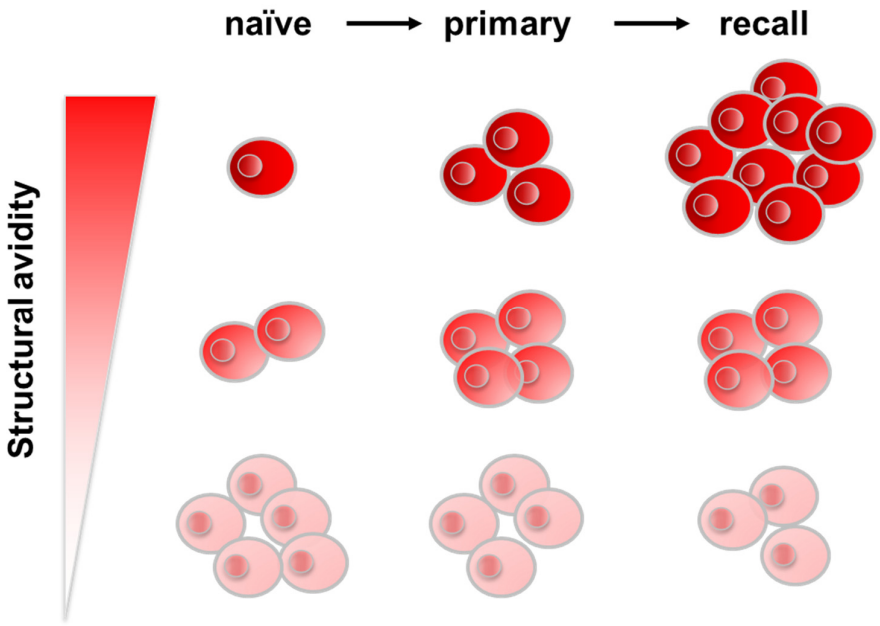

Figure 5. Structural avidity maturation through selective expansion of high avidity T cells. T cells with different structural avidities are recruited during primary infection. During primary and especially during recall/secondary infection high avidity T cells are preferentially enriched, thereby increasing the population's average structural avidity.

1.5 T cell immune response against CMV

Cytomegalovirus (CMV) is a large deoxyribonucleic acid (DNA) virus and member of the β-subfamily of herpesviruses. More than 60 % of the adult population (in developing countries almost 100 %) are CMV-seropositive (P. Griffiths, Baraniak, & Reeves, 2015). Through millions of years of co-evolution with its host, CMV has mastered immune defense and evasion strategies and usually establishes a lifelong chronic latent infection in its host (Loewendorf & Benedict, 2010; McGeoch, Cook, Dolan, Jamieson, & Telford, 1995). Primary infection is generally accompanied by only mild general symptoms and the subsequent chronic infection stays asymptomatic and unnoticed by healthy individuals. CMV is, however, a major cause of morbidity and mortality for immunocompromised individuals. Congenital CMV infection can lead to microcephaly, hepatosplenomegaly and sensorineural hearing loss. Immunosuppressed patients like organ transplant recipients, bone marrow transplant recipients or acquired immune deficiency syndrome (AIDS) patients can develop end-organ disease, such as gastrointestinal ulceration, hepatitis, pneumonitis or retinitis (P. Griffiths et al., 2015).

First evidence that CMV might play a role in immunosenescence in immunocompetent individuals came from two Swedish longitudinal studies performed on non-institutionalized octogenarians and nonagenarians, respectively. They identified an immune risk phenotype (IRP) predictive of mortality, which correlated with CMV seropositivity (Hadrup et al., 2006; Wikby, Maxson, Olsson, Johansson, & Ferguson, 1998). IRP was characterized by an inverted CD4/CD8 ratio, poor proliferative response, and an accumulation of $CD28^{-}CD8$ T cells. Murine cytomegalovirus (mCMV) in old mice also led to an increase of $CD8^{+}$ cells, reduced numbers of naïve T cells and weaker response to superinfection (Cicin-Sain et al., 2012).

1.5.1 Memory inflation

After lytic primary infection, during which infectious virions are shed, CMV enters a phase of chronic latent infection with only occasional episodes of minor reactivation (P. Griffiths et al., 2015). However, controlling CMV requires continuous immune surveillance, especially a T cell mediated cellular immune response (Klenerman & Oxenius, 2016). Epitope expression changes from acute to chronic latent infection, which is reflected in the CMV-specific T cell response. The T cell response can be divided into two groups (see Figure 6): non-inflationary T cell populations are mostly directed against epitopes expressed during acute infection (primary infection, reactivation). Population size kinetics are reminiscent of T cell responses against non-persistent pathogens like expansion during acute infection, then contraction and maintenance as small resting memory populations. Inflationary T cell populations, on the other hand, are mostly directed against epitopes expressed during latency. They increase in size over the course of the infection, a phenomenon called memory inflation (Khan et al., 2007; Munks et al., 2006; O'Hara, Welten, Klenerman, & Arens, 2012). In the following, "inflationary T cell response-inducing epitopes" will be referred to simplistically as "inflationary epitopes", and infections that induce an inflationary T cell response will be referred to as "inflationary infections". Although also described for other viruses (e.g. Epstein–Barr virus (EBV)), memory inflation is most pronounced in CMV

infection. For some individuals, the population size of T cells specific for one inflationary epitope can reach even more than 50 % of all $CD8^+$ T cells (Karrer et al., 2003).

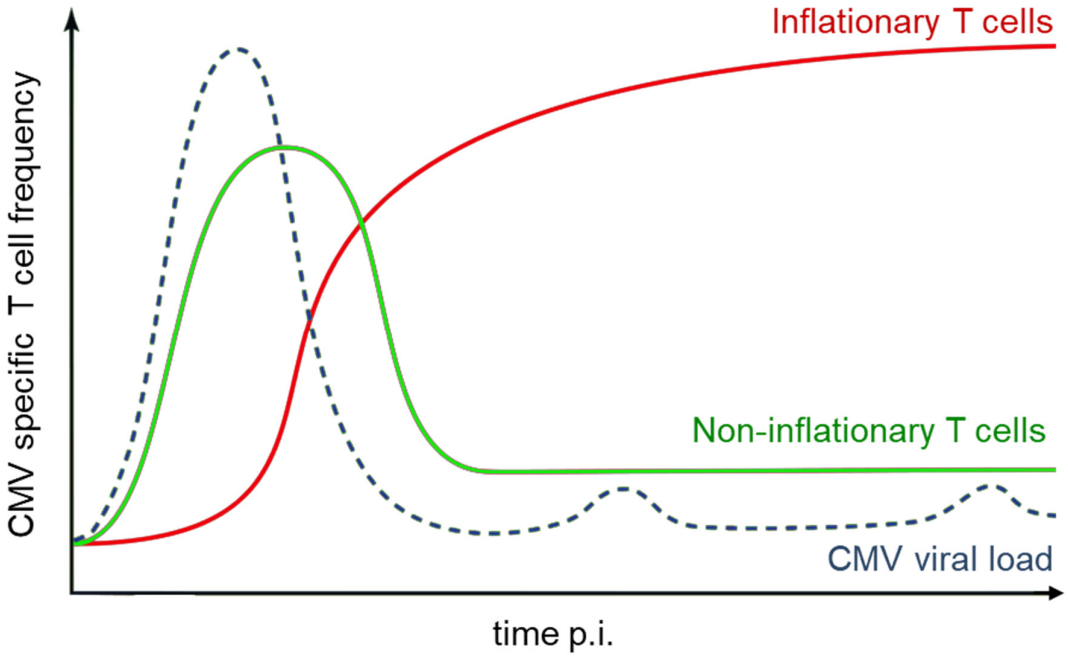

Figure 6. Memory inflation occurs during chronic latent CMV infection. After primary infection, viral load usually stays at undetectable levels with only occasional episodes of minor reactivation. Accordingly, non-inflationary T cells also contract after primary infection and are maintained as small resting memory populations. In contrast, inflationary T cells continuously expand during latency, a phenomenon termed memory inflation. Figure adapted from (O'Hara et al., 2012).

Since CMV has a high species tropism, human CMV cannot be used in animal models. The natural mouse pathogen mCMV, however, shows striking similarity in the host-pathogen interaction also inducing memory inflation. mCMV is therefore widely used as a model system for the human counterpart allowing more systematic research (Krmpotic, Bubic, Polic, Lucin, & Jonjic, 2003; Smith, Turula, & Snyder, 2014).

Although T cell responses against CMV can be directed towards a broad and complex repertoire of antigens, large screenings with peptide pools derived from different CMV genes identified two antigens as major T cell targets for human CMV (Elkington et al., 2003; Sylwester et al., 2016): The major tegument protein pp65 (UL83), which is only expressed during viral replication, and the transcription factor immediate early 1 (IE1; UL123), which is expressed during latency and elicits T cell memory inflation. For mCMV in

C57BL/6 mice the most prominent epitopes are the non-inflationary M45 and M57 and the inflationary M38, M139 and IE3 (Munks et al., 2006; Snyder, 2011).

1.5.2 TCR repertoire changes

During latency, not only the population size of CMV-specific T cells changes, but also the composition of T cell clones participating in the immune response. Increasing oligoclonality over time, in the sense of a more restricted TCRβ-chain usage compared to a polyclonal repertoire at primary infection, was shown for inflationary T cell populations during mCMV infection (Karrer et al., 2003). Longitudinal studies covering such a large part of the individual's lifespan have barely been performed for hCMV. However clonal focusing has been reported to occur during primary infection for T cells specific for the non-inflationary epitope pp65 (Day et al., 2007). Restricted TCRβ-chain usage for pp65-specific T cells was especially found in patients undergoing reactivation or chronic inflammation (Trautmann et al., 2005) or following allogeneic stem cell transplantation (Link et al., 2016). The loss of TCR diversity was suggested to be the result of selection of certain T cell clones, but the mechanisms governing this process are still unclear. Some groups have proposed the selection of high avidity T cells as the key driver of oligoclonality (Day et al., 2007; Price, 2005; Trautmann et al., 2005), potentially in analogy to avidity maturation (Figure 5) seen in non-persistent infections.

The avidity assessments performed in these studies were based on functional avidity measurements or tetramer binding/dissociation assays which have several downsides for avidity-based repertoire analysis (see 1.2). Moreover, few of these studies looked at inflationary T cell populations, for which different factors might need to be considered in shaping the TCR repertoire. Unlike conventional resting memory cells, which are maintained in the absence of antigen, memory inflation is sustained by low level antigen exposure (Lang, Brien, & Nikolich-Zugich, 2009; O'Hara et al., 2012). Somatic cells cannot divide infinitely due to a cell-intrinsic phenomenon known as the Hayflick limit (L Hayflick & Moorhead, 1961; Leonard Hayflick, 1980). Constant stimulation and antigen driven

proliferation can therefore lead to proliferation-associated or replicative senescence. Replicative senescence is well described for T cells, both *in vitro* and *in vivo* (reviewed in (Chou & Effros, 2013) and has also been suggested as a driver of TCR repertoire changes during chronic latent infection (Buchholz, Neuenhahn, & Busch, 2011): According to the model of clonal changing of the guard, T cells of high structural avidity receive the strongest TCR-mediated signal, proliferate the most and therefore dominate the early phase of chronic infection. Over time, however, they will become replication senescent, leading to a successive handover of dominance to T cells with lower avidity (see also Figure 7). Experimental evidence supporting a similar model (senescence model of clonal succession) was found for EBV, for which TCR repertoire and avidity data suggest a gradual loss of high avidity cells (Annels, Callan, Tan, & Rickinson, 2000; Davenport, Fazou, McMichael, & Callan, 2002). Also, oligoclonality of CMV-specific T cell populations was found accentuated by old age (Khan et al., 2002) and in contrast to the reported selection of high avidity T cells during primary infection and early latency (see above) CMV-specific T cells of elderly individuals were found to be of low avidity (S. J. Griffiths et al., 2017; Khan, Cobbold, Cummerson, & Moss, 2010; Ouyang et al., 2003, 2004).

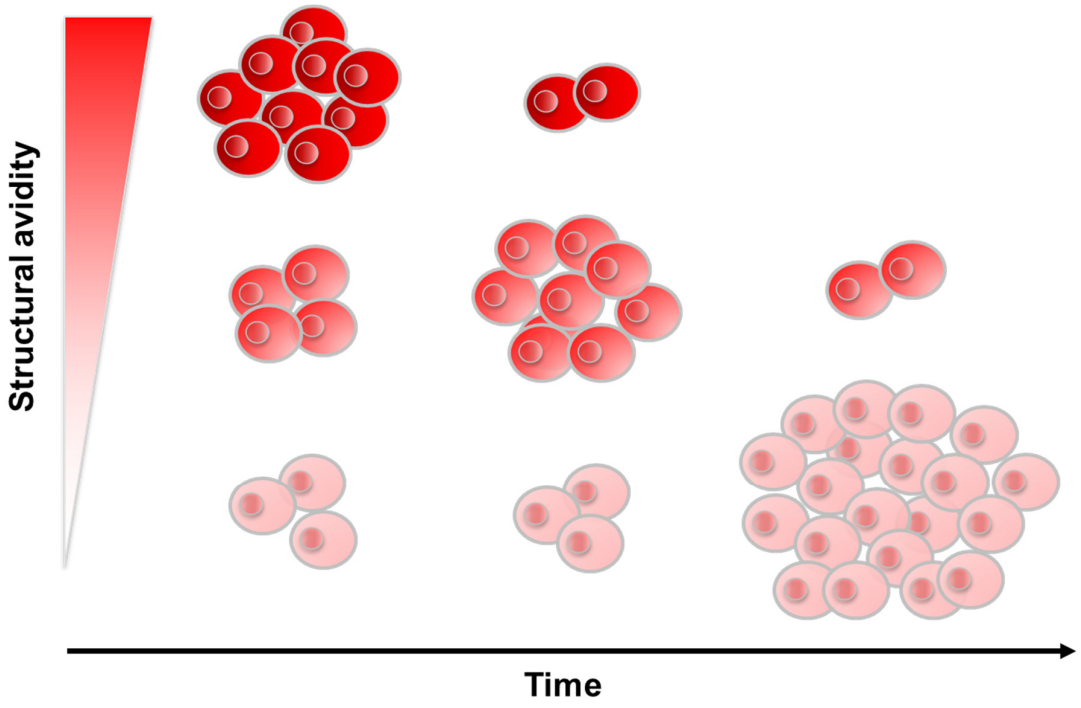

Figure 7. Reverse TCR repertoire evolution: clonal succession through replicative senescence of high avidity T cells during chronic latent infection. T cells of high structural avidity receive the strongest TCR-mediated signal, proliferate the most and therefore dominate the early phase of chronic infection. Over time however, they will become replication senescent leading to a successive handover of dominance to T cells with lower avidity. The T cell population increases in size over time (memory inflation) potentially to compensate for lower avidity. Adapted from: (Buchholz et al., 2011; Davenport et al., 2002).

2 Aims and objectives of this thesis

$CD8^+$ T cells are of particular importance for the control of chronic latent viral infections. The strength of interaction between the TCR plus co-receptor and pMHC (structural avidity) determines activation and recruitment of naïve T cells into the immune response. T cell immune responses against CMV are initially diverse, consisting of many different T cell clones. Driven by repetitive antigen exposure, a certain group of CMV-specific T cells increases in size over time (memory inflation) and becomes progressively oligoclonal. If and how this repertoire focusing reflects selection based on structural avidity of T cells is currently unknown. In principle, several options are conceivable (see 1.5.2):

1. Repertoire focusing is independent of structural avidity.
2. T cells with high structural avidity are preferentially selected, a process called structural avidity maturation, which has been shown to occur for T cell responses against non-persistent pathogens.
3. T cells with high structural avidity are initially preferentially selected, but due to repetitive stimulation and proliferation throughout a lifetime of latent infection, high avidity T cells undergo replicative senescence. Clonal succession then leads to a gradual decrease of the population's average structural avidity.

The aim of this thesis was to investigate this fundamental process of how T cells are selected in the context of chronic latent infection. For this purpose, TCR-ligand k_{off}-rate measurements, which provide a good surrogate for structural avidity, were performed for human $hCMV^+$ blood donors and at different time points after infection using the mCMV model system. In another set of experiments, T cells with different known structural avidity were adoptively transferred and their *in vivo* recruitment into the immune response was monitored during mCMV infection.

3 Material and Methods

3.1 Material

3.1.1 Consumable material

Plastics	Supplier
Falcon Tube CELLSTARR (15 ml, 50 ml)	Greiner bio-one, Kremsmunster, Austria
70 µm Nylon Cell Strainer	Corning, Corning, USA
Minisart Syringe Filters (0,45 µm)	Sartorius, Gottingen, Germany
Discofix-3 (three-way valve)	Braun, Melsungen, Germany
Eppendorf tubes (1,5 ml, 2 ml)	Eppendorf, Hamburg, Germany
Fluorescence-activated cell sorting (FACS) tubes 1,2 ml	Starlab, Hamburg, Germany
FACS tubes 5 ml	Corning, Corning, USA
Filter tips (10 µl, 20 µl, 200 µl, 1000 µl)	Starlab, Hamburg, Germany
Sterican Cannulae (Gr. 18, 20)	Braun, Melsungen, Germany
Syringes (1 ml, 5 ml, 10 ml, 20 ml)	Braun, Melsungen, Germany
Syringe 1 ml Sub-Q	BD, Franklin Lakes, USA
6-, 24-, 48- and 96-well plates (U-bottom, flat-bottom)	Corning, Corning, USA
96-well plates FACS (V-bottom, non-sterile)	Josef Peske GmbH & Co. KG, Aindfing-Arnhofen, Germany
Petri-dish 60 mm	Corning, Corning, USA
Serological pipettes (2 ml, 5 ml, 10 ml, 25 ml)	Greiner Bio-one, Frickenhausen, Germany

3.1.2 Chemicals and Reagents

Chemicals/Reagents	Supplier
Alexa Fluor 488 maleimide	Molecular Probes, Leiden, The Netherlands
Ammonium chloride (NH_4Cl)	Sigma, Taufkirchen, Germany
Atipamezole	EuroVet, Bladel, Netherlands
β-Mercaptoethanol	Sigma, Taufkirchen, Germany
BCA assay reagents	Interchim, Montlucon, France
Bepanthen eye and nose ointment	Bayer Vital GmbH, Leverkusen, Germany
Biocoll Ficoll solution	Biochrom, Berlin, Germany
Bovine serum albumin (BSA)	Sigma, Taufkirchen, Germany
Cytofix/Cytoperm	BD Biosciences, Heidelberg, Germany
D-biotin	Sigma, Taufkirchen, Germany
Dimethyl sulfoxide (DMSO)	Sigma, Taufkirchen, Germany
Ethanol	Klinikum rechts der Isar, Munich, Germany
Ethidium monazide bromide (EMA)	Molecular Probes, Leiden, The Netherlands
Fentanyl	EuroVet, Bladel, Netherlands
Fetal calf serum (FCS)	Biochrom, Berlin, Germany
Flumazenil	Hexal, Holzkirchen, Germany
Gentamycin	GibcoBRL, Karlsruhe, Germany
L-Glutamine	GibcoBRL, Karlsruhe, Germany
Golgi-Plug	BD Biosciences, Heidelberg, Germany
HCl	Roth, Karlsruhe, Germany
HEPES	GibcoBRL, Karlsruhe, Germany
Leupeptin	Sigma, Taufkirchen, Germany
Interleukin 2 (IL-2)	Peprotech, New Jersey, USA
Ionomycin (IONO)	Sigma, Taufkirchen, Germany
Medetomidine	Orion Pharma, Hamburg, Germany

Chemicals/Reagents	Supplier
Midazolam	Hexal, Holzkirchen, Germany
Naloxone	B.Braun, Melsungen, Germany
NaOH	Roth, Karlsruhe, Germany
Penicillin	Roth, Karlsruhe, Germany
Pepstatin	Sigma, Taufkirchen, Germany
Perm Wash	BD Biosciences, Heidelberg, Germany
Phosphate buffered saline (PBS)	Biochrom, Berlin, Germany
Phorbol 12-myristate 13-acetate (PMA)	Sigma, Taufkirchen, Germany
Propidium iodide (PI)	Molecular Probes, Invitrogen, UK
RPMI 1640	GibcoBRL, Karlsruhe, Germany
Sodiumazide (NaN3)	Sigma, Taufkirchen, Germany
Sodium chloride (NaCl)	Roth, Karlsruhe, Germany
Sodium ethylenediaminetetraacetic acid (Na-EDTA)	Sigma, Taufkirchen, Germany
***Strep*-Tactin-Allophycocyanin (APC)**	IBA, Göttingen, Germany
***Strep*tavidin-Phycoerythrin (PE)**	IBA, Göttingen, Germany
***Strep*tomycin**	Sigma, Taufkirchen, Germany
Tris-hydrochloride (Tris-HCl)	Roth, Karlsruhe, Germany
Trypan Blue solution	Sigma, Taufkirchen, Germany

3.1.3 Buffers and Media

Buffers and Media	Content	
Ammonium chloride Tris (ACT)	0,17 M 0,3 M	NH_4Cl Tris-HCl, pH 7,5
Complete freezing medium (CFM)	10 % (v/v)	FCS DMSO
D-biotin 10 M stock solution	244.31 g ad 100 ml	D-biotin H_2O, pH was brought to pH 11 to facilitate solution of D-biotin, then back to pH 7
FACS buffer	1x 0.5 % (w/v) 1.65 % (v/v) pH	PBS BSA NaN3 7,45
RP10$^+$ cell culture medium	1x 10 % (v/v) 5 % (v/v)	RPMI 1640 FCS SC$^+$
Supplement complete (SC$^+$) in 1L RPMI-1640	1 ml 20 ml 23.83 g 4 g 200 ml	β-Mercaptoethanol Gentamicin HEPES L-Glutamine Penicillin/*Strep*tomycin

3.1.4 Human blood samples

Written informed consent was obtained from the donors and use of the blood samples was approved according to national law by the local Institutional Review Board (Ethikkommission der Medizinischen Fakultät der Technischen Universität München). Peripheral blood was obtained from healthy adult donors of both sexes, diluted in PBS and peripheral blood mononuclear cells (PBMCs) were purified over a Ficoll gradient. PBMCs were frozen in CFM, stored in liquid nitrogen and thawed before analysis (performed by AG Neuenhahn).

3.1.5 Viruses

Virus	Manufacturer
wild type (wt) mCMV	Luka Cicin-Sain, Braunschweig
M45-SIINFEKL mCMV	Luka Cicin-Sain, Braunschweig
IE2-SIINFEKL mCMV (N4)	Luka Cicin-Sain, Braunschweig
IE2-SIITFEKL mCMV (T4)	Luka Cicin-Sain, Braunschweig
IE2-SIIVFEKL mCMV (V4)	Luka Cicin-Sain, Braunschweig

3.1.6 Antibody

Dilution as specified by the manufactures were titrated for optimal staining intensity.

Murine Antibody	Clone	Manufacturer
a CD8a fluorescein isothiocyanate (FITC)	53-6.7	eBioscience, San Diego, USA
a CD44 FITC	IM7	eBioscience, San Diego, USA
a CD45.1 FITC	A20	eBioscience, San Diego, USA
a CD45.2 FITC	104	eBioscience, San Diego, USA
a Thy1.1 FITC	OX7	BD Bioscience, Heidelberg, Germany
a PD-1 FITC	J43	eBioscience, San Diego, USA
a CD4 PE	H129.19	BD Bioscience, Heidelberg, Germany
a CD8a PE	53-6.7	eBioscience, San Diego, USA
a IL2 PE	JES6-5H4	eBioscience, San Diego, USA
a CD27 PE	LG7.F9	eBioscience, San Diego, USA
a CD44 PE	IM7	eBioscience, San Diego, USA
a CD19 PE-CF594	1D3	BD Bioscience, Heidelberg, Germany
a CD4 peridinin-chlorophyll-protein complex (PerCP)-Cy5.5	RM4-5	eBioscience, San Diego, USA
a CD8a PerCP-Cy5.5	53-6.7	eBioscience, San Diego, USA
a CD45.2 PerCP-Cy5.5	104	eBioscience, San Diego, USA
a CD45.1 PerCP-Cy5.5	A20	eBioscience, San Diego, USA
a CD3e PE-Cy7	145-2C11	eBioscience, San Diego, USA

Murine Antibody	Clone	Manufacturer
a CD62L PE-Cy7	MEL-14	eBioscience, San Diego, USA
a CD27 PE-Cy7	LG.7F9	eBioscience, San Diego, USA
a CD8a PE-Cy7	5H10	Invitrogen, Carlsbad, USA
a CD8a eF450	53-6.7	eBioscience, San Diego, USA
a CD8a Pacific Blue	5H10	Invitrogen, Carlsbad, USA
a CD8a Pacific Orange	5H10	Invitrogen, Carlsbad, USA
a CD8a APC	5H10	Invitrogen, Carlsbad, USA
a IFNγ APC	XGM1.2	eBioscience, San Diego, USA
a TCRβ chain APC	H57-597	Biolegend, San Diego, USA
CD27 APC	LG7F9	eBioscience, San Diego, USA
a Thy1.1 APCeF780	HIS51	eBioscience, San Diego, USA
a Thy1.2 APCeF780	53-2.1	eBioscience, San Diego, USA
a CD45.2 APC eF780	104	eBioscience, San Diego, USA

human Antibody	Clone	Manufacturer
a CD8a FITC	B9.11	Immunotech, Monrovia, USA
a CD8a PE	3B5	Invitrogen, Carlsbad, USA
a CD19 ECD	J3-119	Beckman Coulter, Brea, USA
a CD8a PE Cy7	OKT8	eBioscience, San Diego, USA
a CD45 Pacific Blue	T29/33	BD Bioscience, Heidelberg, Germany
a CD45 Pacific Orange	HI30	Agilent Technologies, Santa Clara, USA
a CD4 PE	H129.19	Exbio, Vestec, Czech Republic
a CD8a APC	RPA-T8	BioLegend, San Diego, USA

3.1.7 MHC molecules for *Strep*tamer and multimer staining

***Strep*tamers:**

H2-Kb *Strep*-tagIII/mβ2m cys67 Alexa 488/ OVA257−264-*Strep*-Tactin-APC

H2-Kb *Strep*-tagIII/mβ2m cys67 Alexa 488/ M38316−323-*Strep*-Tactin-APC

B8/hβ2m/IE1$_{199\text{-}207K}$ StrepIII tub tag functionalized with Atto488-*Strep*-Tactin-APC

Multimers:

H2-Kb/mβ2m/Ova257-264 *Strep*tavidin-PE/APC

H2-Kb/mβ2m/M38316-323 *Strep*tavidin-PE/APC

H2-Db/mβ2m/M45985-993 *Strep*tavidin-PE/APC

B8/hβ2m/IE1199-207k *Strep*tavidin-PE

3.1.8 Equipment

Equipment	Model	Manufacturer
Flow cytometer	CyAn ADP	Beckman Coulter, Fullerton
	MoFlo Legacy Cell Sorter	Beckman Coulter, Fullerton
	FACSAria III	BD Bioscience, Heidelberg
Microscope	Axiovert S100	Carl Zeiss, Jena
	Leica SP 5	Leica, Bensheim
Centrifuges	Biofuge fresco	Heraeus, Hanau
	Multifuge 3 S-R	Heraeus, Hanau
	Sorvall® RC 26 Plus	Heraeus, Hanau
	Varifuge 3.0RS	Heraeus, Hanau
	Biofuge stratos	Heraeus, Hanau
Incubators	Cytoperm 2	Heraeus, Hanau
	Minitron	Infors, Bottmingen
	BE 500	Memmert, Schwabach
Flow cytometry-based k_{off}-rate		Qutools, Munich
Laminar flow hood	HERA safe	Heraeus, Hanau

Hemocytometer	Neubauer chamber	Schubert, München
Photometer	BioPhotometer	Eppendorf, Hamburg
Stainless Water Bath	LAUDA ecoline 019	Lauda, Königshofen
bench pH/mV meter	MultiCal® pH 526	WTW, Weilheim
Precision weighting balance	CP 124 S	Sartorius, Göttingen

3.1.9 Software

FlowJo V10 Treestar, Ashland, USA

Microsoft Office 2019, Microsoft, Redmond, USA

MetaMorph, Online Molecular Devices, Downingtown, USA

Analyzer.nt, Sebastian Nauerth, Department of Physics, LMU München

GraphPad Prism 5 and 7, GraphPad Software, La Jolla, USA

Inkscape 0.92.2, Oregon, USA

Summit™ Software System, Cytomation Bioinstruments GmbH, Freiburg

3.2 Methods

3.2.1 Procedures performed on laboratory animal

Animal studies were approved by local authorities (Regierung von Oberbayern). Mice were housed under specific pathogen free (SPF) conditions at the Institute of Medical Microbiology, Immunology and Hygiene at the Technical University Munich. Wild-type C57BL/6 mice were purchased from Envigo (Rossdorf, Germany). Recombination activating gene $1^{-/-}$($Rag1^{-/-}$), $Rag2^{-/-}$, OT-I $RAG^{-/-}$ and congenic matrix $Rag^{-/-}$ donor mice were all bred in house on C57BL/6 background (Buchholz et al., 2013). If not stated otherwise, C57BL/6 mice were used for experiments.

3.2.1.1 Infection of mice with mCMV

Sex-matched mice were infected with mCMV at the age of six to eight weeks. Animals were held with a restraining grip and intra-peritoneal (i.p.) injection was performed on the lower left abdomen using a 28-gauge needle (for wt C57BL/6: 5×10^5 plaque-forming unit (PFU); for $Rag^{-/-}$: 5×10^4 PFU in 200 µl PBS).

3.2.1.2 Collection of cell samples

Blood samples were collected via facial vein bleeding. Mice were restrained with one hand and puncture of the facial vein was performed with a 5-mm lancet. No more than 200 µl of blood was taken at a time. To prevent clotting blood samples were immediately mixed with heparinized PBS (1:10, 100 µl total volume). For the collection of organs mice were sacrificed by cervical dislocation.

3.2.1.3 Thymectomy

Thymectomies were performed in cooperation with Kilian Schober, Lorenz Mihatsch and Joel Eggert. The operation was conducted at four weeks of age (pre-adult thymectomy). 18 hours before surgery the mice received pre-emptive analgesia (Meloxicam: 1 mg/kg). The

mice were anaesthetized by i.p. injection (Medetomidine: 0,5 mg/kg, Midazolam: 5 mg/kg, Fentanyl: 0,05 mg/kg) and fixated in a supine position using rubber bands. Cervical extension was achieved by placing a pipette tip underneath the neck. Eye ointment (Bepanthen Eye and Nose Ointment) was applied to prevent corneal dryness. The incision site was wiped with ethanol for disinfection and adequate anesthesia was assured by pinching the front paws. A first 2 mm superficial skin cut was performed horizontally at the cranial third of the sternomental distance, then extended by a 2 cm long median incision towards the sternum. The superficial cervical fascia and muscles were gently pushed laterally by blunt dissection exposing the trachea. After vertical tracing of the pretracheal fascia the superior mediastinum was opened, and the thymus became visible attached to the posterior surface of the sternum. The thymus was then aspirated using a curved Pasteur pipette. After total removal of the thymus a quick external thoracic compression was applied to reduce the induced pneumomediastinum. Wound closure was achieved by staples and anesthesia was antagonized by subcutaneous injection (Atipamezole: 2,5 mg/kg, Flumazenil: 0,5 mg/kg, Naloxone: 1,2 mg/kg). For postoperative analgesia, the mice received oral Meloxicam (1 mg/kg) daily for two days. Wound healing and recovery were monitored daily for 14 days. Staples were removed ten days postoperatively.

3.2.2 Preparation of leukocytes from different organs

3.2.2.1 Blood

Red blood cell lysis was performed using ACT-buffer at room temperature. 10 ml of ACT-buffer was added to blood samples followed by a 10-min incubation. Then the samples were centrifuged at 1500 revolutions per minute (rpm) for 6 min. Supernatant was discarded and the pellet was resuspended with 5 ml of ACT. After 5 min the lysis was stopped by addition of 5 ml of $RP10^{+}$ or FACS buffer, followed by another centrifugation at 1500 rpm for 6 min. The supernatant was discarded, and the cells were transferred to a 96-well V-bottom plate, then washed once in 200 µl of FACS buffer.

3.2.2.2 Spleen

Spleens were transferred to a sterile cell strainer (70 µm pore size) placed in petri dish (3 cm diameter) that contained 5 ml of $RP10^+$. Using the plunger of a 2 ml syringe spleens were mashed through the cell strainer. The thereby created single-cell suspension was transferred into a 15 ml falcon tube. To minimize cell loss the petri dish was washed with 5 ml of $RP10^+$ and this suspension was added into the falcon tube. After centrifugation at 1500 rpm for 6 min the pellet was resuspended with 5 ml of ACT buffer for red blood cell lysis (5 min at room temperature). Lysis was stopped with 5 ml of $RP10^+$ and after another centrifugation cycle (1500 rpm, 6 min) cells were resuspended in 10 ml of FACS buffer. To determine the total splenocytes count a 10 µl aliquot was stained with Trypan Blue solution and living cells were counted using a microscope and a hemocytometer (Neubauer chamber).

3.2.2.3 Lymph node

Leukocyte preparation was performed the same way as spleen preparation (see 3.2.2.2) except, due to the low frequency of erythrocytes in lymph node samples, no red blood cell lysis was performed.

3.2.3 Antibody staining of surface antigens

All following staining or washing steps were conducted in the dark at 4 °C if not specified otherwise. After preparation of leucocytes (see 3.2.2) the cells were transferred to a 96-well V-bottom plate and incubated with a master mix of monoclonal antibodies directed at the surface antigens of interest for 20 min (antibody concentrations were titrated for optimal staining intensity; master mix was prepared in 50 µl of FACS buffer per well). For live/dead staining PI was added (1:100) 5 min before the end of the staining period. After staining the cells were washed in FACS buffer 2,5 times (centrifugation at 1500 rpm for 3 min, washing volume of 200 µl/well). Before FACS analysis cells were filtrated using a nylon mesh.

3.2.4 Non-reversible multimer staining

Non-reversible multimers consisting of biotinylated pMHC molecules bound to a *Strep*tavidin backbone were used for identification of antigen-specific $CD8^+$ T cells. Biotinylated pMHC molecules were generated according to established protocols in cooperation with Anna Hochholzer, Bianca Weißbrich and Manuel Effenberger (Dirk H Busch, Pilip, Vijh, & Pamer, 1998). After preparation of leucocytes (see 3.2.2) cells were counted and rested at 4 °C for 30 min. A multimer mix, consisting of 0,4 µg of the respective biotinylated pMHC I molecule, 0,5 µg of *Strep*tavidin-PE or *Strep*tavidin-APC and 50 µl of FACS buffer for every 5×10^6cells, was preincubated for at least 30 min for multimerization. Cells were transferred to a 96-well plate and incubated with the multimer solution for 30 min. 20 min before the end of the staining period antibodies for the staining of surface antigens were added. PI for live/dead staining was added 5 min before the end of the staining period. After staining cells were washed in FACS buffer 2,5 times (centrifugation at 1500 rpm for 3 min, washing volume of 200µl/well). Before FACS analysis cells were filtrated using a nylon mesh.

3.2.5 *Strep*tamer staining

A *Strep*tamer staining, which is a reversible multimer staining, was used for TCR-ligand k_{off}-rate experiments. Staining was performed according to established protocols with some minor variations (Nauerth et al., 2016, 2013). After preparation of leucocytes (see 3.2.2) cells were counted and rested at 4 °C for 30 min. A multimer mix, consisting of 1 µg of the respective Alexa Fluor 488-conjugated pMHC I molecule (*Strep*-tagIII/mβ2m cys67), 0,75 µg of *Strep*-Tactin-APC and 50 µl of FACS buffer for every 5×10^6cells, was preincubated for at least 30 min for multimerization. Cells were then transferred to a 96-well plate or 15 ml falcon tubes depending on the cell number being stained and incubated with the multimer mix for 45 min. 20 min before the end of the staining period antibodies for the staining of surface antigens were added. PI for live/dead staining was added 5 min before the end of

the staining period. After staining cells were washed in FACS buffer 2,5 times. Before FACS analysis cells were filtrated using a nylon mesh. Absolute cells numbers of *Strep*tamer$^+$ cells per spleen were estimated using the following simple rule of three (total splenocyte count was determined by hemocytometer):

$$\textit{Strep}\text{tamer}^+\text{cells per spleen} = \frac{\textit{Strep}\text{tamer}^+\text{cells [FACS]}}{\text{splenocytes [FACS]}} \times \text{total splenocyte count}$$

3.2.6 Peptide titration and intracellular interferon gamma (IFNγ) staining of SIINFEKL-specific T cells

To prepare solutions of different peptide concentrations the lyophilized SIINFEKL peptide was dissolved in DMSO followed by serial dilution with RP10$^+$. Spleen preparation was performed as described in 3.2.2.2 and splenocytes (2×10^6/well) were transferred to a flat-bottom tissue culture plate together with the respective peptide solution plus negative (RP10$^+$ only) and positive controls (PMA: 1:4000 and Ionomycin: 1:250). Samples were then incubated at 37 °C for five hours all together, after one hour 2 µg/well of Golgi Plug was added without resuspension. After incubation, samples were transferred to a 96-well V-bottom plate and all following staining steps were done at 4 °C. EMA/Fc-block staining (EMA 1:1000, Fc-Block 1:400) was performed for 20 min with exposure to light followed by the staining of surface antigens (CD8-pacific blue (PB), CD19-ECD; see 3.2.3). To allow intracellular cytokine staining fixation and permeabilization of cells were performed using Cytofix/Cytoperm (20 min incubation period). After washing 2,5 times in Perm/Wash buffer cells were stained with an anti-IFNγ antibody for 30 min. Cells were then washed 2x in Perm/Wash buffer and 1x in FACS buffer before suspension in 1 % PFA.

3.2.7 Microscopic TCR-ligand k_{off}-rate assay

Microscopic k_{off}-rate measurements allow for the assessment of structural avidity of epitope-specific T cells at the single-cell level. Measurements were performed according

established protocols with some minor variations (Knall, 2007; Nauerth, 2012; Nauerth et al., 2013; Weißbrich, 2015). After preparation of leucocytes (see 3.2.2) a *Strep*tamer staining was performed (see 3.2.5). Epitope-specific T cells were then sorted on a MoFlo Legacy cell sorter gating on living, $CD19^-$, $CD8^+$, *Strep*tamer$^+$ cells (double positive for the *Strep*-Tactin-APC backbone and the pMHC Alexa Fluor 488; see Supplementary Figure 1). Sorted cells were collected in a 15 ml Falcon tube filled with 1 ml of filtered FCS on ice. After washing 2,5 x in FACS buffer and transferal to a 96-well plate cells were resuspended in 5-10 µl FACS buffer and kept on ice protected from light. Microscopic k_{off}-rate measurements were conducted on a Leica SP5 confocal laser scanning microscope. The experimental setup of the microscopic k_{off}-rate assay was as follows: As the k_{off}-rate dissociation kinetics are temperature dependent and higher temperatures can lead to internalization of the MHC molecules, measurement at constant and low temperatures was assured by connecting a Peltier cooler (water cooling device) to the buffer reservoir (set temperature: 4 °C; actual temperature in buffer reservoir according to measurements by Bianca Weißbrich: 10 °C). Usually about 1 µl of the cell suspension was pipetted into the buffer reservoir which consisted of a customized metal insert that fitted into the Peltier cooler and a glass cover slip that could be attached to the bottom side of the metal insert using a hydrophobic pen. To prevent excessive cell movement during dissociation cells were covered with a polycarbonate membrane and a small metal shim on top of the membrane for fixation. After addition of 600 µl of FACS buffer the cells were focused. To record the fluorescence intensity of the *Strep*-Tactin APC backbone and the MHC-Alexa Fluor 488 signal over time images were taken every 10 s. The dissociation was started by addition of 600 µl of D-biotin after the first image had been recorded and was subsequently observed until the fluorescence intensity of all cells had dropped to levels of auto fluorescence of unstained cells (about 15 min depending on the dissociation kinetics). Usually at least three dissociations of each sample were recorded as technical replicates.

Since the cells were exposed to the laser beam for an extended period of time photo bleaching which is a photochemical alteration of the dye resulting in impaired fluorescence

had to be accounted for. To calculate this bleaching constant k_{bleach} for either *Strep*-Tactin–coated beads (multimerized with Alexa Fluor 488-conjugated MHC molecules) or *Strep*tamer stained T cells a k_{off}-rate measurement was performed without addition of D-biotin but otherwise identical settings. At least one bleaching movie was recorded for every experimental day. k_{bleach} turned out to be quite stable throughout all microscopic k_{off}-rate experiments (mean = 0,00052; standard deviation (SD) = 0,00011; see Supplementary Figure 3).

Data analysis was performed using the MetaMorph Online Molecular Devices software. Only cells that showed only minor movement during the dissociation could be analyzed. For each cell, a gate was drawn containing the cell and the integrated fluorescence intensity of that gate was calculated for every image of the dissociation. To account for changes in the background fluorescence intensity a gate of same size and shape was placed in close proximity to the cell (but not containing the cell or any other cell) and its integrated fluorescence intensity was acquired for all time points. The intensity values for the gate containing the cell and the background gate for every image of the dissociation were transferred to Microsoft Excel. Using the “Analyzer nt software” (developed by S. Nauerth) k_{off}-rate values and the corresponding $t_{1/2}$ could be calculated automatically. For every time point individual background fluorescence intensity was subtracted from the cell’s fluorescence intensity. Start and endpoint of the dissociation were defined manually. The starting point of MHC-dissociation was set as the time point when *Strep*-Tactin APC dissociation was completed (when APC fluorescence intensity was at auto fluorescence levels) which usually coincided with an MHC-Alexa Fluor 488 fluorescence intensity of approximately 80 % of the initial value. The endpoint of the dissociation was set as the last point of the plateau of the fitted curve. These raw values of k_{off} and $t_{1/2}$ were then corrected for the influence of photo bleaching by subtracting k_{bleach} from raw k_{off} values and recalculating $t_{1/2}$. The k_{bleach} value was determined by plotting the fluorescence intensity values of the bleaching movie in GraphPad Prism 5 (mean k_{bleach} of about 10 k_{bleach} values analyzed). Dead cells or cells with internalized *Strep*tamers were

excluded from the analysis (cells with relatively high initial fluorescence intensity but no substantial decrease over time except for photo bleaching and a $t_{1/2}$ in the range of photobleaching).

3.2.8 Flow cytometry-based TCR-ligand k_{off}-rate assay

The flow cytometry-based TCR-ligand k_{off}-rate assay follows the same principles as the microscopic k_{off}-rate assay. However instead of determining the k_{off}-rate on the single-cell level, the average or mean k_{off}-rate of an epitope-specific population is measured. Measurements were performed according to established protocols with some minor variations (Nauerth et al., 2016; Weißbrich, 2015). After preparation of leucocytes (see 3.2.2) a *Strep*tamer staining was performed (see 3.2.5), followed by a non-reversible multimer staining of the same specificity for 10 min (see 3.2.4). This non-reversible multimer staining allowed a sort-free approach even for samples not only containing epitope-specific cells by making it possible to stably gate on the epitope-specific population and observe *Strep*tamer dissociation at the same.

Dissociations were conducted inside a k_{off}-rate tube which is a modification of a regular polypropylene FACS sample tube. It allowed the addition of D-biotin into the tube without discontinuation of sample acquisition thereby making it possible to also observe the critical start of dissociation directly after D-biotin addition. To this goal the FACS tube was pierced at its lower quarter by a 20 G canula and the entry site was sealed airtight using silicon. The canula was then connected to a 3-way-valve which in turn could be connected to a 1 ml syringe containing D-biotin. A Peltier-controlled cooling device encasing the k_{off}-rate tube was used to ensure measurement at constant and low temperature comparable to the microscopic assay (T = 5,5 °C). Experiments were performed on Cyan FACS machines and for each sample at least two replicates were recorded. After transfer of the sample into the k_{off}-rate tube (sample volume: 1 ml) the tube was placed into the cooling device and inserted into the FACS machine. Acquisition was started and the initial *Strep*tamer staining intensity was recorded for 30 s. Then 1 ml of D-biotin (2 mM) was

injected into the k_{off}-rate tube via the canula and the dissociation was observed for the remainder of 15 min.

Color-coding, which was mainly established by Manuel Effenberger, allowed simultaneous measurements of multiple k_{off}-rates. Samples were labelled with a unique combination of surface antibodies directed at the ubiquitous leucocyte/lymphocyte surface marker CD45.2 or CD90.2. The use of different fluorochromes generated distinct combinations and therefore allowed simultaneous measurements at the same time (number of possible combinations C: $C = 2^n$; n: number of different fluorochromes used for color coding). The color code staining was performed together with the standard surface staining against CD8 and CD19. After staining the samples were pooled into one k_{off}-rate tube and k_{off}-rate measurements were run as usual.

FlowJo was used for flow cytometry data analysis. Samples were gated on lymphocytes, singlets, living $CD19^-$, $CD8^+$, color code and non-reversible multimer. After gating on the specific population, for every cell within that gate the computed time value and intensity values for Alexa Fluor 488 and *Strep*-Tactin-APC were exported to MS Excel. Using the “single cell Flow Analysis” app programmed by Philipp Lückemeier data could then be transferred to Graph Pad Prism creating dot plots of the fluorescence decay over time. k_{off}-rate values and $t_{1/2}$ could then be calculated by fitting one-phase exponential decay curves to the dot plot. To eliminate the interference of the *Strep*-Tactin-APC dissociation with the MHC-Alexa Fluor 488 dissociation, for fitting of the MHC-Alexa Fluor 488 exponential decay curve only data points after complete *Strep*-Tactin dissociation were considered.

Constrained fitting (developed by Philipp Lückemeier) was applied for dissociations with steep initial decay, where normal fitting could lead to long $t_{1/2}$ by mistake. Here, the mean of MHC-intensity before the start of dissociation was calculated and taken as y-intercept (y0), thereby forcing the one-phase exponential decay curve to include this point.

3.2.9 *In vivo* competition of epitope-specific T cells of known structural avidity via co-transfer and mCMV infection

For *in vivo* competition experiments defined numbers of different T cells of known structural avidity towards the model epitope SIINFEKL were transferred to recipient animals. Recipients were infected with IE2-SIINFEKL mCMV on the day after cell transfer and the number of transferred cells was monitored over time by repeated blood screenings. TCR retrogenic mice which served as donors for the T cell transfer were generated as follows:

In a first step SIINFEKL-specific TCRs were isolated (performed by Kilian Schober with support of Thomas Müller and Simon Grassmann): C57/BL6 mice were infected with IE2-SIINFEKL mCMV and splenocytes were harvested during acute infection (d15 post infectionem (p.i.)) or during late chronic infection. A single-cell sort of $CD8^+$, $CD19^-$ and *Strep*tamer$^+$ cells was performed which was followed by a single-cell polymerase chain reaction (PCR) of the TCR and Sanger sequencing (according to an adapted protocol of (Dössinger et al., 2013)). This led to the identification of several full αβ TCRs.

Next retrogenic mice were generated according to the protocol described in (Bettini, Bettini, Nakayama, Guy, & Vignali, 2013; Holst et al., 2006) with some minor variations (Generation was performed by Simon Grassmann, Kilian Schober, Justin Leube). Bone marrow of $RAG1^{-/-}$ mice on a distinct congenic marker background (Buchholz et al., 2013) was retrovirally transduced with the constructs of interest. Before bone marrow transfer mice received sublethal irradiation (2 x 4,5 Gy for C57Bl/6 recipients and 1 x 4,5 Gy for $RAG^{-/-}$ recipients).

4 Results

4.1 Validation of the TCR-ligand k_{off}-rate assay

The TCR-ligand k_{off}-rate assay allows the precise acquisition of an important part of the structural avidity of the TCR, the k_{off}-rate. It combines reversible MHC multimer technology with real-time microscopy or flow cytometry. Development and initial validation of the assay was mainly performed by Magdalena Nauerth, Bianca Weißbrich, Robert Knall and others (Knall, 2007; Nauerth, 2012; Nauerth et al., 2016, 2013; Weißbrich, 2015). The following experiments address some additional questions of the validation process, namely the influence of a surface antibody staining against CD8 or CD45.2/CD90.2 on the k_{off}-rate and the maintenance of the k_{off}-rate *in vivo* over time.

4.1.1 Influence of CD8 antibody staining on TCR-ligand k_{off}-rate assay

CD8 is a transmembrane glycoprotein that serves as a co-receptor for the TCR. It specifically binds to the MHC I molecule and is the defining marker of cytotoxic T cells. Including CD8 in the staining panel for the identification of antigen-specific cytotoxic T cells increases the specificity of the panel by eliminating unspecific *Strep*tamer/multimer binding cells of other cell types. But due to the close interaction of the CD8 receptor with the TCR, an influence of CD8 antibody staining on the k_{off}-rate needed to be taken into consideration.

In a first experiment, blood samples of OT-$I^{tg/tg}$ mice, which are TCR transgenic mice that exclusively express a defined TCR specific for the ovalbumin residue SIINFEKL, were stained with SIINFEKL-*Strep*tamer and different monoclonal CD8 antibodies (see Figure 8). Flow cytometry-based TCR-ligand k_{off}-rate assay showed that CD8 antibody clone 53.67 more than doubled dissociation $t_{1/2}$ compared to no CD8 staining, whereas clone 5H10 did not show any significant influence. Also, the choice of fluorochrome of the CD8 antibody (PB vs. PE) did not show any influence on the k_{off}-rate.

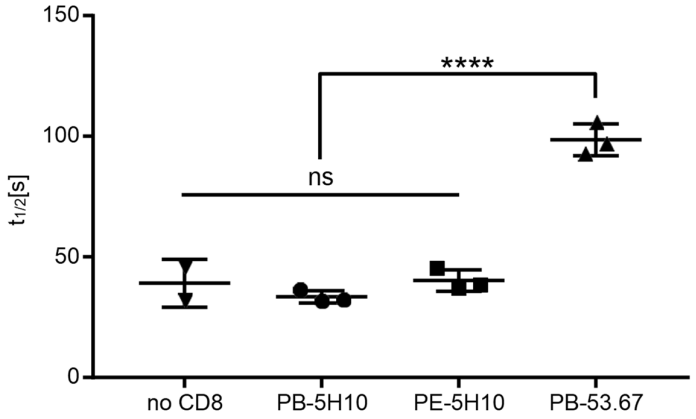

Figure 8. Type of clone but not fluorochrome of the CD8 antibody influences dissociation $t_{1/2}$ of OT-I T cells. Blood samples of OT-$I^{tg/tg}$ were stained with SIINFEKL-*Strep*tamer and different CD8 antibody clones or fluorochromes: no CD8 antibody, CD8-PB-clone 5H10, CD8-PE-clone 5H10 and CD8-PB-clone 53.67. TCR- k_{off}-rate half-life time ($t_{1/2}$) was measured by the flow cytometry-based TCR-ligand k_{off}-rate assay. Data are shown as mean ± standard error of mean (SEM). Statistical analysis was performed using one-way analysis of variance (ANOVA) and Tukey's multiple comparisons test. ns, non-significant. **** P < 0,0001.

In a next experiment, the CD8-PB clone 5H10, which did not show any influence on the k_{off}-rate $t_{1/2}$ for OT-I T cells, was tested in the setting of staining an endogenous T cell response against mCMV (see Figure 9). SIINFEKL-specific splenocytes of an IE2-SIINFEKL mCMV infected mouse were stained either with CD8-PB clone 5H10 or not, and microscopic TCR-ligand k_{off}-rate measurements were performed. The single-cell k_{off}-rate measurements revealed a great diversity of k_{off}-rate $t_{1/2}$ for this polyclonal T cell population. Nonetheless, the staining of CD8-PB clone 5H10 did not show a significant influence on the mean k_{off}-rate or the $t_{1/2}$ distribution.

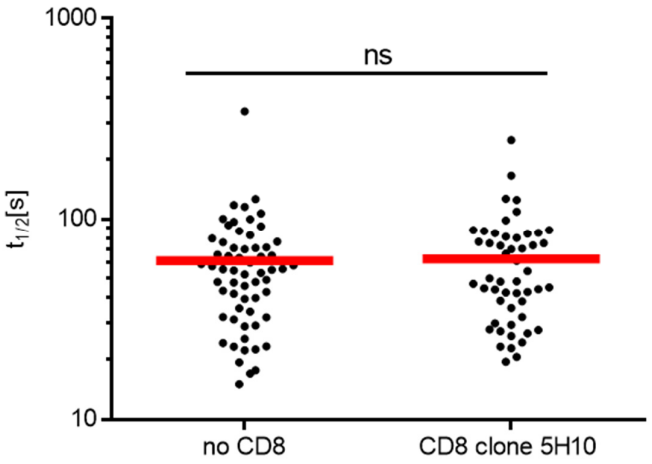

Figure 9. CD8 antibody clone 5H10 does not influence k_{off}-rate $t_{1/2}$ of endogenous SIINFEKL-mCMV-specific T cells. Splenocytes of an IE2-SIINFEKL mCMV infected C57BL/6 mouse were stained with SIINFEKL-*Strep*tamers, a monoclonal antibody directed at CD19 and a live/dead dye (PI). Additionally, the sample was split in half and either stained with CD4-PE clone H129.19 or CD8 antibody CD8-PB-clone 5H10. CD4 stained cells were sorted for $CD19^-$, $CD4^-$ and *Strep*tamer$^+$ cells; CD8 stained cells were sorted for $CD19^-$, $CD8^+$, *Strep*tamer$^+$ cells. TCR- k_{off}-rate half-life time ($t_{1/2}$) of sorted cells were measured by the microscopic TCR-ligand k_{off}-rate assay. Each dot represents one cell. Red lines indicate geometric mean. Significance was assessed by unpaired two-tailed Student t test (p = 0,8748). ns, non-significant.

In the setting of the microscopic TCR-ligand k_{off}-rate assay, Pacific Blue (PB) is preferable to Phycoerythrin (PE) since it does not have an emission overspill into the Alexa Fluor 488 detection channel of the *Strep*tamer. Therefore, all following microscopic TCR-ligand k_{off}-rate experiments and for consistency reasons also all murine flow cytometry-based TCR-ligand k_{off}-rate experiments were conducted using the CD8-PB clone 5H10 antibody (except for the first couple of microscopic k_{off}-rate experiments for which the CD8-PB clone 5H10 was unavailable and CD8-PE clone 5H10 was used instead).

4.1.2 Flow cytometry-based k_{off}-rate dissociations of multiple murine samples can be analyzed simultaneously using color coding

Dissociations of the flow cytometry-based k_{off}-rate assay are recorded for 15 min and at least two replicates per sample are desirable as a standard of quality. To save time and allow high-throughput k_{off}-rate measurements, our laboratory developed a combinatorial labelling system (“color coding”), making it feasible to perform flow cytometry-based k_{off}-rate dissociations of multiple samples simultaneously. It was first tested and validated for human

samples using a staining against human CD45 on different fluorophores, but for the purpose of this project color coding was tested using murine CD45.2 and CD90.2 (number of possible combinations C: $C = 2^n$; n: number of different fluorochromes used for color coding). Since the additional antibodies also bind to the T cell surface, potential interference with the dissociation of the *Strep*tamer's pMHCs had to be examined. To test for the influence of color coding on the k_{off}-rate $t_{1/2}$, measurements of the same sample were performed under the following conditions: all four combinations of the color code and also a classical single-sample dissociation without any color code (see Figure 10). The additional antibody staining of CD45.2 and CD90.2 did not alter the dissociations $t_{1/2}$ compared to the same sample measured without a color code.

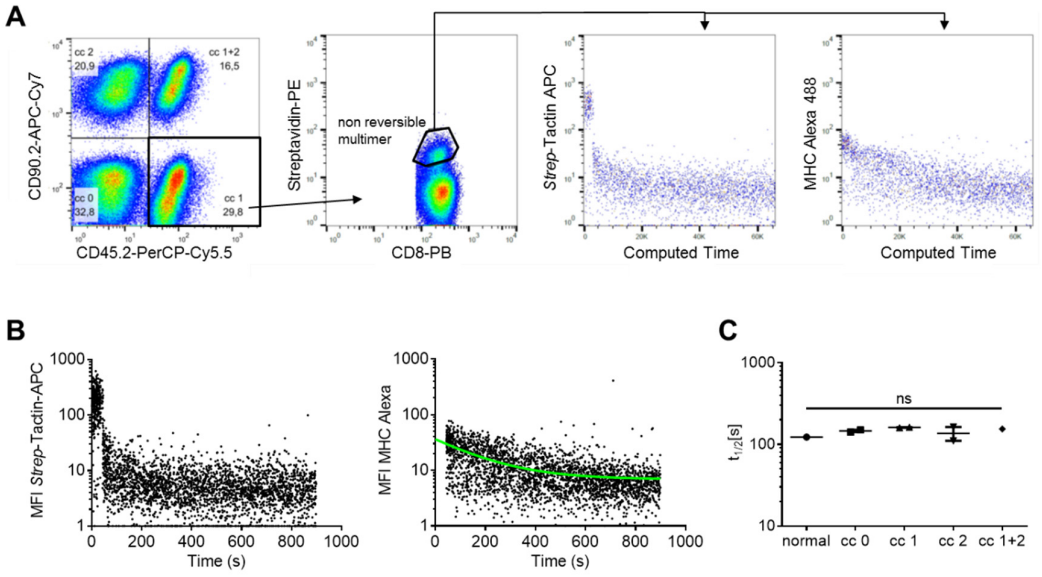

Figure 10. Color-code directed against murine CD45.2 and CD90.2 does not influence $t_{1/2}$. Different combinations of CD45.2 and CD90.2 antibodies were tested for interference with k_{off}-rate dissociation. Splenocytes of a wt mCMV infected mouse (d 202 p.i.) were stained with M38-*Strep*tamer, non-reversible M38-multimer and surface antibodies against CD8 and CD19. The sample was split into four and the following color code was applied: cc 0: no additional antibody, cc 1: CD45.2-PerCP-Cy5.5, cc 2: CD90.2 APC-Cy7, cc 1+2: CD45.2-PerCP-Cy5.5 and CD90.2 APC-Cy7. After staining the four samples were pooled and analyzed at the same time. As a control a classical single-sample dissociation without any color code was performed of the same specimen. **(A)** pseudocolor FACS-plot of flow cytometry-based k_{off}-rate assay of color-coded samples cc 0, cc 1, cc 2 and cc 1+2; pre-gated on lymphocytes, singlets, living non-B cells, $CD8^+$. **(B)** dot plot of flow cytometry-based k_{off}-rate dissociation of cc 1 (see (A)) **(C)** $t_{1/2}$ of single-sample dissociation (normal) and multiple-sample dissociation using color coding. Statistical testing was performed using one-way ANOVA. ns, not significant.

4.1.3 TCR-ligand k_{off}-rate is a stable characteristic of T cells

Unlike B cells, T cells cannot undergo classical affinity maturation, a process by which the antigen receptor can increase its affinity towards an epitope through somatic hypermutation and clonal selection. Therefore, TCR structural avidity is a stable parameter of T cells, largely independent of the cell's phenotype, activation status or proliferative history (as discussed above, the phenotype can in principle change the avidity – in contrast to the affinity – but for simplification purposes and in general reality, the structural avidity is "hardwired" in the TCR sequence). If the TCR-ligand k_{off}-rate was to be considered a valid surrogate for TCR avidity, it should in principle also be independent of the afore mentioned parameters. Indeed, Nauerth et al. could show that the k_{off}-rate was independent of the activation status of T cells and did not change after transgenic expression in Jurkat76 cells (Nauerth et al., 2013). To investigate if prolonged *in vivo* persistence and proliferation would influence the k_{off}-rate, naïve OT-I T cells were transferred into a wildtype C57/BL6 mouse infected with IE2-SIINFEKL mCMV. 390 days after transfer, k_{off}-rate measurements of the transferred OT-I T cells were performed in comparison to naïve OT-I T cells. Half-life time ($t_{1/2}$) did not show any significant change even after more than one-year of *in vivo* persistence (see Figure 11).

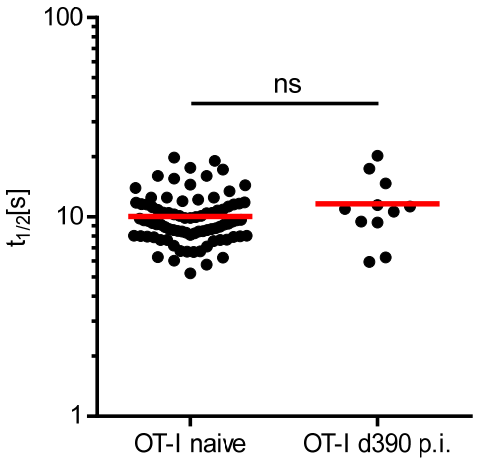

Figure 11. TCR- k_{off}-rate $t_{1/2}$ of OT-I T cells is maintained after adoptive transfer and prolonged *in vivo* proliferation during chronic mCMV infection. After adoptive transfer of 100 OT-I T cells, a C57BL/6 mouse was infected with IE2-SIINFEKL mCMV. At d390 p.i. splenocytes of this mouse and of one naïve OT-I mouse were stained with a SIINFEKL-*Strep*tamer staining, a monoclonal antibody staining directed at CD19 and CD8 and live/dead dye (PI). Cells were sorted for $CD19^-$, $CD8^+$, *Strep*$tamer^+$ cells. Half-life times $t_{1/2}$ of sorted cells were measured using the microscopic TCR-ligand k_{off}-rate assay; Each dot represents one cell. Red lines indicate geometric mean. Statistical testing was performed by unpaired two-tailed Student t test (p = 0,13). ns, non-significant.

4.2 Analysis of human inflationary CMV-specific T cell populations suggests non-linear inverse correlation between population size and structural avidity

Great interindividual variability has been shown for population sizes of $CD8^+$ T cells specific for CMV (both hCMV and mCMV), with some inflationary epitope-specific populations comprising more than 30 % of all $CD8^+$ T cells (see 1.5.1). During the course of infection, inflationary populations increase over time and large populations are more common in elder individuals (Klenerman & Oxenius, 2016). Previous microscopic k_{off}-rate experiments of blood samples from human leukocyte antigen (HLA) B8+ $hCMV^+$ healthy donors had shown an inverse correlation between population size and structural avidity (Schober et al., 2020; experiments performed by Bianca Weißbrich; sample acquisition and storage performed by AG Neuenhahn).

To expand the dataset, all suitable samples stored in the AG Neuenhahn facility were analyzed using the flow cytometry-based k_{off}-rate assay (some of the samples used for the microscopic assay were reanalyzed: blood donors were anonymous and repeated donations were allowed). Population size for the HLA-B8 restricted inflationary epitope $IE1_{199\text{-}207KM}$ showed a wide interindividual range from 0,21 % up to over 35 % of living $CD19^-$ lymphocytes (exemplary depiction: see Figure 12 A). Flow cytometry-based k_{off}-rate measurements suggested a non-linear inverse correlation between population size and $t_{1/2}$ (see Figure 12 B and C).

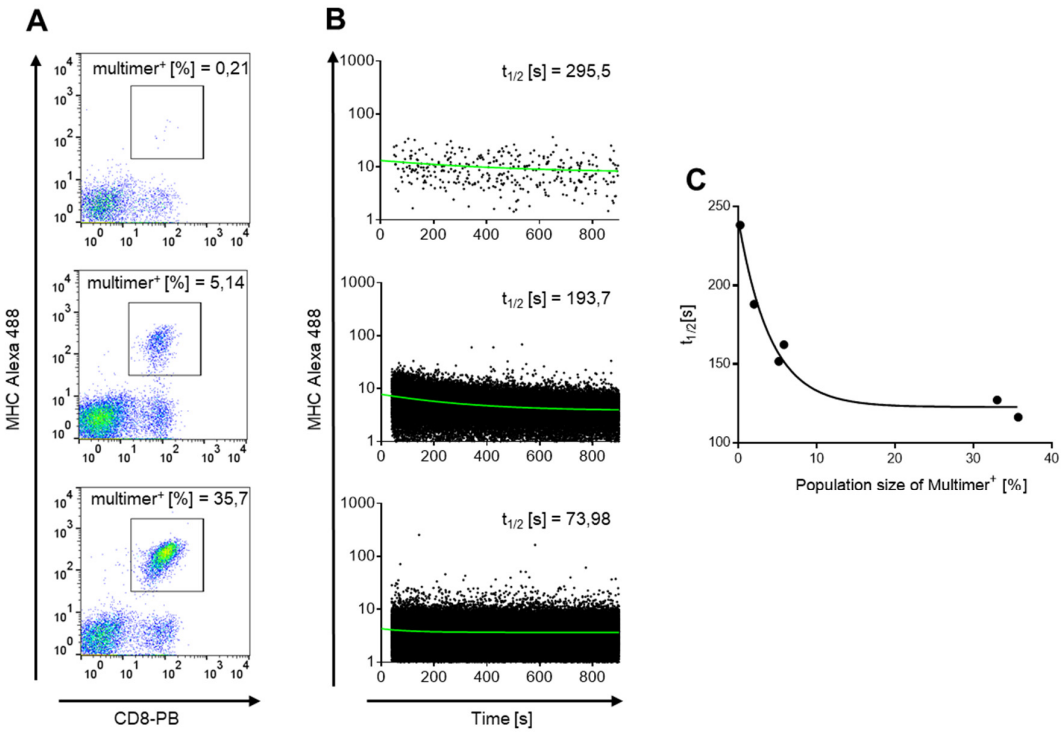

Figure 12. Human inflationary CMV-specific T cell populations show inverse correlation between population size and structural avidity. K_{off}-rate analysis of human inflationary HLA-B8/IE1$_{199-207KM}$-specific T cell populations of healthy CMV positive blood donors. **(A)** Exemplary pseudocolor plots of non-reversible multimer staining for the HLA-B8/IE1$_{199-207KM}$ epitope. Pre-gated on living CD19$^-$ lymphocytes. Numbers next to the gate show population size of multimer$^+$ cells of living CD19$^-$ lymphocytes. **(B)** Exemplary dot plots of flow cytometry-based k_{off}-rate dissociation of multimer$^+$ cells seen in (A). At least two dissociations were performed for each sample. **(C)** Nonlinear fit (one-phase exponential decay curve) of $t_{1/2}$ and population size (N = 6). Dissociation curves were fitted using constrained fit.

4.3 The SIINFEKL mCMV model for the study of avidity dependent evolution of the TCR repertoire during chronic viral infection

During chronic latent viral infections like CMV, the antiviral T cell response undergoes tremendous changes in terms of size (memory inflation; see 1.5.1) and clonality (repertoire focusing; see 1.5.2).

The aim of this project was to study if and how repertoire focusing reflects selection based on structural avidity of T cells. Different kinetics of T cell responses (inflationary or non-inflationary) were investigated to study the role of antigen expression. To eliminate a putative influence of the epitope itself on the repertoire composition and T cell avidity, two recombinant mCMV viruses expressing the same model epitope (SIINFEKL) either under an inflationary (IE2) or a non-inflationary (M45) promotor were used (Dekhtiarenko, Jarvis,

Ruzsics, & Čičin-Šain, 2013). This approach allowed the study of T cell populations directed against the same epitope and therefore also recruited out of a similar naïve repertoire.

4.3.1 IE2-SIINFEKL-specific T cell populations show phenomenon of memory inflation at late time points of mCMV infection

To see if the recombinant mCMV viruses could indeed induce inflationary or non-inflationary T cell responses, population sizes of IE2- and M45-SIINFEKL mCMV infected mice was assessed at different time points after infection.

The relative population size of sorted *Strep*tamer$^+$ cells was quantified as percentage of CD8$^+$ cells. Cells were considered *Strep*tamer$^+$ when double positive for the *Strep*tamer backbone *Strep*-Tactin-APC and the *Strep*tamer MHC-Alexa Fluor 488. M45-SIINFEKL induced populations were maintained as relatively small populations at all time points of the infection. In contrast IE2-SIINFEKL induced populations massively accumulated over time and in some mice composed more than thirty percent of all CD8$^+$ T cells at late time points (see Figure 13 A and B).

Changes in relative population size do not necessarily translate to changes in absolute cell numbers of a specific populations per organ. For example, changes in organ size or the size of the CD8$^+$ compartment could have a substantial effect on the absolute cell number while not affecting relative population size. To determine the absolute number of *Strep*tamer$^+$ cells per spleen, the total splenocyte count was estimated via a hemocytometer and relative frequencies of *Strep*tamer$^+$ cells and splenocytes was assessed via FACS (see 3.2.5 and Figure 13 C). Absolute numbers of *Strep*tamer$^+$ cells for M45-SIINFEKL mCMV infected mice slightly decreased after acute infection and were maintained thereafter. In contrast, absolute numbers of *Strep*tamer$^+$ cells for IE2-SIINFEKL mCMV infected mice increased continuously over the course of the infection. For the late d200+ time point the number of *Strep*tamer$^+$ cells per spleen had more than quintupled compared to d8. Thus, changes in relative population size of antigen-specific CD8$^+$ T cells paralleled those in absolute cell number.

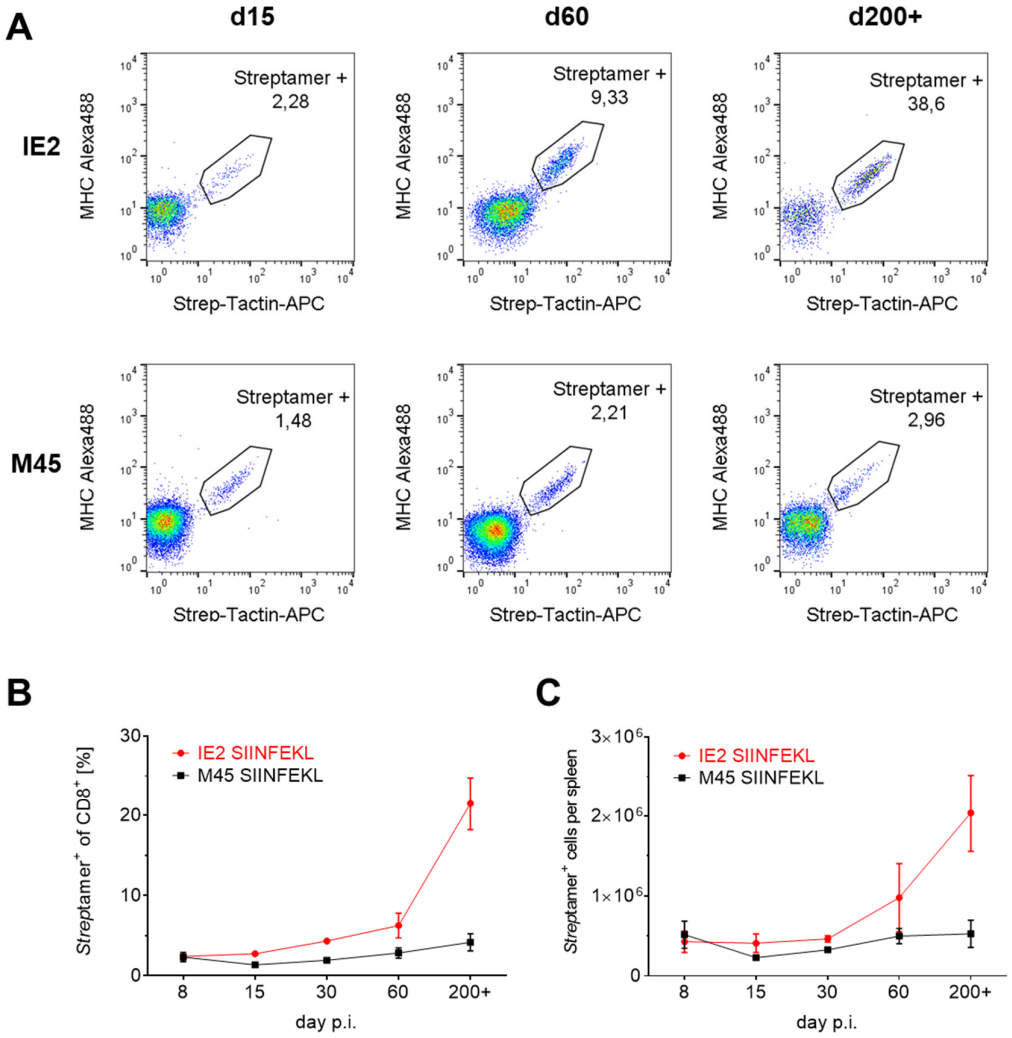

Figure 13. Memory inflation: Population size for inflationary epitope IE2-SIINFEKL increases over the course of mCMV infection. Mice were infected i.p. with recombinant IE2-SIINFEKL mCMV or M45-SIINFEKL mCMV and sacrificed at the indicated time points. Splenocytes were FACS-sorted for CD8$^+$, CD19$^-$, SIINFEKL-*Strep*tamer$^+$ cells. **(A)** Representative pseudocolor FACS plots show relative population size of SIINFEKL-*Strep*tamer$^+$ T cells in the spleen for IE2- and M45-SIINFEKL mCMV infection at different time points. Plots are pre-gated on lymphocytes, singlets, living CD19$^-$ and CD8$^+$ cells. **(B)** Mean percentage of SIINFEKL-*Strep*tamer$^+$ T cells of CD8$^+$ cells in the spleen for IE2- and M45-SIINFEKL mCMV derived populations at different time points. **(C)** Mean number of SIINFEKL-*Strep*tamer$^+$ T cells per spleen is calculated by estimating the total splenocytes count per spleen via hemocytometer and using relative frequencies of *Strep*tamer$^+$ cells and splenocytes determined via FACS. Data are mean ± SEM of N = 2-7 mice at each time point.

4.3.2 In-depth TCR repertoire analysis reveals decreasing diversity and clonal succession during inflationary IE2-SIINFEKL mCMV infection

Clonal focusing has been described to occur during chronic CMV infection (both in hCMV and mCMV; see 1.5.2). To decipher the role of population dynamics (inflationary vs. non-inflationary), in-depth TCR repertoire analysis was performed for IE2-SIINFEKL and M45-SIINFEKL mCMV infection (experiments mainly performed by Kilian Schober and

Thomas Müller). Analysis of the TRBV usage using TCR Vβ staining and flow cytometry revealed progressive oligoclonality during inflationary IE2-SIINFEKL mCMV infection. During M45-SIINFEKL mCMV infection however only some repertoire focusing occurred early on, but it remained stable thereafter (Schober, Voit, et al., 2020). Single-cell sequencing of TCR α and β chains using TCR SCAN (Dössinger et al., 2013) further showed highly comparable results in terms of TRBV usage. Longitudinal sequencing of TCR CDR3 α and CDR3 β of IE2-SIINFEKL-specific T cell populations throughout the course of infection again showed decreasing diversity over time. Interestingly, when looking at the ten most abundant clonotypes within individual mice over time, the dominators changed several times over the course of the infection, suggestive of clonal succession (Schober, Voit, et al., 2020). In line with these findings, decreasing diversity was also observed for inflationary M38-specific T cell populations during wildtype mCMV infection and lowering the precursor frequencies through thymectomy appeared to accelerate this process. Again, longitudinal data revealed clonal succession over time (Schober, Voit, et al., 2020).

4.3.3 Microscopic k_{off}-rate measurements of inflationary T cell populations reveal dominance of low avidity T cells at late time points of IE2-SIINFEKL mCMV infection

The massive increase in size and especially the increased oligoclonality of inflationary mCMV-specific T cell populations at late time points of infection raised the question if the changes in the composition of the repertoire reflected changes based at least partly on TCR avidity. To answer this question, repeated measurements of TCR avidity at different time points of the infection were performed. Both TCR avidity data of inflationary mCMV-specific T cell populations and as a control also of non-inflationary mCMV-specific T cell populations were gathered. As a surrogate for TCR avidity the k_{off}-rate was assessed using the microscopic TCR k_{off}-rate assay.

When looking at exemplary TCR-ligand k_{off}-rate measurements of IE2-SIINFEKL mCMV infected mice at the peak of acute infection at d15, T cell populations covered a wide

spectrum of TCR avidities (see Figure 14 A). Half-lives ranged between slightly below 10 s up to 500 s with no apparent clustering. At the late phase of chronic infection (d200+) the distribution of $t_{1/2}$ had narrowed substantially with $t_{1/2}$ usually confined to only one or two sectors of the $t_{1/2}$ spectrum (see Figure 14 B). Based on the TCR repertoire data, we hypothesize that the "$t_{1/2}$ sector groups" represent T cell clones with distinct structural avidities.

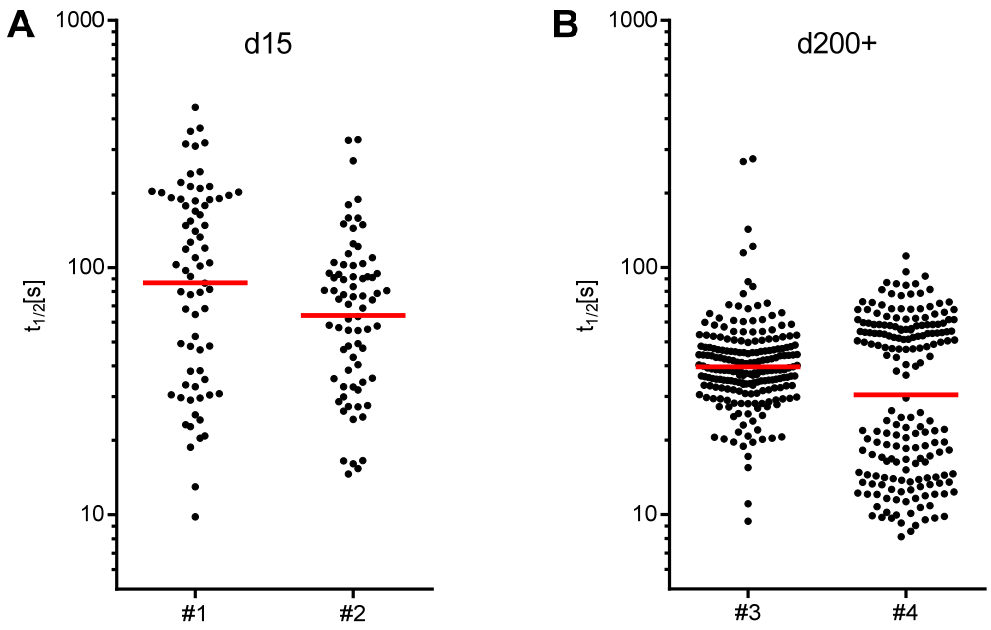

Figure 14. Microscopic k_{off}-rate measurements reveal wide initial TCR avidity spectrum that narrows at late time points for IE2-SIINFEKL mCMV infected mice. Half-life time ($t_{1/2}$) of exemplary k_{off}-rate measurements of IE2-SIINFEKL mCMV infected mice at d15 and d200+ p.i. Splenocytes were FACS sorted for $CD8^+$, $CD19^-$, SIINFEKL-*Strep*tamer$^+$ cells and microscopic k_{off}-rate measurements were performed. **(A)** Half-life time ($t_{1/2}$) of individual cells of mice at d15 p.i. **(B)** Half-life time ($t_{1/2}$) of individual cells of mice at d200+ p.i.; Each dot represents one cell. Each column (#) represents one mouse. Red lines show geometric mean of $t_{1/2}$ for each mouse.

K_{off}-rate measurements like the ones exemplified in Figure 14 were conducted for multiple time points and for both the inflationary IE2- and the non-inflationary M45-SIINFEKL mCMV group. To compare the results of these measurements to one another, one way is to reduce the single-cell $t_{1/2}$ data for each mouse to one value best capturing the typical $t_{1/2}$. For this purpose, the geometric mean seemed most appropriate. It is less affected by outliers than the arithmetic mean, yet unlike the median does not completely ignore extreme values that might have physiological significance.

Measurements for the non-inflationary M45-SIINFEKL mCMV infection showed constant geometric mean $t_{1/2}$ values of around 60 s for all time points except for one d60 sample with a particularly long $t_{1/2}$ (see Figure 15 A). The IE2-SIINFEKL group on the other hand displayed an interesting progression. At d15 p.i. $t_{1/2}$ was very diverse not only within specimens but also in between specimens. Nonetheless, on average, long $t_{1/2}$ and therefore high avidity T cells were most abundant at this time point. At late time points of infection (d200+), however, T cells with very short $t_{1/2}$ dominated the responses in most cases. The overall $t_{1/2}$ significantly decreased from d15 to d200+ (see Figure 15 A).

Using the geometric mean to summarize the acquired k_{off}-rate data provides a good overview. Nonetheless a lot of information about the distribution of single-cell data points is lost that way. As an attempt to illustrate the whole data set and keep the single-cell resolution, a cell number adjusted pooled sample approach was performed (see Figure 15 B). The number of cells analyzed for each mouse varied substantially due to experimental conditions. In order to pool the single-cell data from different mice for one time point and make sure that each mouse is accounted for equally, representative draws were conducted to equalize cell numbers. Serial random draws of samples with more cells were performed until a draw that matched the original population in terms of geometric mean and coefficient of variation was obtained. Then all representative samples of each time point were pooled. For IE2-SIINFEKL this depiction showed the diversity of TCR avidity and the abundance of high avidity T cells at d15. Subsequently there was a progression towards lower avidity in the chronic phase of infection, which coincided with a loss of TCR avidity diversity in terms of evenness of distribution due to the focusing on lower avidity. M45-SIINFEKL infected mice on the other hand maintained their diverse distribution of TCR avidity with a medium to high average avidity.

T cells with a $t_{1/2}$ of over 100 s in the microscopic k_{off}-rate assay can be considered to be of high avidity (Nauerth et al., 2013). The fraction of cells with that property was calculated for every individual mouse (see Figure 15 C). For the M45-SIINFEKL group this percentage amounted to somewhat over 20 % on average for all time points examined. For

the IE2-SIINFEKL group this fraction increased during acute infection from d8 to d15. Thereafter the percentage decreased continuously, accounting for less than 10 % of cells analyzed in most of the d200+ mice.

Taken together, for inflationary IE2-SIINFEKL mCMV-specific T cell populations the overall TCR avidity decreased after acute infection. At late time points of the chronic infection, low avidity T cells dominated while the fraction of high avidity T cells became increasingly scarce.

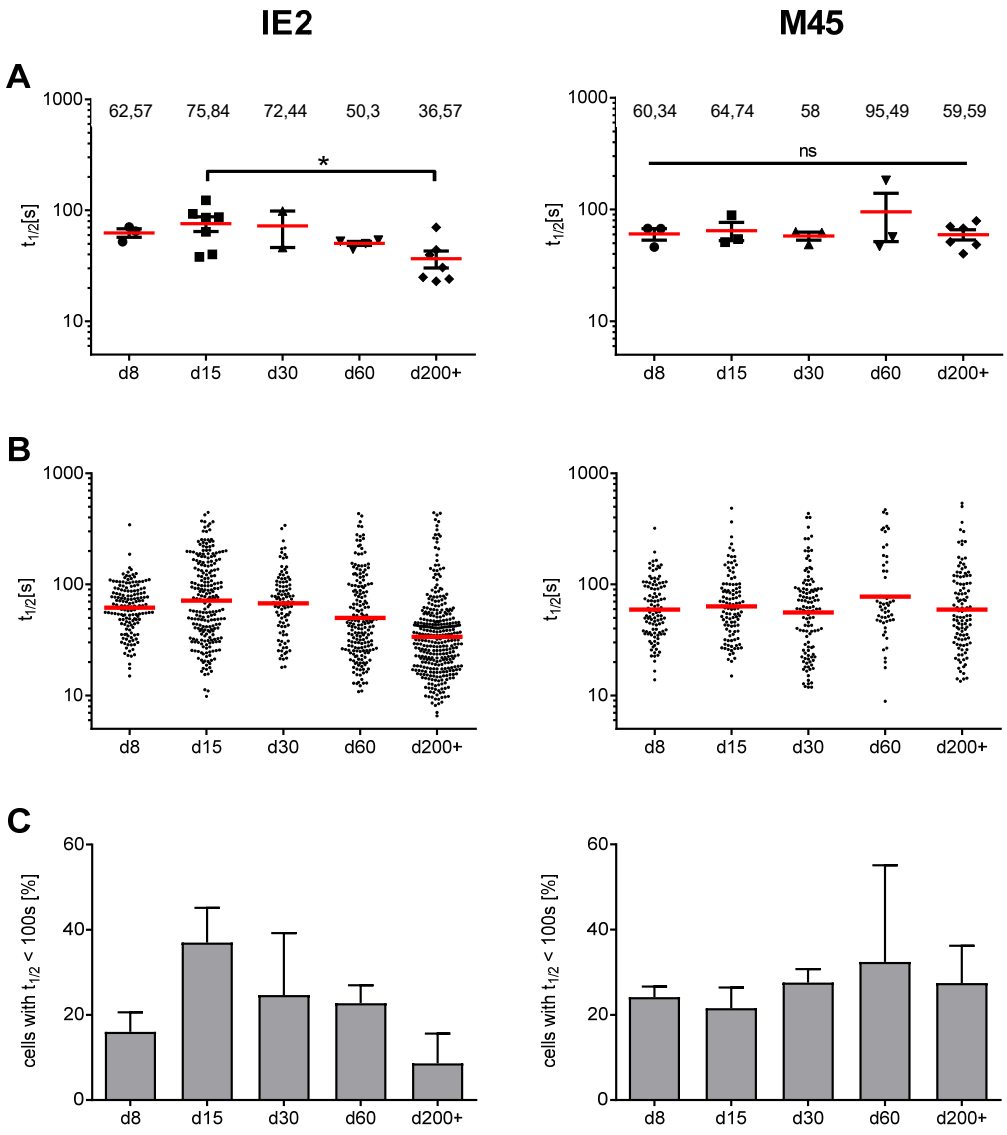

Figure 15. Dominance of low avidity T cells at late time points of inflationary IE2-SIINFEKL mCMV infection. Mice were infected i.p. with recombinant IE2-SIINFEKL mCMV or M45-SIINFEKL mCMV and sacrificed at the indicated time points. Splenocytes were FACS sorted for $CD8^+$, $CD19^-$, SIINFEKL-*Strep*tamer$^+$ cells and microscopic k_{off}-rate measurements were performed. **(A)** Geometric means of $t_{1/2}$; each dot represents the geometric mean of $t_{1/2}$ of all cells analyzed for one mouse. Red lines and numbers noted above show the mean of the geometric mean of $t_{1/2}$ for each time point, the value is depicted at the top. **(B)** Pooled single-cell data of $t_{1/2}$: to adjust for differences in the cell number analyzed per mouse, representative draws reduced cell number to the lowest of each time point. Adjusted samples were then pooled for each time point; each dot represents one cell. Red lines indicate geometric mean. **(C)** Percentage of T cells with $t_{1/2}$ < 100 s was computed for each mouse; On average N = 70 cells were analyzed for each mouse (see Supplementary Figure 2). Error bars indicate SEM. Statistical analysis was performed using one-way ANOVA and Tukey's multiple comparisons test. ns, non-significant. * P < 0,05. N = 2-7 mice per time point.

The observed relative decrease in T cells with a $t_{1/2}$ of over 100 s during chronic inflationary IE2-SIINFEKL mCMV infection raised the question of the fate of these high avidity T cells. All previous k_{off}-rate measurements were conducted with spleen samples. One possible

explanation of the disappearance of high avidity T cells at late time points in the spleen would be preferential homing of those cells to other organs. So, in a next experiment, k_{off}-rate measurements for an IE2-SIINFEKL mCMV infected d200+ mouse were also performed for a blood and lymph node sample (see Figure 16). Population size of *Strep*tamer$^+$ cells differed considerably in the different organs (see Figure 16 A). In the lymph node sample, *Strep*tamer$^+$ cells only accounted for about 3 % of CD8$^+$ cells, whereas in the blood, memory inflation was even more pronounced than in the spleen with *Strep*tamer$^+$ cells reaching almost 50 % of CD8$^+$ cells. Although population size differed greatly, k_{off}-rate $t_{1/2}$ was not significantly different for all organs tested. In fact, in all organs the overall TCR avidity was equally low and the fraction of high avidity was equally small as in the spleen (see Figure 16 B). In addition, comparative k_{off}-rate measurements were performed in bone marrow and liver samples (at d200+ after IE2-SIINFEKL mCMV infection), which also showed no significant difference compared to the spleen sample (Schober et al., 2020; experiment performed by Joel Eggert).

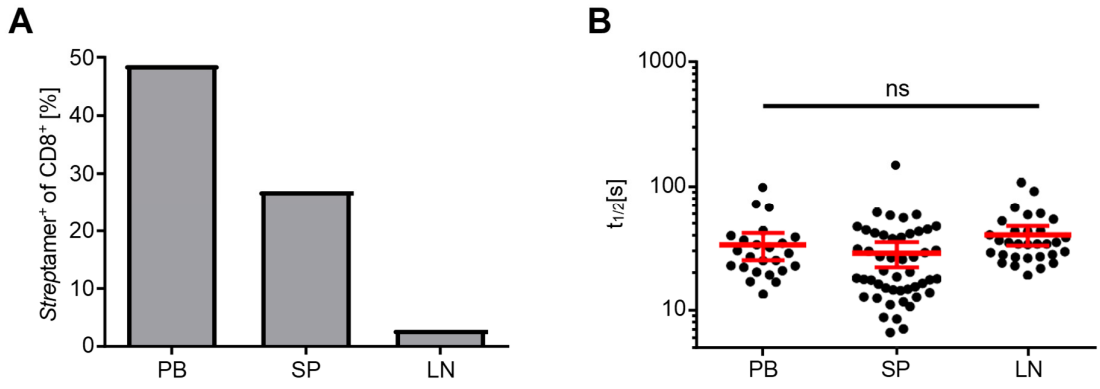

Figure 16. At late time point of IE2-SIINFEKL mCMV infection low avidity T cell populations dominate in different organs. An IE2-SIINFEKL mCMV infected mouse was sacrificed at d404 p.i. Peripheral blood (PB), spleen (SP) and lymph nodes (LN) were FACS sorted for CD8$^+$, CD19$^-$, *Strep*tamer$^+$ cells and microscopic koff-rate measurements were performed. **(A)** Frequency of SIINFEKL-*Strep*tamer$^+$ cells of CD8$^+$ cells. **(B)** Microscopic TCR-ligand $t_{1/2}$ values of SIINFEKL-*Strep*tamer$^+$ cells of different organs; each dot represents one cell. Red lines indicate geometric mean and SEM. Statistical analysis was performed using one-way ANOVA. ns, not significant.

4.3.4 Longitudinal flow cytometry-based TCR-ligand k_{off}-rate measurements confirm dominance of low avidity T cells during late IE2-SIINFEKL mCMV infection – influence of thymectomy

To formally show that significant changes of TCR avidity occur for inflationary IE2-SIINFEKL mCMV-specific T cell populations, longitudinal k_{off}-rate measurements in the same individuals need to be performed. These longitudinal experiments were performed using the flow cytometry-based TCR-ligand k_{off}-rate assay because of the following advantages: The cell number required for k_{off}-rate measurements is lower for the flow cytometry-based assay, making longitudinal measurements of murine blood samples possible. Furthermore, the performance and especially data analysis are a lot faster making high-throughput analysis and therefore bigger test groups feasible.

To further explore the influence of thymic output on the evolution of TCR avidity, pre-adult thymectomy was performed (see Figure 17 A). The population size of SIINFEKL-specific T cells was slightly bigger in the thymectomized group at all time points, although these differences were not significant (see Figure 17 B). Cross-sectional microscopic k_{off}-rate measurements had revealed a maximum $t_{1/2}$ for d15 and decreasing $t_{1/2}$ for later time points (see Figure 15). A similar pattern was observed in longitudinal measurements of individual non-thymectomized mice (see Figure 17 C and D wt). Mean $t_{1/2}$ of all 12 mice showed a significant decrease between d15 and d170, confirming the results of the previous cross-sectional measurements (see Figure 17 E wt). K_{off}-rate measurements of thymectomized mice revealed high intra- and interindividual diversity. Half-life times began to decrease even earlier than in the non-thymectomized group, but changes over time were not significant overall (see Figure 17 D thy and E thy).

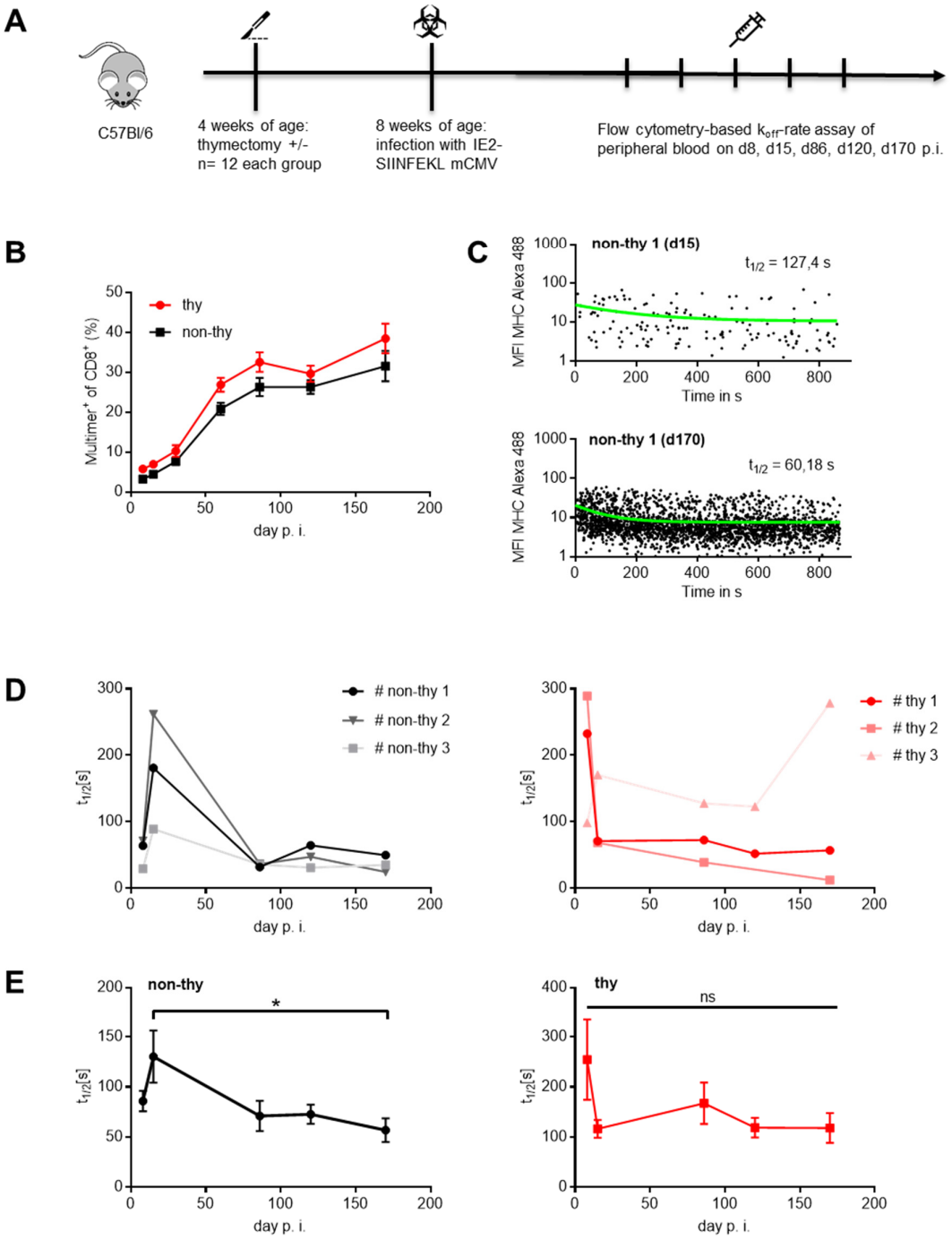

Figure 17. Longitudinal k_{off}-rate measurements confirm decrease of TCR avidity during inflationary IE2-SIINFEKL mCMV infection. **(A)** Experimental setup for the longitudinal measurements; **(B)** Population size displayed as percentage of SIINFEKL-*Strep*tamer$^+$ T cells (Multimer$^+$) of CD8$^+$ cells in peripheral blood; **(C)** Exemplary dot plots of flow cytometry-based k_{off}-rate dissociation of one individual non-thymectomized mouse at d15 and d170 **(D)** Exemplary longitudinal $t_{1/2}$ of three individual mice per group. Data represent mean of two dissociations per mouse and time point. **(E)** Longitudinal mean $t_{1/2}$ for non-thymectomized (left) and thymectomized (right) group. thy: thymectomized; non-thy: non-thymectomized; data in (B) and (E) display mean and SEM; dissociation curves were fitted using constrained fit; Statistical analysis in (E) was performed using one-way ANOVA. * $P < 0,05$. ns, not significant. N = 12 mice per group.

The analysis of the thymectomized group in particular was hampered by the occasional occurrence of “two-band dissociations” potentially skewing the result (exemplary data see Figure 18), likely reflecting selection of two clones with very high and very low structural avidities (also see 5.5).

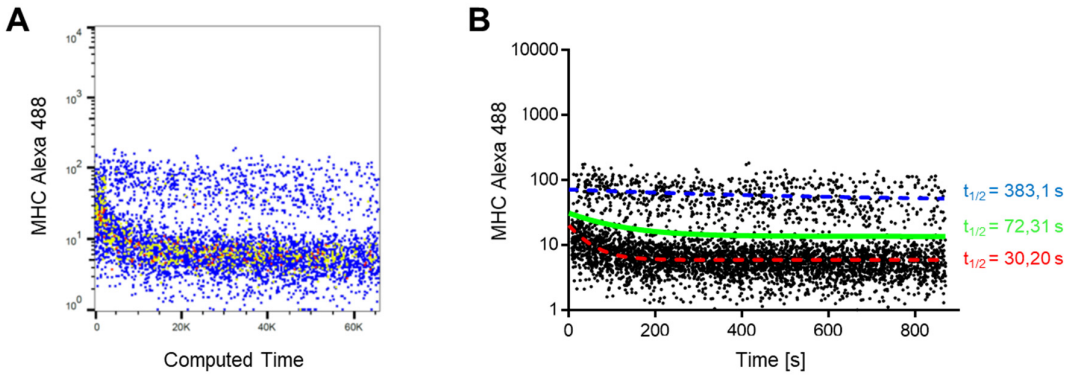

Figure 18. Two-band dissociations occasionally occurred at late time points of infection, especially in the thymectomized group. Exemplary depiction of two-band dissociation. Data show dissociation of one thymectomized mouse at d170 p.i. with IE2-SIINFEKL mCMV (see Figure 17). **(A)** Pseudocolor plot of flow cytometry-based k_{off}-rate assay, pre-gated on SIINFEKL-multimer positive. **(B)** dot plot of dissociation shown in (A). Green curve shows regular one-phase exponential decay curve. In addition, decay curves were calculated separately for upper (blue) and lower (red) band.

4.3.5 Functional avidity of inflationary or non-inflationary SIINFEKL mCMV-specific T cells does not decrease between acute and late chronic infection

Inflationary IE2- and non-inflationary M45-SIINFEKL mCMV-specific T cell populations were examined for their functional avidity at different phases of infection. Functional avidity can be assessed by incubating T cells with different amounts of their cognate antigen and measuring their cytokine response. T cells with high functional avidity will respond to lower amounts of antigen. Here IFN-γ production of splenocytes was determined after incubation with SIINFEKL peptide (see Figure 19). For M45-SIINFEKL mCMV infected mice, functional avidity did not decrease from acute infection at d15 to late chronic infection at d200+ (in fact, a small but significant increase was observed), consistent with measurements of their structural avidity (see Figure 15). Despite showing a significantly lower structural avidity (see Figure 15, Figure 17), IE2-SIINFEKL mCMV infected mice did not exhibit lower functional avidity at late time points of chronic infection at d200+ than at d15.

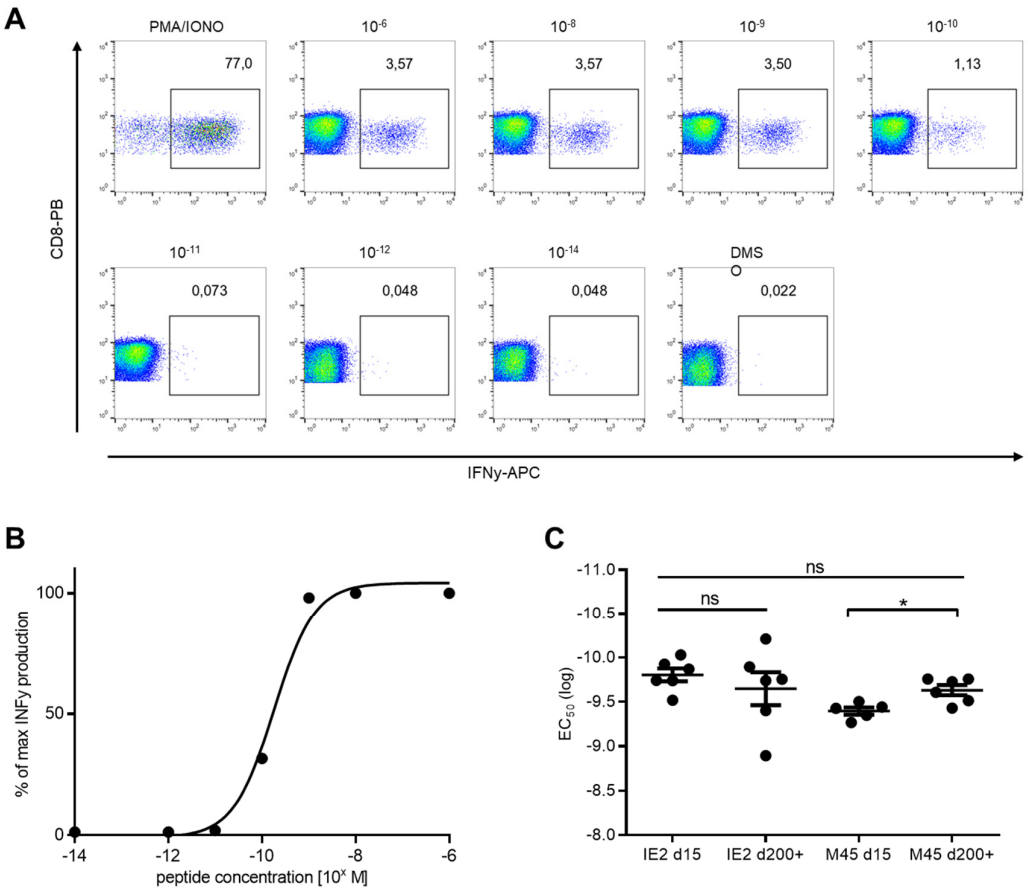

Figure 19. Functional avidity of inflationary or non-inflationary SIINFEKL mCMV-specific T cells does not decrease between acute and late chronic infection. Mice were infected i.p. with recombinant IE2- or M45-SIINFEKL mCMV and sacrificed at d15 or d200+ p.i. Splenocytes were incubated with indicated amounts of SIINFEKL peptide and IFN-γ production was analyzed by intracellular cytokine staining. **(A)** Exemplary FACS plots show IFN-γ production upon stimulation with indicated amounts of SIINFEKL peptide. Numbers above gate indicate percentage of IFN-γ^+ cells. Pre-gated on $CD8^+$. PMA/IONO represents positive control. **(B)** Values of (A) were normalized to maximal IFN- γ production, and the EC_{50} was calculated by nonlinear regression. **(C)** EC_{50} values of IE2 d15, IE2 d200+, M45 d15 and M45 d200+; Note that smaller numbers (bigger negative exponent) signify higher sensitivity to peptide. Each dot represents one mouse. Lines show the mean ± SEM for each group. Statistical testing for all four groups was performed by one-way ANOVA (p = 0,13). Statistical testing for the IE2 and M45 groups separately was conducted by a two-tailed unpaired Student's t-tests. *P < 0,05. N = 6 for each group.

4.4 Avidity measurements of thymectomized and non-thymectomized mice during wt mCMV infection

So far, all mCMV experiments had been performed using recombinant IE2- and M45-SIINFEKL mCMV strains. This had the major advantage of enabling measurement of k_{off}-rates of inflationary and non-inflationary T cell population under very controlled and well-defined conditions. Both had the same epitope specificity and therefore were also recruited out of a similar naïve repertoire. Furthermore, the same *Strep*tamer reagents could be used

for all experiments. Having observed the gradual loss of high avidity T cells over time for IE2-SIINFEKL mCMV derived T cell populations, the question was if a similar progression could also be observed for the more physiological and general case of wt mCMV infection. To this end, TCR k_{off}-rate measurements of T cell populations specific for the inflationary wt mCMV epitope M38 were conducted.

4.4.1 Memory inflation is more pronounced in thymectomized mice than in non-thymectomized mice for inflationary M38 epitope

For wt mCMV infection, memory inflation is a well described phenomenon for some epitopes. To check if thymectomy would influence the extent of memory inflation, relative population sizes of T cells specific for one inflationary mCMV epitope (M38) and one non-inflationary mCMV epitope (M45) were determined at different time points after infection. Acute infection was dominated in both groups by M45-specific T cell populations to a similar degree (see Figure 20). Also, M38-specific T cell populations were initially similar in size in both groups. During chronic infection, although M38-specific T cell populations dominated in both groups and increased in size over time, they did so even more in the group of thymectomized mice. To control for unspecific effects of the thymectomy operation, an additional group of mice received sham thymectomy. The population size of sham-thymectomized mice behaved similarly to those of non-thymectomized mice and did not show enhanced memory inflation.

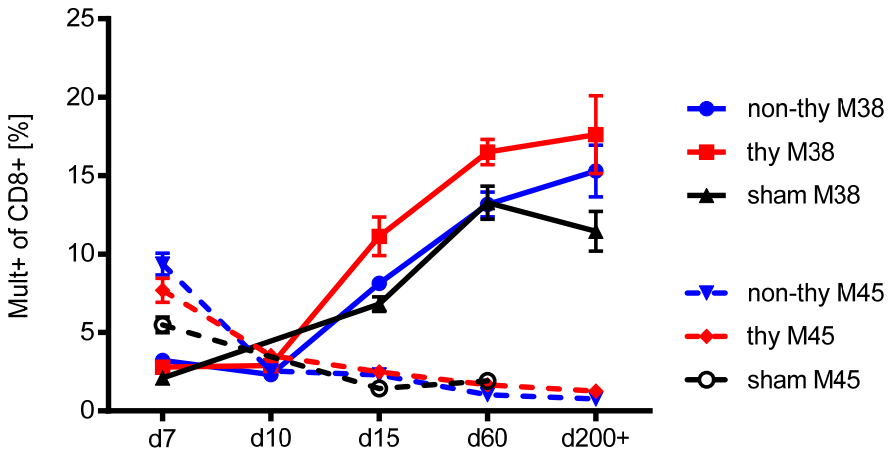

Figure 20. Memory inflation is more pronounced in thymectomized mice than in non-thymectomized mice for inflationary wt mCMV epitope. At four weeks of age mice were either thymectomized (thy), sham operated (sham) or not operated at all (non-thy). After three weeks of recovery mice were infected i.p. with wt mCMV and sacrificed at the indicated time points. A non-reversible multimer blood staining was performed for the inflationary H_2Kb-M38 and the non-inflationary H_2Db-M45 epitope for each mouse. Fraction of multimer$^+$ of CD8$^+$ is depicted for different time points. Data are mean ± SEM of N = 8-18 mice at each time point and group (except sham group: N = 6 mice).

4.4.2 Decrease of structural avidity of inflationary M38-specific T cell populations during wt mCMV infection

Microscopic k_{off}-rate measurements of inflationary M38-specific T cell populations of wt mCMV infected mice were performed as described previously (see 4.3.3). Consistent with results obtained using the IE2-SIINFEKL mCMV model, inflationary M38-specific T cell populations of wt mCMV infected mice showed a significant decrease in structural avidity over time (see Figure 21).

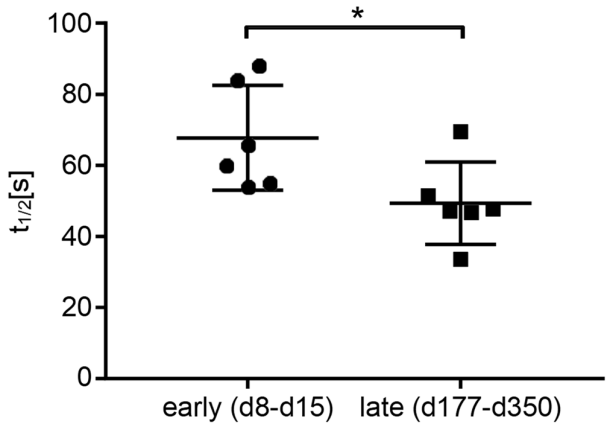

Figure 21. Microscopic k_{off}-rate measurements reveal decrease of structural avidity of inflationary M38-specific T cell populations during wt mCMV infection. Microscopic k_{off}-rate $t_{1/2}$ of inflationary M38-specific T cell populations of wt mCMV infected mice at different time points after infection. C57/BL6 mice were infected i.p. with wildtype mCMV and sacrificed at the indicated time points (early: d8-d15; late: d177-d350). Splenocytes were used for k_{off}-rate measurements. Each dot represents geometric mean $t_{1/2}$ of ≤ 13 replicates per mouse. Lines show mean with SEM. Statistical analysis was performed using a two-tailed unpaired t-test. *P < 0,05. N = 6 per group.

4.4.3 Half-life time of M38-specific T cell populations of thymectomized and non-thymectomized mice increases at late time points of chronic wt mCMV infection

Flow cytometry-based TCR-ligand k_{off}-rate assay measurements were performed for inflationary wt mCMV epitope M38-specific T cell populations for thymectomized and non-thymectomized groups. The $t_{1/2}$ measurements revealed remarkably high interindividual variability for both groups at all time points. Additionally, both groups showed a surprising triphasic $t_{1/2}$ pattern over time (see Figure 22). Both groups showed an increase of mean $t_{1/2}$ during acute infection. Mean $t_{1/2}$ decreased thereafter until d60 (for the thymectomized group $t_{1/2}$ had already decreased after d10, for the non-thymectomized group $t_{1/2}$ only decreased after d15). After d60 however, the overall $t_{1/2}$ increased gradually for both groups, which coincided with the more frequent occurrence of two-band-dissociations (see Figure 18). Currently, no final explanation for this surprising phenomenon can be offered (see 5.5).

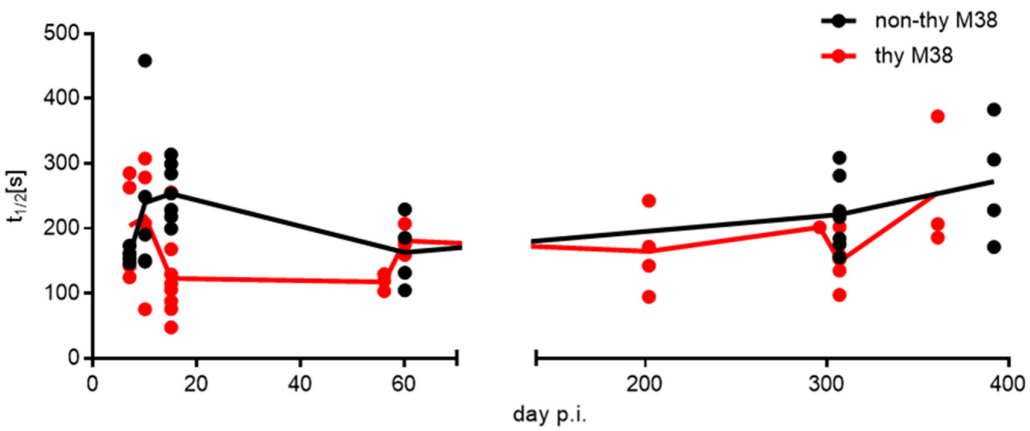

Figure 22. Half-life time of M38-specific T cell populations of thymectomized and non-thymectomized mice increases at late time points of chronic wt mCMV infection. Flow cytometry-based k_{off}-rate $t_{1/2}$ of inflationary M38-specific T cell populations of thymectomized or non-thymectomized wt mCMV infected mice at different time points after infection. At three weeks of age mice were either thymectomized (thy) or not operated (non-thy). After three weeks of recovery mice were then infected i.p. with wt mCMV and sacrificed at the indicated time points. Splenocytes were used for k_{off}-rate measurements. Each dot represents mean $t_{1/2}$ of ≤ 2 replicates per mouse. Lines connect means of each time point. N = 3-6 mice per time point and group.

4.5 *In vivo* competition of epitope-specific T cells of different avidities – prospective adoptive transfer experiments

The previous experiments suggested a significant decrease of the overall avidity over time and dominance of low avidity T cells at late time points of the inflationary IE2-SIINFEKL mCMV infection (see 4.3). To validate this hypothesis in a prospective manner, adoptive transfer experiments were performed to observe *in vivo* competition of epitope-specific T-cells of different avidities.

4.5.1 *In vivo* competition of adoptively transferred OT-I T cells during infection with altered peptide ligand (APL) variants of IE2-SIINFEKL mCMV

APL variants are generated by single amino acid replacements in the sequence of an immunogenic epitope. APL variants of the native SIINFEKL epitope (N4) differ in their potency of stimulating OT-I T cells. SIITFEKL (T4) has been described to mark the avidity threshold between positive and negative selection of OT-I T cells (Enouz, Carrié, Merkler, Bevan, & Zehn, 2012). The potency of SIIVFEKL (V4) has been described to be even less (about 700-fold lower than N4) (Zehn et al., 2009).

Adoptive transfer of 100 naïve CD44low OT-I T cells into C57BL/6 mice and subsequent infection with APL variants of IE2-SIINFEKL mCMV were performed. In the setting of N4-infection OT-I T cells can be viewed as high avidity T cells, in the setting of T4- or V4-infection they resemble low avidity cells. Population size of transferred cells in peripheral blood was monitored longitudinally.

In N4-infected mice transferred OT-I T cells expanded vigorously, reaching approximately 10 % of the CD8 T cell compartment at d200. At late time points, the population slightly contracted (see Figure 23 B). The large OT-I T cell population together with a strong endogenous N4-specific response (data not shown) led to suppression of the endogenous M38-specific response (in comparison with T4 or V4 infected mice; see Figure 23 A). At early time points in T4- and V4-infected mice the population size of transferred OT-I T cells was at the limit of detection. Only at very late time points of infection (< d300 p.i.) they expanded significantly to form small but robustly detectable populations, potentially suggesting late recruitment.

The OT-I-APL experimental system, however, has the following limitations: competition of a defined set of high and low avidity T cells cannot be observed within the same host, but rather they compete separately against a polyclonal endogenous response. The use of OT-I T cells is also problematic given their unusually fast k_{off}-rate in relation to their high overall affinity (Nauerth et al., 2013; Rosette et al., 2001). Also, the affinity of individual APLs to the MHC complex itself may differ, which would represent a confounding effect.

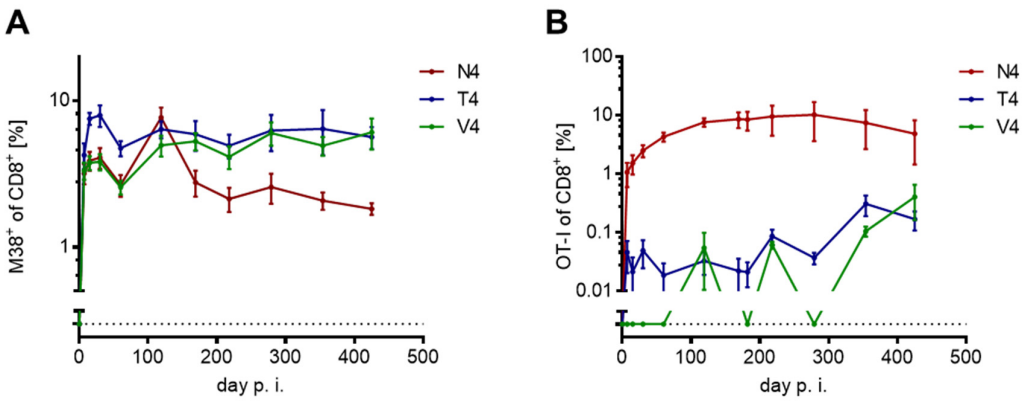

Figure 23. ***In vivo*** **competition of adoptively transferred OT-I T cells during infection with APL variants of IE2-SIINFEKL mCMV.** 100 CD45.1+ OT-I T cells were adoptively transferred into C57BL/6 mice and infected with APL variants of IE2-SIINFEKL mCMV one day later. Population size of endogenous M38-specific T cells (via multimer staining) and transferred OT-I T cells (via congenic marker staining) were tracked longitudinally. **(A)** Percentage of $M38^+$ cells of $CD8^+$ cells. **(B)** Percentage of transferred OT-I T cells of $CD8^+$ cells. Data represent mean and SEM. Lines connect mean of each time point. The dashed horizontal line at the bottom indicated zero percent. N = 3 per group.

4.5.2 TCR library for $H2K^b$-SIINFEKL

In order to build up a library containing TCRs covering a wide spectrum of avidities for $H2K^b$-SIINFEKL to choose from for transfer experiments, TCRs were isolated at different time points of IE2-SIINFEKL mCMV infection. Using TCR SCAN single-cell PCR (Dössinger et al., 2013), 15 different fully paired $\alpha\beta$ TCRs were identified. After re-expression in retrogenic mice functional testing of the TCRs revealed full functionality: stainability with SIINFEKL multimer, antigen-specific proliferation *in vivo* and dose-dependent cytokine release upon antigen-specific stimulation *in vitro* (Schober, Voit, et al., 2020). The TCRs differed substantially in their $t_{1/2}$ determined by the flow cytometry-based k_{off}-rate assay, indeed showing coverage of a wide spectrum of avidities (see Figure 24). The experiments described above were performed by Kilian Schober with support by Simon Grassmann, Thomas Müller, Joel Eggert and Sebastian Jarosch.

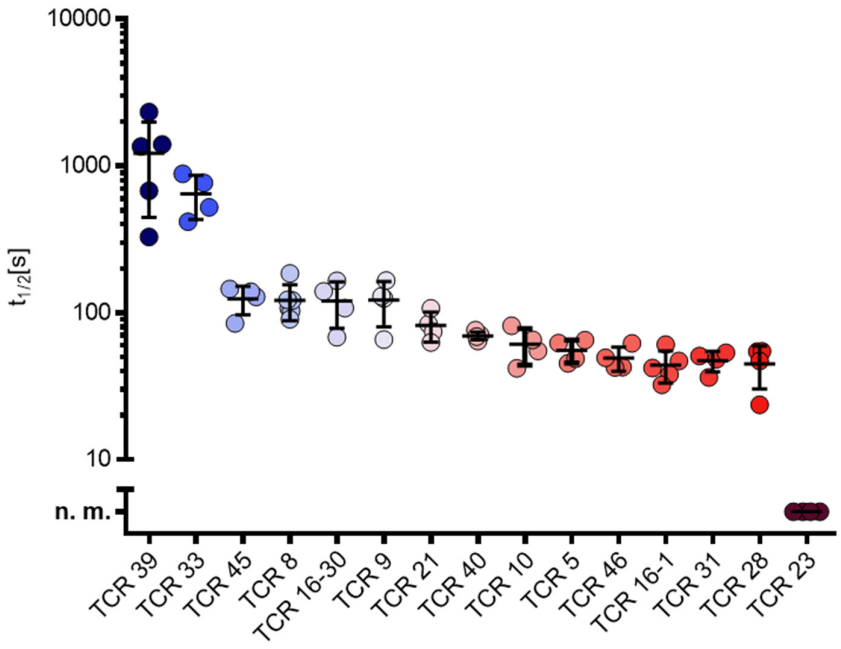

Figure 24. TCR library for H2Kb-SIINFEKL covers wide spectrum of structural avidities. Half-life time ($t_{1/2}$) of 15 SIINFEKL-specific TCRs color coded according to their structural avidity determined by flow cytometry-based k_{off}-rate assay. Every dot represents one measurement with two technical replicates, lines depict mean and SEM. Figure adapted from (Schober, Voit, et al., 2020).

4.5.3 *In vivo* competition of co-transferred SIINFEKL-specific T cells of different avidities

4.5.3.1 Determination of physiological cell number of transferred cells

The number of cells that should be adoptively transferred needs to be chosen carefully, because it can have a big effect on the outcome of the experiment. Transfer of excessive numbers would lead to saturation effects preventing competition to occur. For this reason, RAG$^{-/-}$ mice were used as recipients to prevent the endogenous response from “buffering the system". On the other hand, for transfers of less than about 50 cells, large stochastic effects would be expected (Buchholz et al., 2013). Furthermore, to recreate physiological conditions as closely as possible, the total cell number of transferred cells should resemble the precursor number of a given epitope in the naïve repertoire. For the SIINFEKL epitope the precursor number is estimated to be in the range of a few hundred cells per mouse (Obar et al., 2008).

Expansion capacity of high avidity TCR 33 during IE2-SIINFEKL mCMV infection was tested in comparison to endogenous response in C57BL/6 mice. A cell number of 100, 300 or 1000 naïve, CD44^{low} was transferred and the population size of transferred cells (via congenic marker staining) and endogenous SIINKFEKL-specific cells (via multimer staining) was monitored longitudinally in peripheral blood. Transfer of at least 300 cells elicited an expansion size of a similar magnitude compared to the endogenous response (see Figure 25; see also (Schober, Voit, et al., 2020)).

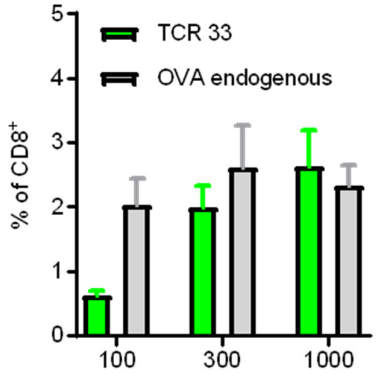

Figure 25. Competition of transferred TCR 33 with endogenous SIINKFEKL-specific response. 100, 300 or 1000 naïve, CD44^{low}, CD 45.1^{+} cells of TCR 33 were transferred into C57Bl/6 recipients which were infected with IE2-SIINFEKL mCMV subsequently. Population size of transferred and endogenous SIINFEKL-specific cells was tracked longitudinally in peripheral blood. Bar graphs show population size as percentage of CD8^{+} cells on d8. Data represent mean and SEM. N = 3 per group.

4.5.3.2 Longitudinal tracking of co-transferred SIINFEKL-specific T cells of different avidities

TCRs of different avidities were re-expressed in retrogenic donor mice (see 4.5.2), also expressing the congenic markers CD45.1 and/or CD90.1 in a homo- or heterozygous fashion, to allow discrimination of cells after transfer (Buchholz et al., 2013). Rag$^{-/-}$ mice served as recipients to eliminate “buffering effects” of the endogenous response. Different combinations of TCRs were tested for transfer experiments (only a representative selection of the experiments that were performed in a collaborative effort are shown in this thesis). The following experiment shows co-transfer of high avidity TCR 33 ($t_{1/2}$ = 647s), intermediate avidity TCR 9 ($t_{1/2}$ = 122s) and low avidity TCR 28 ($t_{1/2}$ = 50s) (100 naïve CD44^{low} CD8^{+} T cells each; see Figure 26 A and B). Infection with IE2-SIINFEKL mCMV was performed the following day. Population size and phenotype of transferred cells was tracked over time in peripheral blood (see Figure 26 C). All three TCRs were recruited into

the immune response with domination of high avidity TCR 33 at early time points of infection (see Figure 26 D). Over time, however, intermediate TCR 9 became more prominent, matching TCR 33 in size at around d100. Even later, low avidity TCR 28 began to increase in size continuously, making up a relative share of almost 20 % at around d300. Relative changes in the compartment of transferred cells were accompanied by similar kinetics in relation to the population of living lymphocytes (see Figure 26 E). Phenotypic analysis revealed an increasing proportion of central memory T cells (Tcm) over time, and interestingly a greater proportion of Tcms for lower avidity TCRs compared to a more effector-differentiated phenotype of the higher avidity TCR (see Figure 26 F).

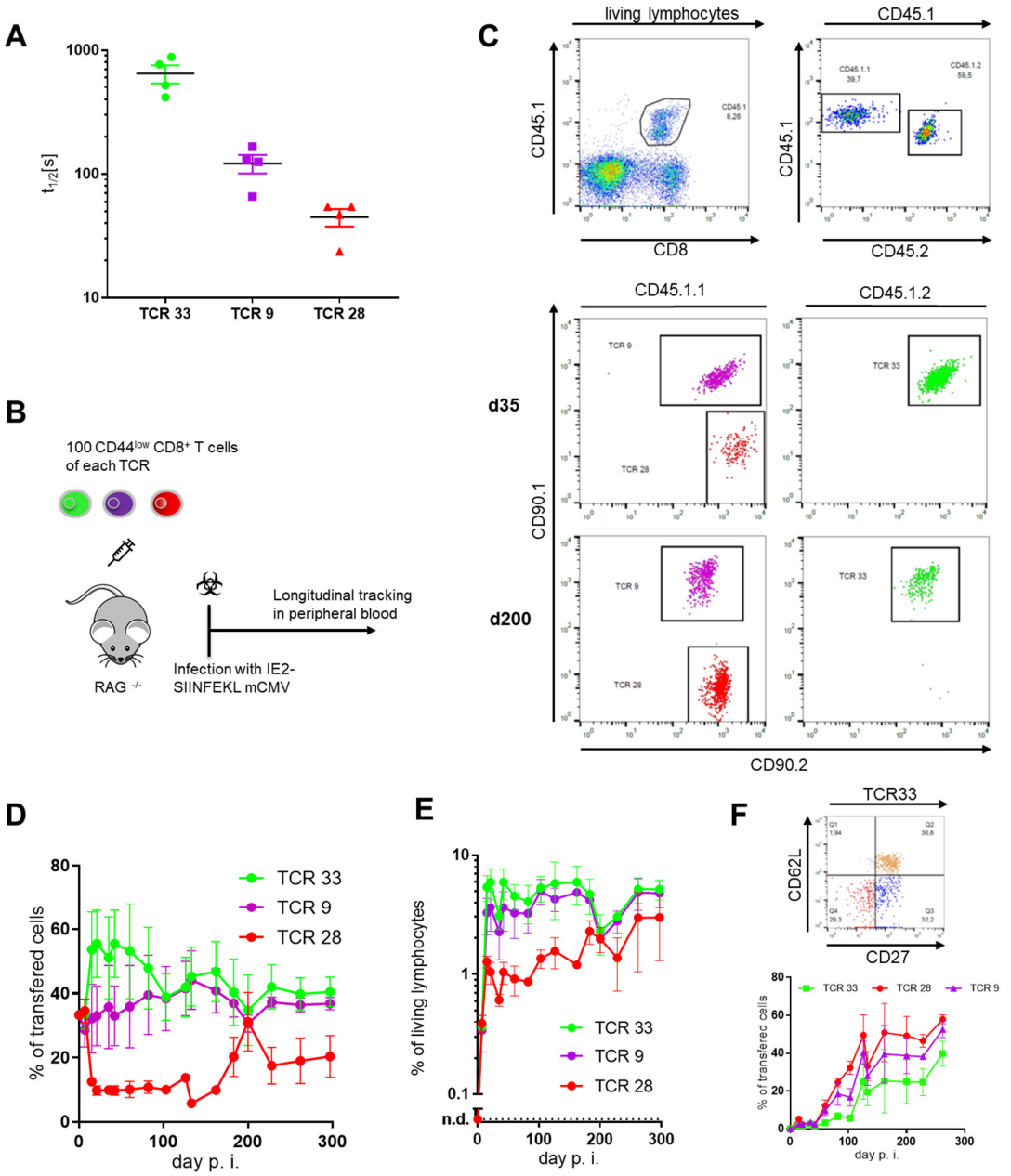

Figure 26. Co-transfer of high, intermediate and low avidity TCRs shows dynamic changes of progeny size during chronic IE2-SIINFEKL mCMV infection. 100 CD44^{low} CD8^{+} T cells of each TCR shown in **(A)** (see also Figure 24) were co-transferred into RAG$^{-/-}$ recipients which were infected with IE2-SIINFEKL mCMV one day later **(B)**. Population size of transferred cells was tracked longitudinally in peripheral blood. TCRs were distinguishable by different congenic marker expression (CD45.1, CD90.1). **(C)** Pseudocolor and color dot plots show representative gating strategy; legend above plot shows gating history. **(D)** Population size of different transferred cells shown as percentage of total transferred cells. **(E)** Population size of different transferred cells shown as percentage of living lymphocytes. **(F)** Phenotype gating: representative dot plot shows CD27 and CD62L staining, pre-gated on TCR33 (top graph); graph below shows percentage of central memory cells (CD27^{+}, CD62L^{+}) of all transferred TCRs over time.; Data represent mean and SEM; n.d.: not defined; N = 3 mice.

To see if a further reduction of the initial transfer cell number would reinforce the expansion of low avidity T cells, the following experiment focused on the transfer of TCR 33

($t_{1/2}$ = 647s) and TCR 28 ($t_{1/2}$ = 50s) only (the rest of the experimental setup was unchanged (see Figure 27 A and B). Again, both TCRs were recruited into the immune response with early domination of high avidity TCR 33 (see Figure 27 C). After around d30 p.i., however, the relative shares of both TCRs (as percentage of transferred cells) began to converge over time with even a temporary change of dominance at around d200. Similar kinetics were observed in relation to the population of living lymphocytes. Phenotypic analysis revealed an increasing proportion of central memory cells (Tcm) over time and again a greater proportion Tcms for the lower avidity TCR (see Figure 26 F and Figure 27 E).

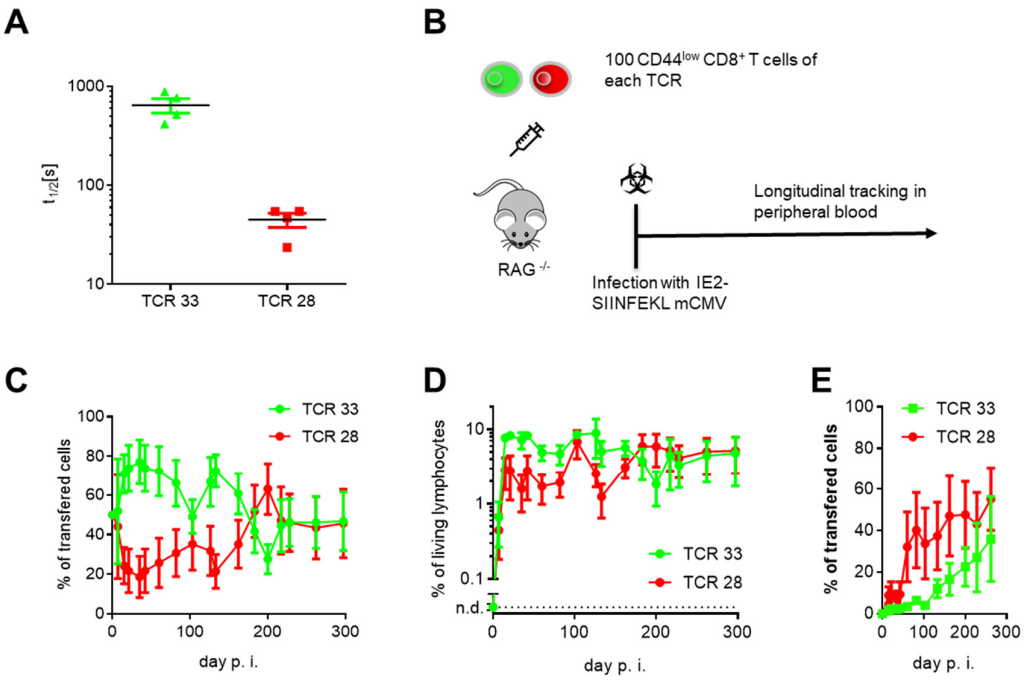

Figure 27. Co-transfer of high and low avidity TCRs reveals late expansion of low avidity T cells. 100 CD44l^{ow} CD8^{+} T cells of high avidity TCR33 and low avidity TCR9 (see **(A)**) were co-transferred into RAG$^{-/-}$ recipients which were infected with IE2-SIINFEKL mCMV one day later **(B)**. Population size of transferred cells was tracked longitudinally in peripheral blood. TCRs were distinguishable by different congenic marker expression (CD45.1, CD90.1). **(C)** Population size of different transferred cells shown as percentage of total transferred cells. **(D)** Population size of different transferred cells shown as percentage of living lymphocytes. **(E)** Percentage of central memory cells (CD27^{+}, CD62L^{+}) of different transferred TCRs over time.; Data represent mean and SEM. N = 3 mice.

In order to examine the transcriptional signatures associated with the change of dominance, T cells of both TCRs were sorted to perform ribonucleic acid (RNA) sequencing before the change of dominance had occurred (d103 p.i.) (Schober, Voit, et al., 2020). Low avidity TCR 28 T cells were found to be enriched for gene clusters related to “naïve and late memory”

or “memory precursors” whereas high avidity TCR 33 T cells were enriched for genes related to a highly differentiated, senescent phenotype (data not shown; RNA sequencing experiments and analysis performed by Kilian Schober and further colleagues).

5 Discussion

5.1 Validation of the TCR-ligand k_{off}-rate assay

Development and main validation of the TCR-ligand k_{off}-rate assay was mainly performed by Nauerth, Weißbrich, Knall and others (Knall, 2007; Nauerth, 2012; Nauerth et al., 2016, 2013; Weißbrich, 2015). For the application of the assay for this project, some additional validation issues had to be addressed.

Including the cytotoxic T cell marker CD8 in the staining/sorting panel of k_{off}-rate experiments increases the specificity of the panel by eliminating unspecific *Strep*tamer/multimer binding cells of other cell types. But due to close interaction of CD8 with the TCR, a potential influence of a CD8 antibody staining on the k_{off}-rate dissociation needed to be taken into consideration. Indeed, CD8 clone 53.6-7 turned out to have a tremendous influence on the k_{off}-rate $t_{1/2}$ and should therefore not be used for k_{off}-rate experiments (see 4.1.1). Clone 5H10, however, did not show any influence on the k_{off}-rate $t_{1/2}$ both in the setting of monoclonal OT-I T cells and polyclonal endogenous T cells compared to no CD8 staining. The choice of fluorochrome did not show any influence on the k_{off}-rate. Nonetheless for the microscopic k_{off}-rate assay PB is preferable to PE since it does not have an emission overspill into the Alexa Fluor 488 detection channel. Thus, for murine k_{off}-rate experiments CD8-PB clone 5H10 should be the antibody of choice.

The newly developed combinatorial labelling system “color coding” made it possible to perform flow cytometry-based k_{off}-rate dissociations of multiple samples simultaneously. Again, an influence of an additional surface antibody staining (here CD45.2 and CD90.2) on the k_{off}-rate had to be excluded. As no significant influence could be detected (see 4.1.2) color coding for murine samples can be applied using the presented antibody combination.

TCR avidity is an overall fairly stable parameter of T cell functionality. If the TCR-ligand k_{off}-rate was to be considered a valid surrogate for TCR avidity it should at best be largely independent from the cell's phenotype, activation status or proliferative history. Indeed, Nauerth et al. could show that the k_{off}-rate was independent of the activation status of T cells and did not change after transgenic expression in Jurkat76 cells (Nauerth et al.,

2013). As this project focused on T cell fate after prolonged *in vivo* proliferation it was of particular importance to check if the proliferative history of a cell in this particular infection setting would influence its k_{off}-rate. It could be shown that even after adoptive transfer, mCMV infection and more than one year of *in vivo* proliferation, k_{off}-rate $t_{1/2}$ had not changed significantly compared to naïve T cells (see 4.1.3) thereby again confirming the validity of the k_{off}-rate as a surrogate for T cell structural avidity.

5.2 Inverse correlation between population size and structural avidity in human inflationary CMV-specific T cell populations

The population size of inflationary T cell populations increases continuously over time (memory inflation), thus big populations are more frequent at late time points after infection. K_{off}-rate measurements of inflationary T cell populations of human HLA $B8^+$ $hCMV^+$ healthy blood donors revealed an inverse correlation between population size and $t_{1/2}$ (see 4.2). Even though age and time point of infection of donors were unknown and sample size was small, these finding argue against avidity maturation (see 1.4) and are more compatible with decreasing avidity over the course of infection.

5.3 The SIINFEKL mCMV model

The aim of this thesis was to investigate the role of structural avidity on the evolution of the T cell repertoire during chronic latent CMV infection. The processes governing naïve repertoire generation, T cell recruitment and maintenance of epitope-specific T cells during infection are highly complex and many factors may influence repertoire evolution. Thus, for an in-depth study of one influencing factor a reductionistic model system with well-defined conditions is advantageous.

In contrast to the study of T cell responses in human subjects, a mouse model system not only allows to control the time of infection, viral inoculum dose and genetic background, but also makes targeted interventions feasible. mCMV, which closely

resembles its human counterpart, is a well-established model for a chronic latent infection. Two different types of T cell responses against mCMV can be distinguished (see Figure 6): non-inflationary T cell populations, most prominent during acute infection (primary infection, reactivation), and inflationary T cell populations, accumulating throughout latency (memory inflation). Those groups show vastly different expansion kinetics, thus their comparative repertoire analysis both in terms of diversity and structural avidity seemed particularly interesting. In wt mCMV different viral epitopes are responsible for the induction of inflationary and non-inflationary T cell populations, which makes their comparative assessment of T cell avidity problematic. To eliminate the influence of the epitope itself, two recombinant mCMV viruses expressing the same model epitope (SIINFEKL) either under an inflationary (IE2) or a non-inflationary (M45) promotor were used. Infection with either of the viral recombinants induced a SIINFEKL-specific T cell response readily detectible by multimer staining. Depending on the promotor used indeed either an inflationary or a non-inflationary T cell response was observed in a robust manner (see Figure 13).

5.4 Avidity changes during chronic SIINFEKL mCMV infection favor model of clonal succession

Analysis of the TRBV usage and single-cell sequencing of TCR α and β chains showed decreasing diversity over the course of the infection for inflationary T cell populations in IE2-SIINFEKL mCMV infection as well as in wt mCMV infection. For non-inflationary populations, repertoire changes were only mild. Additionally, longitudinal experiments of inflationary populations revealed clonal succession of the dominating clonotypes over time (see 4.3.2).

This begs the question if and how changes in the repertoire during chronic mCMV infection are determined by structural avidity. Due to the lack of adequate methods to assess structural avidity, this question had previously not been answered in a conclusive manner (see 1.5). Using the SIINFEKL mCMV model (see 5.3) structural avidity of inflationary (IE2) and non-inflationary (M45) T cell responses was assessed at different time points of infection (see 4.3.3 and 4.3.4) Microscopic k_{off}-rate measurements, which offer

single-cell resolution, revealed insights about the composition of inflationary T cell populations in terms of avidity. At early time points of infection populations covered a wide spectrum of $t_{1/2}$ with no apparent clustering. At the late phase of chronic infection (d200+) the distribution of $t_{1/2}$ had narrowed substantially with $t_{1/2}$ usually confined to only one or two sectors of the $t_{1/2}$ spectrum (see Figure 14) thus reflecting the changes observed by TRBV or next generation sequencing (NGS) analysis (see also Schober et al., 2020).

Not only had the distribution of $t_{1/2}$ narrowed at late time points for inflationary T cell population, also the overall TCR avidity decreased continuously after acute infection. At late time points of the chronic infection low avidity T cells dominated while the fraction of high avidity T cells became increasingly scarce. Of note, this was not observed for M45-SIINFEKL mCMV-specific resting memory T cell population which maintained an intermediate to high overall structural avidity. This is in line with M45 being transcribed only during the acute phase of infection, and therefore not eliciting a continuous change in the responding TCR repertoire during CMV latency.

To demonstrate that the differences in avidity at different time points truly reflect changes within individual mice, longitudinal measurements in peripheral blood were performed (see 4.3.4). The pattern of initial increase and subsequent decrease of avidity observed by the cross-sectional microscopic measurements was confirmed by the longitudinal flow cytometry-based measurements (see Figure 17).

Of note, the marked decrease in structural avidity for inflationary T cell populations was not accompanied by a decrease in functional avidity (see 4.3.5). This is in line with findings from Synder and others, who showed that mCMV-specific T cells, despite a phenotype that suggests extensive antigen-driven differentiation, remain functional and do not show classic features of exhaustion (Klenerman & Oxenius, 2016; Snyder et al., 2009; Wherry, 2011). One might speculate that functionality is maintained by compensatory adjustments in cell phenotype or TCR expression levels.

5.5 Avidity changes during chronic wt mCMV infection

Microscopic k_{off}-rate measurements of inflationary M38-specific T cell populations of wt mCMV showed a significant decrease in structural avidity over time, consistent with results in the SIINFEKL setting (see 4.4.2).

Flow cytometry-based k_{off}-rate measurements during wt mCMV infection, however, revealed a surprising triphasic $t_{1/2}$ pattern over time (see 4.4.3). After an initial increase during acute infection, $t_{1/2}$ decreased during early chronic infection, reminiscent of the pattern observed for IE2-SIINFEKL mCMV. At late time point of chronic infection (d200+) $t_{1/2}$ began to gradually increase again. Currently, no final explanation for this surprising phenomenon can be offered. One aspect might be the concurrent occurrence of “two-band dissociations” for some samples, which were also occasionally observed at late time points of IE2-SIINFEKL mCMV (see Figure 18). Two-band-dissociations complicate fitting the one-phase exponential decay curve, cause greater technical variability and generally lead to longer $t_{1/2}$ due to the presence of the upper band. If the impaired dissociation of the upper band truly reflects “super-high” avidity T cells is unclear. Interestingly, by reanalyzing a two-band dissociation sample after 60 min, Sebastian Jarosch could show that fluorescence intensity of the upper band could return to background levels (unpublished data). This is in line with an actual long dissociation and argues against an intrinsically higher signal for example caused by auto-fluorescence. However, even if that was the case, the functionality of these “super-high” avidity T cells is unclear. Supraphysiologically long TCR dissociation have been shown to correlate with decreased T cell functionality (Irving et al., 2012). Along these lines, TRC 39, the TCR with the longest $t_{1/2}$ of our TCR library for H2Kb-SIINFEKL showed the poorest functionality (data not shown; see 4.5.2). However, more TCRs with such a behavior would need to be observed to corroborate this line of thinking.

5.6 Influence of thymectomy

At late time points of the inflationary IE2-SIINFEKL mCMV infection, mice showed a lower overall structural avidity and relative reduction of high avidity T cells (see 4.3.3). One

possible explanation of this phenomenon would be a higher proliferative rate of high avidity T cells leading to their replicative senescence over time (see Figure 7). If that was the case, then decreasing the naïve T cell pool before infection by thymectomy (thereby reducing the initial total number of T cells and proportionally also the number of high avidity T cells recruited into the immune response) should accelerate the process of replicative senescence of high avidity T cells.

Indeed, during wt mCMV infection, TRBV usage showed an accelerated loss of diversity upon thymectomy, and memory inflation was more pronounced than in non-thymectomized mice (see 4.3.2 and 4.4.1). Additionally, both in the setting of IE2-SIINFEKL and wt mCMV peak structural avidity and the decrease thereafter occurred earlier in the thymectomized group than in the non-thymectomized group, again arguing for an accelerated clonal changing due to reduced precursor frequencies (see 4.3.4 and 4.4.3). It is interesting to speculate if earlier thymectomy would accentuate the effects described above.

Of note, it is worth noting that even at late time points of infection, thymectomized mice did not show any signs of uncontrolled mCMV infection (e.g. weight loss or increased mortality; data not shown), which argues against an essential role of constant replenishment of the T cell pool by thymic output for mCMV control. By performing extensive longitudinal repertoire sequencing of inflationary T cell populations of thymectomized and non-thymectomized individuals during IE2-SIINFEKL mCMV infection, Kilian Schober et al. could show a remarkable stabilization of the repertoire at late time points in both groups in the sense of a plateau of cumulative unique CDR3 sequences over time, which argues against major nourishment of the antigen-specific pool from novel thymic emigrants (Schober, Fuchs, et al., 2020). Along these lines, Snyder et al. have shown that, although naïve T cells can be recruited into the immune response during chronic mCMV infection, maintenance of the antigen-specific T cell pool is dependent mainly on memory precursor cells primed early in infection (Snyder et al., 2008).

5.7 Probing the model by prospective co-transfer experiments

The previous findings (see 4.3 and 4.4) supported the hypothesis of reverse TCR repertoire evolution, possibly through clonal succession due to replicative senescence of high avidity T cells. To validate this hypothesis in a prospective manner adoptive transfer experiments were performed to observe *in vivo* competition of epitope-specific T-cells of different avidities. A library containing TCRs that cover a wide spectrum of avidities for $H2K^b$-SIINFEKL was created and co-transfers of TCRs of different avidities were performed (see 4.5). Different experiments revealed early domination of high avidity TCR T cells followed by late expansion of the low avidity TCR T cells. Furthermore, RNA sequencing showed that low avidity T cells were enriched for gene clusters related to “naïve and late memory” or “memory precursors” whereas high avidity T cells were enriched for genes related to a highly differentiated, senescent phenotype.

5.8 Clonal succession through replicative senescence of high avidity T cells

T cell immune responses against non-persistent pathogens have been shown to undergo structural avidity maturation through selective expansion of high avidity T cells (see 1.4; D H Busch & Pamer, 1999). However, by performing extensive k_{off}-rate measurements both in humans and in mouse models of CMV, evidence for decreasing avidity over the course of chronic viral infection (see 4.2, 4.3 and 4.4) was found. The decrease in avidity was accompanied by a loss of diversity and clonal succession on a genetic level (see 4.3.2). Rebuilding an *in vivo* T cell response by transfer of TCRs of known avidity revealed early dominance of high avidity T cells, which was lost over time. The loss of dominance of high avidity T cells was preceded by relative senescence in their RNA profile. These data argue against progressive avidity maturation during chronic latent infection and are rather compatible with the model of clonal succession through replicative senescence of high avidity T cells (see Figure 7). In this respect the phenomenon of memory inflation might be

a compensatory mechanism for the decreasing avidity of inflationary T cell populations over time. One could also conjecture that the domination of low avidity T cells resemble an “evolutionary compromise” to avoid immunopathology in a setting, in which viral clearance is not possible (Schober, Voit, et al., 2020).

However, the high interindividual diversity of the avidity distribution of epitope-specific T cell populations suggests that avidity is not the only determinant of repertoire evolution. The naïve precursor number for a given epitope, which only lies in the range of a few hundred per mouse (Obar et al., 2008), is believed to contain only a low number of high avidity T cells (Arstila et al., 1999; Hombrink et al., 2013). It can therefore be assumed that the expansion kinetics of the few high avidity T cells are in part established by stochasticity, as experiments by Buchholz showed for monoclonal populations in an acute infection (Buchholz et al., 2013) and an mCMV setting (Grassmann et al., 2020).

5.9 Clinical Implications

In recent years, T cell immunotherapy has made tremendous advances in treatment of infections and especially cancer. Immune checkpoint inhibitors have revolutionized treatment for melanoma, non-small-cell lung carcinoma (NSCLC), renal cell carcinoma and others (Dine, Gordon, Shames, Kasler, & Barton-Burke, 2017; Shih, Arkenau, & Infante, 2014). Adoptive T cell therapy is now available in the form of chimeric antigen receptor (CAR) T cells and in development for TCR-engineered T cells for the treatment of B cell malignancies and has recently yielded very promising results (Ping, Liu, & Zhang, 2018; Wilkins, Keeler, & Flotte, 2017). In the case of persistent CMV infections after allogeneic hematopoietic stem cell transplantation adoptive transfer of CMV-specific donor derived T cells showed promising virological response rates (Neuenhahn et al., 2017; Riddell et al., 1992; Walter et al., 1995).

Clinical success of these therapies greatly relies on T cell functionality and persistence *in vivo*. However, it remains unclear what kind of T cells best provides these characteristics. In the case of TCR-engineered T cells a big challenge is to isolate TCRs

with optimal structural avidity. The findings presented here suggest directing this search to situations where long-term antigen exposure has not occurred, in order to isolate TCRs from a diverse repertoire with a broad spectrum of different avidities.

Optimal avidity does not necessarily mean TCRs of the highest structural avidity. Indeed, although high avidity T cells are generally viewed as functionally superior to low avidity T cells, the loss of dominance during chronic CMV infection however raises questions about their long-term persistence (see 4.5.3 and 5.7). Additionally high avidity T cells can be more susceptible to apoptosis and tolerance (Brentville, Metheringham, Gunn, & Durrant, 2012) and concerns have also be raised about their specificity and induction of autoimmunity (Hurwitz, Cuss, Stagliano, & Zhu, 2014).

The findings presented here suggest that in immunotherapeutic approaches, where target elimination is not possible, transfer of low avidity T cells could represent the more physiological and durable option.

6 Summary

The aim of this thesis was to investigate if and how repertoire focusing of epitope-specific T cells during chronic viral infection reflects selection based on structural avidity. To this end, extensive k_{off}-rate measurements both in humans and in mouse models of CMV were performed, accompanied by in-depth repertoire analysis. Furthermore, *in vivo* T cell responses were rebuilt by transfer of T cells of known avidity, and the resulting artificial repertoires were monitored over time.

The following conclusions can be drawn from the presented data:

1. During the acute phase of the infection, the TCR repertoire of inflationary mCMV-specific T cell populations is diverse and high avidity T cells are preferentially recruited.
2. Structural avidity gradually decreases during chronic infection and is associated with expansion of low avidity T cells.
3. Loss of immunodominance of high avidity T cells is most likely caused by replicative senescence. Clonal succession towards lower avidity TCRs would in turn explain the observed reverse TCR repertoire evolution.

7 Supplement

Enrichment of SIINFEKL-*Strep*tamer positive T cells via high purity FACS sorting

To efficiently perform the microscopic TCR-ligand k_{off}-rate assay for *ex vivo* T cell populations only comprising a small fraction of the sample's leucocytes sorting those T cells prior to k_{off}-rate analysis is prerequisite. For the microscopic k_{off}-rate measurements of Figure 11, Figure 14, Figure 15 and Figure 16 staining and sorting was performed as follows: Preparation of leucocytes was conducted as described in 3.2.2 and for 5×10^7 cells a *Strep*tamer staining was performed (described in 3.2.5). *Strep*tamer positive cells were then sorted on a MoFlo Legacy cell sorter using the sorting strategy displayed in Supplementary Figure 1 A. A high sort purity of over 95 % was achieved (see Supplementary Figure 1 B).

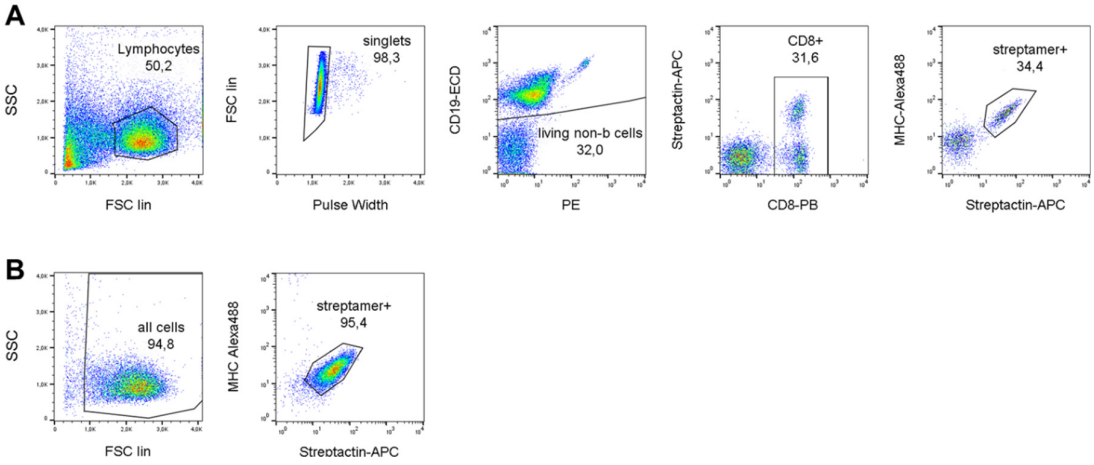

Supplementary Figure 1. *Strep*tamer staining allows high purity sort of SIINFEKL-specific cells. Splenocytes of IE2-SIINFEKL mCMV or M45-SIINFEKL mCMV infected C57BL/6 mice were stained with a SIINFEKL-*Strep*tamer staining, a monoclonal antibody staining directed at CD19 and CD8 and a live/dead dye (PI). **(A)** Pseudocolor plots show a representative sorting strategy for the sort of SIINFEKL-*Strep*tamer$^+$ cells. From left to right: Sorting of lymphocytes, singlets (elimination of doublets), living non-B cells, CD8$^+$ cells and cells double positive for both *Strep*tamer fluorochromes. **(B)** sort purity control: Sorted cells were reanalyzed to assess sort purity.

Microscopic k_{off}-rate assay: cell number analyzed per sample and bleaching constant

Microscopic k_{off}-rate measurements of polyclonal endogenous T cell populations require a large number of single-cell measurements to reliably determine the populations average $t_{1/2}$ and the distribution of $t_{1/2}$. Therefore, on average more than 70 cells were analyzed per mouse (see Supplementary Figure 2).

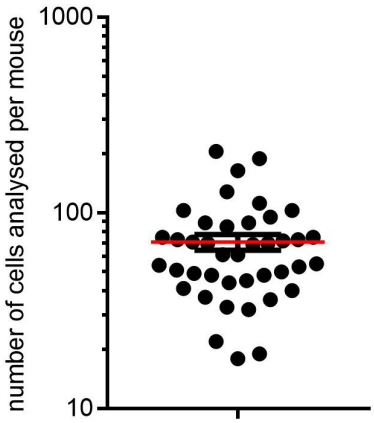

Supplementary Figure 2. Microscopic k_{off}-rate measurements of IE2-SIINFEKL mCMV or M45-SIINFEKL mCMV infected mice: Number of cells analyzed per mouse. Mice were infected i.p. with recombinant IE2-SIINFEKL mCMV or M45-SIINFEKL mCMV. Splenocytes were FACS sorted for $CD8^+$, $CD19^-$, *Strep*tamer$^+$ cells and microscopic koff-rate measurements were performed. Each dot represents number of cells analyzed for one mouse. Red line indicates mean. Number of cells analyzed per mouse: Mean = 70,93 (red); Error bars indicate SEM (black lines), N = 41.

To correct for the influence of photo bleaching on microscopic k_{off}-rate values a bleaching constant k_{bleach} was measured for every experimental day (see 1.2.2 and 3.2.7). Mean k_{bleach} of all microscopic k_{off}-rate experimental days was roughly 0,00052.

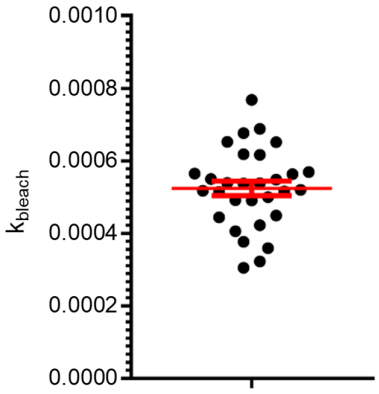

Supplementary Figure 3. Bleaching constant k_{bleach} corrects effect of photo bleaching. k_{bleach} was measured every experimental day for microscopic k_{off}-rate measurements. At least one k_{off}-rate dissociation for either *Strep*-Tactin–coated beads multimerized with Alexa Fluor 488-conjugated MHC molecules or *Strep*tamer stained T cells was performed without addition of D-biotin but otherwise identical settings. Photobleaching caused loss of intensity in a logarithmic manner. One-phase exponential decay curves were fitted using GraphPad Prism; Dots represent mean of at least five events measured for one experimental day. Lines are mean and SEM (red). N = 30.

8 Bibliography

Alam, S. M., Travers, P. J., Wung, J. L., Nasholds, W., Redpath, S., Jameson, S. C., & Gascoigne, N. R. J. (1996). T cell-receptor affinity and thymocyte positive selection. *Nature*, *381*(6583), 616–620. https://doi.org/10.1038/381616a0

Alanio, C., Lemaitre, F., Law, H. K. W., Hasan, M., & Albert, M. L. (2010). Enumeration of human antigen-specific naive CD8+ T cells reveals conserved precursor frequencies. *Blood*, *115*(18), 3718–3725. https://doi.org/10.1182/blood-2009-10-251124

Altman, J. D., Moss, P. A., Goulder, P. J., Barouch, D. H., McHeyzer-Williams, M. G., Bell, J. I., … Davis, M. M. (1996). Phenotypic analysis of antigen-specific T lymphocytes, *274*(5284), 94–96. Retrieved from http://www.ncbi.nlm.nih.gov/entrez/query.fcgi?cmd=Retrieve&db=PubMed&dopt=Citation&list_uids=8810254

Annels, N. E., Callan, M. F., Tan, L., & Rickinson, A. B. (2000). Changing patterns of dominant TCR usage with maturation of an EBV-specific cytotoxic T cell response. *Journal of Immunology (Baltimore, Md. : 1950)*, *165*(9), 4831–4841. Retrieved from http://www.ncbi.nlm.nih.gov/pubmed/11046006

Arstila, T. P., Casrouge, A., Baron, V., Even, J., Kanellopoulos, J., & Kourilsky, P. (1999). A direct estimate of the human alpha beta T cell receptor diversity. *Science (New York, N.Y.)*, *286*(5441), 958–961. https://doi.org/10.1126/science.286.5441.958

Bettini, M. L., Bettini, M., Nakayama, M., Guy, C. S., & Vignali, D. A. A. (2013). Generation of T cell receptor–retrogenic mice: improved retroviral-mediated stem cell gene transfer. *Nature Protocols*, *8*(10), 1837–1840. https://doi.org/10.1038/nprot.2013.111

Blattman, J. N., Antia, R., Sourdive, D. J. D., Wang, X., Kaech, S. M., Murali-Krishna, K., … Ahmed, R. (2002). Estimating the precursor frequency of naive antigen-specific CD8 T cells. *The Journal of Experimental Medicine*, *195*(5), 657–664. https://doi.org/10.1084/JEM.20001021

Brentville, V. A., Metheringham, R. L., Gunn, B., & Durrant, L. G. (2012). High avidity cytotoxic t lymphocytes can be selected into the memory pool but they are exquisitely

sensitive to functional impairment. *PLoS ONE*, *7*(7), e41112. https://doi.org/10.1371/journal.pone.0041112

Buchholz, V. R., Flossdorf, M., Hensel, I., Kretschmer, L., Weissbrich, B., Gräf, P., … Busch, D. H. (2013). Disparate individual fates compose robust CD8+ T cell immunity. *Science (New York, N.Y.)*, *340*(6132), 630–635. https://doi.org/10.1126/science.1235454

Buchholz, V. R., Neuenhahn, M., & Busch, D. H. (2011). CD8+ T cell differentiation in the aging immune system: until the last clone standing. *Current Opinion in Immunology*, *23*(4), 549–554. https://doi.org/10.1016/j.coi.2011.05.002

Burnet, F. M. (1959). The clonal selection theory of acquired immunity. *Cambridge University Press*, 1–232. https://doi.org/10.5962/bhl.title.8281

Busch, D H, & Pamer, E. G. (1999). T Cell Affinity Maturation by Selective Expansion during Infection. *Journal of Experimental Medicine*, *189*(4), 701–710. https://doi.org/10.1084/jem.189.4.701

Busch, Dirk H, Pilip, I. M., Vijh, S., & Pamer, E. G. (1998). Coordinate Regulation of Complex T Cell Populations Responding to Bacterial Infection, *8*, 353–362.

Casrouge, A., Beaudoing, E., Dalle, S., Pannetier, C., Kanellopoulos, J., & Kourilsky, P. (2000). Size Estimate of the TCR Repertoire of Naive Mouse Splenocytes. *The Journal of Immunology*, *164*(11), 5782–5787. https://doi.org/10.4049/jimmunol.164.11.5782

Chou, J. P., & Effros, R. B. (2013). T cell replicative senescence in human aging. *Current Pharmaceutical Design*, *19*(9), 1680–1698. Retrieved from http://www.ncbi.nlm.nih.gov/pubmed/23061726

Chu, H. H., Moon, J. J., Kruse, A. C., Pepper, M., & Jenkins, M. K. (2010). Negative selection and peptide chemistry determine the size of naive foreign peptide-MHC class II-specific CD4+ T cell populations. *Journal of Immunology (Baltimore, Md. : 1950)*, *185*(8), 4705–4713. https://doi.org/10.4049/jimmunol.1002276

Cicin-Sain, L., Brien, J. D., Uhrlaub, J. L., Drabig, A., Marandu, T. F., & Nikolich-Zugich, J. (2012). Cytomegalovirus infection impairs immune responses and accentuates T-cell

pool changes observed in mice with aging. *PLoS Pathogens*, *8*(8), e1002849. https://doi.org/10.1371/journal.ppat.1002849

Crawford, F., Kozono, H., White, J., Marrack, P., & Kappler, J. (1998). Detection of antigen-specific T cells with multivalent soluble class II MHC covalent peptide complexes. *Immunity*, *8*(6), 675–682. https://doi.org/10.1016/S1074-7613(00)80572-5

Davenport, M. P., Fazou, C., McMichael, A. J., & Callan, M. F. C. (2002). Clonal selection, clonal senescence, and clonal succession: the evolution of the T cell response to infection with a persistent virus. *Journal of Immunology (Baltimore, Md. : 1950)*, *168*(7), 3309–3317. https://doi.org/10.4049/jimmunol.168.7.3309

Day, E. K., Carmichael, A. J., ten Berge, I. J. M., Waller, E. C. P., Sissons, J. G. P., & Wills, M. R. (2007). Rapid CD8+ T Cell Repertoire Focusing and Selection of High-Affinity Clones into Memory Following Primary Infection with a Persistent Human Virus: Human Cytomegalovirus. *The Journal of Immunology*, *179*(5), 3203–3213. https://doi.org/10.4049/jimmunol.179.5.3203

Dekhtiarenko, I., Jarvis, M. a, Ruzsics, Z., & Čičin-Šain, L. (2013). The context of gene expression defines the immunodominance hierarchy of cytomegalovirus antigens. *Journal of Immunology (Baltimore, Md.: 1950)*, *190*(7), 3399–3409. https://doi.org/10.4049/jimmunol.1203173

Dine, J., Gordon, R., Shames, Y., Kasler, M. K., & Barton-Burke, M. (2017). Immune Checkpoint Inhibitors: An Innovation in Immunotherapy for the Treatment and Management of Patients with Cancer. *Asia-Pacific Journal of Oncology Nursing*, *4*(2), 127–135. https://doi.org/10.4103/apjon.apjon_4_17

Dössinger, G., Bunse, M., Bet, J., Albrecht, J., Paszkiewicz, P. J., Weißbrich, B., … Busch, D. H. (2013). MHC multimer-guided and cell culture-independent isolation of functional T cell receptors from single cells facilitates TCR identification for immunotherapy. *PloS One*, *8*(4), e61384. https://doi.org/10.1371/journal.pone.0061384

Echchakir, H., Dorothee, G., Vergnon, I., Menez, J., Chouaib, S., & Mami-Chouaib, F. (2002). Cytotoxic T lymphocytes directed against a tumor-specific mutated antigen

display similar HLA tetramer binding but distinct functional avidity and tissue distribution. *Proceedings of the National Academy of Sciences*, *99*(14), 9358–9363. https://doi.org/10.1073/pnas.142308199

Elkington, R., Walker, S., Crough, T., Menzies, M., Tellam, J., Bharadwaj, M., & Khanna, R. (2003). Ex vivo profiling of CD8+-T-cell responses to human cytomegalovirus reveals broad and multispecific reactivities in healthy virus carriers. *Journal of Virology*, *77*(9), 5226–5240. Retrieved from http://www.ncbi.nlm.nih.gov/pubmed/12692225

Enouz, S., Carrié, L., Merkler, D., Bevan, M. J., & Zehn, D. (2012). Autoreactive T cells bypass negative selection and respond to self-antigen stimulation during infection. *Journal of Experimental Medicine*, *209*(10), 1769–1779. https://doi.org/10.1084/jem.20120905

Fägerstam, L. G., Frostell-Karlsson, A., Karlsson, R., Persson, B., & Rönnberg, I. (1992). Biospecific interaction analysis using surface plasmon resonance detection applied to kinetic, binding site and concentration analysis. *Journal of Chromatography*, *597*(1–2), 397–410. Retrieved from http://www.ncbi.nlm.nih.gov/pubmed/1517343

Grassmann, S., Mihatsch, L., Mir, J., Kazeroonian, A., Rahimi, R., Flommersfeld, S., … Buchholz, V. R. (2020). Early emergence of T central memory precursors programs clonal dominance during chronic viral infection. *Nature Immunology*, *21*(12), 1563–1573. https://doi.org/10.1038/s41590-020-00807-y

Griffiths, P., Baraniak, I., & Reeves, M. (2015). The pathogenesis of human cytomegalovirus. *Journal of Pathology*, *235*(2), 288–297. https://doi.org/10.1002/path.4437

Griffiths, S. J., Riddell, N. E., Masters, J., Libri, V., Henson, S. M., Wertheimer, A., … Rivino, L. (2017). Age-Associated Increase of Low-Avidity Cytomegalovirus-Specific CD8 + T Cells That Re-Express CD45RA. *Journal of Immunology (Baltimore, Md.: 1950)*, *190*(11), 5363–5372. https://doi.org/10.4049/jimmunol.1203267

Hadrup, S. R., Strindhall, J., Kollgaard, T., Seremet, T., Johansson, B., Pawelec, G., … Wikby, A. (2006). Longitudinal Studies of Clonally Expanded CD8 T Cells Reveal a Repertoire Shrinkage Predicting Mortality and an Increased Number of Dysfunctional

Cytomegalovirus-Specific T Cells in the Very Elderly. *The Journal of Immunology*, *176*(4), 2645–2653. https://doi.org/10.4049/jimmunol.176.4.2645

Hayflick, L, & Moorhead, P. S. (1961). The serial cultivation of human diploid strains. *Exp. Cell Res.*, *25*(January 2018), 585–621. Retrieved from http://www.ncbi.nlm.nih.gov/pubmed/13905658

Hayflick, Leonard. (1980). Recent advances in the cell biology of aging. *Mech Ageing Dev*, *14*(1–2), 59–79. Retrieved from http://www.ncbi.nlm.nih.gov/pubmed/7010011

Holmberg, K., Mariathasan, S., Ohteki, T., Ohashi, P. S., & Gascoigne, N. R. J. (2003). TCR Binding Kinetics Measured with MHC Class I Tetramers Reveal a Positive Selecting Peptide with Relatively High Affinity for TCR. *The Journal of Immunology*, *171*(5), 2427–2434. https://doi.org/10.4049/jimmunol.171.5.2427

Holst, J., Szymczak-Workman, A. L., Vignali, K. M., Burton, A. R., Workman, C. J., & Vignali, D. A. A. (2006). Generation of T-cell receptor retrogenic mice. *Nature Protocols*, *1*(1), 406–417. https://doi.org/10.1038/nprot.2006.61

Hombrink, P., Raz, Y., Kester, M. G. D., De Boer, R., Weißbrich, B., Von dem Borne, P. A., … Heemskerk, M. H. M. (2013). Mixed functional characteristics correlating with TCR-ligand koff-rate of MHC-tetramer reactive T cells within the naive T-cell repertoire. *European Journal of Immunology*, *43*(11), 3038–3050. https://doi.org/10.1002/eji.201343397

Hurwitz, A. A., Cuss, S. M., Stagliano, K. E., & Zhu, Z. (2014). T cell avidity and tumor immunity: problems and solutions. *Cancer Microenvironment : Official Journal of the International Cancer Microenvironment Society*, *7*(1–2), 1–9. https://doi.org/10.1007/s12307-013-0143-1

Irving, M., Zoete, V., Hebeisen, M., Schmid, D., Baumgartner, P., Guillaume, P., … Michielin, O. (2012). Interplay between T Cell Receptor Binding Kinetics and the Level of Cognate Peptide Presented by Major Histocompatibility Complexes Governs CD8 $^{+}$ T Cell Responsiveness. *Journal of Biological Chemistry*, *287*(27), 23068–23078. https://doi.org/10.1074/jbc.M112.357673

Jenkins, M. K., Chu, H. H., McLachlan, J. B., & Moon, J. J. (2010). On the Composition of the Preimmune Repertoire of T Cells Specific for Peptide–Major Histocompatibility Complex Ligands. *Annual Review of Immunology*, *28*(1), 275–294. https://doi.org/10.1146/annurev-immunol-030409-101253

Johnson, L. A., Heemskerk, B., Powell, D. J., Cohen, C. J., Morgan, R. A., Dudley, M. E., … Rosenberg, S. A. (2006). Gene Transfer of Tumor-Reactive TCR Confers Both High Avidity and Tumor Reactivity to Nonreactive Peripheral Blood Mononuclear Cells and Tumor-Infiltrating Lymphocytes. *The Journal of Immunology*, *177*(9), 6548–6559. https://doi.org/10.4049/jimmunol.177.9.6548

Karrer, U., Sierro, S., Wagner, M., Oxenius, A., Hengel, H., Koszinowski, U. H., … Klenerman, P. (2003). Memory inflation: continuous accumulation of antiviral CD8+ T cells over time. *Journal of Immunology (Baltimore, Md. : 1950)*, *170*(4), 2022–2029. https://doi.org/IS0127

Kenneth, M. (2013). *Janeway immunobiology*. *Journal of Chemical Information and Modeling*. https://doi.org/10.1017/CBO9781107415324.004

Kenneth Murphy, C. W. (2016). *Janeway's Immunobiology, Ninth Edition*.

Khan, N., Best, D., Bruton, R., Nayak, L., Rickinson, A. B., & Moss, P. A. H. (2007). T cell recognition patterns of immunodominant cytomegalovirus antigens in primary and persistent infection. *The Journal of Immunology*, *178*(7), 4455–4465. https://doi.org/10.4049/jimmunol.178.7.4455

Khan, N., Cobbold, M., Cummerson, J., & Moss, P. A. H. (2010). Persistent viral infection in humans can drive high frequency low-affinity T-cell expansions. *Immunology*, *131*(4), 537–548. https://doi.org/10.1111/j.1365-2567.2010.03326.x

Khan, N., Shariff, N., Cobbold, M., Bruton, R., Ainsworth, J. A., Sinclair, A. J., … Moss, P. A. H. (2002). Cytomegalovirus seropositivity drives the CD8 T cell repertoire toward greater clonality in healthy elderly individuals. *Journal of Immunology (Baltimore, Md. : 1950)*, *169*(4), 1984–1992. https://doi.org/10.4049/jimmunol.169.4.1984

Klenerman, P., & Oxenius, A. (2016). T cell responses to cytomegalovirus. *Nature Reviews.*

Immunology, *16*(6), 367–377. https://doi.org/10.1038/nri.2016.38

Knabel, M., Franz, T. J., Schiemann, M., Wulf, A., Villmow, B., Schmidt, B., … Busch, D. H. (2002). Reversible MHC multimer staining for functional isolation of T-cell populations and effective adoptive transfer. *Nature Medicine*, *8*(6), 631–637. https://doi.org/10.1038/nm0602-631

Knall, R. A. (2007). Direct ex vivo identification of individual antigen-specific T cells with optimal avidity for protection. *Dissertation Fakultät Wissenschaftszentrum Weihenstephan TUM*, 1–112. Retrieved from http://nbn-resolving.de/urn/resolver.pl?urn:nbn:de:bvb:91-diss-20070727-625568-1-2

Krmpotic, A., Bubic, I., Polic, B., Lucin, P., & Jonjic, S. (2003). Pathogenesis of murine cytomegalovirus infection. *Microbes and Infection*, *5*(13), 1263–1277. Retrieved from http://www.ncbi.nlm.nih.gov/pubmed/14623023

Lang, A., Brien, J. D., & Nikolich-Zugich, J. (2009). Inflation and long-term maintenance of CD8 T cells responding to a latent herpesvirus depend upon establishment of latency and presence of viral antigens. *Journal of Immunology (Baltimore, Md. : 1950)*, *183*(12), 8077–8087. https://doi.org/10.4049/jimmunol.0801117

Lawson, T. M., Man, S., Wang, E. C., Williams, S., Amos, N., Gillespie, G. M., … Borysiewicz, L. K. (2001). Functional differences between influenza A-specific cytotoxic T lymphocyte clones expressing dominant and subdominant TCR. *International Immunology*, *13*(11), 1383–1390. Retrieved from http://www.ncbi.nlm.nih.gov/pubmed/11675370

Laydon, D. J., Bangham, C. R. M., & Asquith, B. (2015). Estimating T-cell repertoire diversity: limitations of classical estimators and a new approach. *Philosophical Transactions of the Royal Society B: Biological Sciences*, *370*(1675), 20140291. https://doi.org/10.1098/rstb.2014.0291

Lever, M., Maini, P. K., van der Merwe, P. A., & Dushek, O. (2014). Phenotypic models of T cell activation. *Nature Reviews Immunology*, *14*(9), 619–629. https://doi.org/10.1038/nri3728

Li, D., Li, X., Zhou, W.-L., Huang, Y., Liang, X., Jiang, L., … Wang, W. (2019). Genetically engineered T cells for cancer immunotherapy. *Signal Transduction and Targeted Therapy*, *4*(1), 35. https://doi.org/10.1038/s41392-019-0070-9

Link, C. S., Eugster, A., Heidenreich, F., Rücker-Braun, E., Schmiedgen, M., Oelschlägel, U., … Bonifacio, E. (2016). Abundant cytomegalovirus (CMV) reactive clonotypes in the CD8(+) T cell receptor alpha repertoire following allogeneic transplantation. *Clinical and Experimental Immunology*, *184*(3), 389–402. https://doi.org/10.1111/cei.12770

Loewendorf, A., & Benedict, C. A. (2010). Modulation of host innate and adaptive immune defenses by cytomegalovirus: timing is everything. *Journal of Internal Medicine*, *267*(5), 483–501. https://doi.org/10.1111/j.1365-2796.2010.02220.x

Martinez, R. J., & Evavold, B. D. (2015). Lower affinity T cells are critical components and active participants of the immune response. *Frontiers in Immunology*, *6*(SEP), 468. https://doi.org/10.3389/fimmu.2015.00468

McGeoch, D. J., Cook, S., Dolan, A., Jamieson, F. E., & Telford, E. A. R. (1995). Molecular Phylogeny and Evolutionary Timescale for the Family of Mammalian Herpesviruses. *Journal of Molecular Biology*, *247*(3), 443–458. https://doi.org/10.1006/jmbi.1995.0152

Merwe, P. A. van der, & Davis, S. J. (2003). Molecular Interactions Mediating T Cell Antigen Recognition. *Annual Review of Immunology*, *21*(1), 659–684. https://doi.org/10.1146/annurev.immunol.21.120601.141036

Miles, J. J., Douek, D. C., & Price, D. A. (2011). Bias in the αβ T-cell repertoire: implications for disease pathogenesis and vaccination. *Immunology and Cell Biology*, *89*(3), 375–387. https://doi.org/10.1038/icb.2010.139

Munks, M. W., Cho, K. S., Pinto, A. K., Sierro, S., Klenerman, P., & Hill, A. B. (2006). Four Distinct Patterns of Memory CD8 T Cell Responses to Chronic Murine Cytomegalovirus Infection. *The Journal of Immunology*, *177*(1), 450–458. https://doi.org/10.4049/jimmunol.177.1.450

Nauerth, M. (2012). [Thesis] Development of a novel TCR avidity assay for human CD8 + T cells. *Dissertation Fakultät Wissenschaftszentrum Weihenstephan TUM*. Retrieved

from https://push-zb.helmholtz-muenchen.de/frontdoor.php?source_opus=24763&la=de#extra

Nauerth, M., Stemberger, C., Mohr, F., Weißbrich, B., Schiemann, M., Germeroth, L., & Busch, D. H. (2016). Flow cytometry-based TCR-ligand Koff-rate assay for fast avidity screening of even very small antigen-specific T cell populations ex vivo. *Cytometry Part A*, *89*(9), 816–825. https://doi.org/10.1002/cyto.a.22933

Nauerth, M., Weißbrich, B., Knall, R., Franz, T., Dössinger, G., Bet, J., … Busch, D. H. (2013). TCR-ligand koff rate correlates with the protective capacity of antigen-specific CD8+ T cells for adoptive transfer. *Science Translational Medicine*, *5*(192), 192ra87. https://doi.org/10.1126/scitranslmed.3005958

Neuenhahn, M., Albrecht, J., Odendahl, M., Schlott, F., Dössinger, G., Schiemann, M., … Grigoleit, G. U. (2017). Transfer of minimally manipulated CMV-specific T cells from stem cell or third-party donors to treat CMV infection after allo-HSCT. *Leukemia*, *31*(10), 2161–2171. https://doi.org/10.1038/leu.2017.16

O'Hara, G. a, Welten, S. P. M., Klenerman, P., & Arens, R. (2012). Memory T cell inflation: understanding cause and effect. *Trends in Immunology*, *33*(2), 84–90. https://doi.org/10.1016/j.it.2011.11.005

Obar, J. J., Khanna, K. M., & Lefrançois, L. (2008). Endogenous Naive CD8+ T Cell Precursor Frequency Regulates Primary and Memory Responses to Infection. *Immunity*, *28*(6), 859–869. https://doi.org/10.1016/j.immuni.2008.04.010

Ouyang, Q., Wagner, W. M., Wikby, A., Walter, S., Aubert, G., Dodi, A. I., … Pawelec, G. (2003). Large numbers of dysfunctional CD8+ T lymphocytes bearing receptors for a single dominant CMV epitope in the very old. *Journal of Clinical Immunology*, *23*(4), 247–257. https://doi.org/10.1023/A:1024580531705

Ouyang, Q., Wagner, W. M., Zheng, W., Wikby, A., Remarque, E. J., & Pawelec, G. (2004). Dysfunctional CMV-specific CD8+ T cells accumulate in the elderly. *Experimental Gerontology*, *39*(4), 607–613. https://doi.org/10.1016/j.exger.2003.11.016

Palermo, B., Campanelli, R., Mantovani, S., Lantelme, E., Manganoni, A. M., Carella, G.,

… Giachino, C. (2001). Diverse expansion potential and heterogeneous avidity in tumor-associated antigen-specific T lymphocytes from primary melanoma patients. *European Journal of Immunology*, *31*(2), 412–420. https://doi.org/10.1002/1521-4141(200102)31:2<412::AID-IMMU412>3.0.CO;2-4

Ping, Y., Liu, C., & Zhang, Y. (2018). T-cell receptor-engineered T cells for cancer treatment: current status and future directions. *Protein & Cell*, *9*(3), 254–266. https://doi.org/10.1007/s13238-016-0367-1

Price, D. A. (2005). Avidity for antigen shapes clonal dominance in CD8+ T cell populations specific for persistent DNA viruses. *Journal of Experimental Medicine*, *202*(10), 1349–1361. https://doi.org/10.1084/jem.20051357

Qi, Q., Liu, Y., Cheng, Y., Glanville, J., Zhang, D., Lee, J. Y., … Goronzy, J. J. (2014). Diversity and clonal selection in the human T-cell repertoire. *Proceedings of the National Academy of Sciences of the United States of America*, *111*(36), 13139–13144. https://doi.org/10.1073/pnas.1409155111

Quigley, M. F., Greenaway, H. Y., Venturi, V., Lindsay, R., Quinn, K. M., Seder, R. A., … Price, D. A. (2010). Convergent recombination shapes the clonotypic landscape of the naive T-cell repertoire. *Proceedings of the National Academy of Sciences*, *107*(45), 19414–19419. https://doi.org/10.1073/pnas.1010586107

Riddell, S. R., Watanabe, K. S., Goodrich, J. M., Li, C. R., Agha, M. E., & Greenberg, P. D. (1992). Restoration of viral immunity in immunodeficient humans by the adoptive transfer of T cell clones. *Science*, *257*(5067), 238–241. https://doi.org/10.1126/science.1352912

Rosette, C., Werlen, G., Daniels, M. A., Holman, P. O., Alam, S. M., Travers, P. J., … Jameson, S. C. (2001). The Impact of duration versus extent of TCR occupancy on T cell activation: A revision of the kinetic proofreading model. *Immunity*, *15*(1), 59–70. https://doi.org/10.1016/S1074-7613(01)00173-X

Savage, P. A., Boniface, J. J., & Davis, M. M. (1999). A kinetic basis for T cell receptor repertoire selection during an immune response. *Immunity*, *10*(4), 485–492.

https://doi.org/10.1016/S1074-7613(00)80048-5

Scherer, A., Noest, A., & de Boer, R. J. (2004). Activation-threshold tuning in an affinity model for the T-cell repertoire. *Proceedings. Biological Sciences / The Royal Society*, *271*(1539), 609–616. https://doi.org/10.1098/rspb.2003.2653

Schober, K., Fuchs, P., Mir, J., Hammel, M., Fanchi, L., Flossdorf, M., & Busch, D. H. (2020). The CMV-Specific CD8+ T Cell Response Is Dominated by Supra-Public Clonotypes with High Generation Probabilities. *Pathogens*, *9*(8), 650. https://doi.org/10.3390/pathogens9080650

Schober, K., Voit, F., Grassmann, S., Müller, T. R., Eggert, J., Jarosch, S., … Busch, D. H. (2020). Reverse TCR repertoire evolution towards dominant low affinity clones during chronic CMV infection. *Nature Immunology*, (in press). https://doi.org/10.1038/s41590-020-0628-2

Shih, K., Arkenau, H.-T., & Infante, J. R. (2014). Clinical impact of checkpoint inhibitors as novel cancer therapies. *Drugs*, *74*(17), 1993–2013. https://doi.org/10.1007/s40265-014-0305-6

Slifka, M. K., & Whitton, J. L. (2001). Functional avidity maturation of CD8(+) T cells without selection of higher affinity TCR. *Nature Immunology*, *2*(8), 711–717. https://doi.org/10.1038/90650

Smith, C. J., Turula, H., & Snyder, C. M. (2014). Systemic hematogenous maintenance of memory inflation by MCMV infection. *PLoS Pathogens*, *10*(7), e1004233. https://doi.org/10.1371/journal.ppat.1004233

Snyder, C. M. (2011). Buffered memory: A hypothesis for the maintenance of functional, virus-specific CD8 + T cells during cytomegalovirus infection. *Immunologic Research*, *51*(2–3), 195–204. https://doi.org/10.1007/s12026-011-8251-9

Snyder, C. M., Cho, K. S., Bonnett, E. L., van Dommelen, S., Shellam, G. R., & Hill, A. B. (2008). Memory inflation during chronic viral infection is maintained by continuous production of short-lived, functional T cells. *Immunity*, *29*(4), 650–659. https://doi.org/10.1016/j.immuni.2008.07.017

Snyder, C. M., Cho, K. S., Morrison, E. L., Van, S., Shellam, G. R., Hill, A. B., … Hill, A. B. (2009). Memory Inflation During Chronic Viral Infection is Maintained by Continuous Production of Short-Lived Functional T Cells. *Immunity*, *29*(4), 650–659. https://doi.org/10.1016/j.immuni.2008.07.017.Memory

Stone, J. D., Chervin, A. S., & Kranz, D. M. (2009). T-cell receptor binding affinities and kinetics: impact on T-cell activity and specificity. *Immunology*, *126*(2), 165–176. https://doi.org/10.1111/j.1365-2567.2008.03015.x

Sylwester, A., Nambiar, K. Z., Caserta, S., Klenerman, P., Picker, L. J., & Kern, F. (2016). A new perspective of the structural complexity of HCMV-specific T-cell responses. *Mechanisms of Ageing and Development*, *158*, 14–22. https://doi.org/10.1016/J.MAD.2016.03.002

Trautmann, L., Cerundolo, V., Bonneville, M., Saulquin, X., Neveu, B., Dechanet, J., … Echasserieau, K. (2005). Selection of T Cell Clones Expressing High-Affinity Public TCRs within Human Cytomegalovirus-Specific CD8 T Cell Responses. *J Immunol References*, *175*, 6123–6132. https://doi.org/10.4049/jimmunol.175.9.6123

Turner, S. J., Kedzierska, K., Komodromou, H., La Gruta, N. L., Dunstone, M. A., Webb, A. I., … Doherty, P. C. (2005). Lack of prominent peptide–major histocompatibility complex features limits repertoire diversity in virus-specific CD8+ T cell populations. *Nature Immunology*, *6*(4), 382–389. https://doi.org/10.1038/ni1175

Venturi, V., Kedzierska, K., Price, D. A., Doherty, P. C., Douek, D. C., Turner, S. J., & Davenport, M. P. (2006). Sharing of T cell receptors in antigen-specific responses is driven by convergent recombination. *Proceedings of the National Academy of Sciences*, *103*(49), 18691–18696. https://doi.org/10.1073/pnas.0608907103

Viganò, S., Utzschneider, D. T., Perreau, M., Pantaleo, G., Zehn, D., & Harari, A. (2012). Functional avidity: A measure to predict the efficacy of effector T cells? *Clinical and Developmental Immunology*, *2012*. https://doi.org/10.1155/2012/153863

Walter, E. A., Greenberg, P. D., Gilbert, M. J., Finch, R. J., Watanabe, K. S., Thomas, E. D., & Riddell, S. R. (1995). Reconstitution of Cellular Immunity against

Cytomegalovirus in Recipients of Allogeneic Bone Marrow by Transfer of T-Cell Clones from the Donor. *New England Journal of Medicine*, *333*(16), 1038–1044. https://doi.org/10.1056/NEJM199510193331603

Wang, X. L., & Altman, J. D. (2003). Caveats in the design of MHC class I tetramer/antigen-specific T lymphocytes dissociation assays. *Journal of Immunological Methods*, *280*(1–2), 25–35. https://doi.org/10.1016/S0022-1759(03)00079-6

Weißbrich, B. (2015). T cell receptor binding avidity of antigen-specific CD8 + cytotoxic T cells in chronic infection. *Dissertation Fakultät Für Medizin TU München*. Retrieved from http://nbn-resolving.de/urn/resolver.pl?urn:nbn:de:bvb:91-diss-20160224-1254464-1-9

Wherry, E. J. (2011, June 18). T cell exhaustion. *Nature Immunology*. Nature Publishing Group. https://doi.org/10.1038/ni.2035

Wikby, A., Maxson, P., Olsson, J., Johansson, B., & Ferguson, F. G. (1998). Changes in CD8 and CD4 lymphocyte subsets, T cell proliferation responses and non-survival in the very old: the Swedish longitudinal OCTO-immune study. *Mechanisms of Ageing and Development*, *102*(2–3), 187–198. Retrieved from http://www.ncbi.nlm.nih.gov/pubmed/9720651

Wilkins, O., Keeler, A. M., & Flotte, T. R. (2017). CAR T-Cell Therapy: Progress and Prospects. *Human Gene Therapy Methods*, *28*(2), 61–66. https://doi.org/10.1089/hgtb.2016.153

Williams, M. A., & Bevan, M. J. (2007). Effector and memory CTL differentiation. *Annual Review of Immunology*, *25*(1), 171–192. https://doi.org/10.1146/annurev.immunol.25.022106.141548

Yee, C., Savage, P. A., Lee, P. P., Davis, M. M., & Greenberg, P. D. (1999). Isolation of high avidity melanoma-reactive CTL from heterogeneous populations using peptide-MHC tetramers. *Journal of Immunology*, *162*(4), 2227–2234. https://doi.org/10.4049/jimmunol.171.5.2393

Zarnitsyna, V. I., Evavold, B. D., Schoettle, L. N., Blattman, J. N., & Antia, R. (2013).

Estimating the diversity, completeness, and cross-reactivity of the T cell repertoire. *Frontiers in Immunology*, *4*(DEC), 1–11. https://doi.org/10.3389/fimmu.2013.00485

Zeh, H. J., Perry-Lalley, D., Dudley, M. E., Rosenberg, S. A., & Yang, J. C. (1999). High avidity CTLs for two self-antigens demonstrate superior in vitro and in vivo antitumor efficacy. *Journal of Immunology (Baltimore, Md.: 1950)*, *162*(2), 989–994. Retrieved from http://www.ncbi.nlm.nih.gov/pubmed/9916724

Zehn, D., Lee, S. Y., & Bevan, M. J. (2009). Complete but curtailed T-cell response to very low-affinity antigen. *Nature*, *458*(7235), 211–214. https://doi.org/10.1038/nature07657

9 Acknowledgements

First and foremost, I would like to thank Prof. Dr. Dirk Busch for offering me this interesting and challenging project, the excellent supervision as thesis advisor of my dissertation and the profound scientific education I could gain in his group.

My special thanks go to Dr. Kilian Schober, who as a great mentor and supervisor helped the joint project to reach new dimensions.

I would like to thank Dr. Bianca Weißbrich for her competent introduction to the methods and the preliminary work for this project, as well as Dr. Magdalena Nauerth and Dr. Veit Buchholz for mentoring me in my early days. I would like to thank Dr. Simon Grassmann, Thomas Müller, Joel Eggert, Sebastian Jarosch, Lorenz Mihatsch, Philipp Lückemeier, Justin Leube, and Anna Purcarea for their active cooperation in the joint project and for contributing valuable data.

A big thank you goes to the Busch group. The friendly and collegial atmosphere and the mutual support created an environment in which even long experimental days could be mastered. Many thanks to the TAs Anna Hochholzer Inge Hensel, Katrin Molter, Monika Hammel, Füsun Gökmen and Franziska Graml for their great support. I would also like to thank AG Schiemann for running the many sort experiments, at this point a special thanks to Dr. Immanuel Andrä for rescuing many experiments when there were technical problems with the FACS machines. Furthermore, I would like to thank the members of the “AG Kicker” for the top-class sporting competition at the table during incubation breaks.

And finally, my heartfelt thanks go to my parents, my sister and especially to Alisa, for their mental support and for always being there in times of need during the last years.